



January 2013

Experimental Investigation Of The Effect Of Turbulence On Slot-Fed Film Cooling Adiabatic Effectiveness And Downstream Heat Transfer

Mitch Busche

Follow this and additional works at: <https://commons.und.edu/theses>

Recommended Citation

Busche, Mitch, "Experimental Investigation Of The Effect Of Turbulence On Slot-Fed Film Cooling Adiabatic Effectiveness And Downstream Heat Transfer" (2013). *Theses and Dissertations*. 1405.
<https://commons.und.edu/theses/1405>

This Thesis is brought to you for free and open access by the Theses, Dissertations, and Senior Projects at UND Scholarly Commons. It has been accepted for inclusion in Theses and Dissertations by an authorized administrator of UND Scholarly Commons. For more information, please contact zeinebyousif@library.und.edu.

EXPERIMENTAL INVESTIGATION OF THE EFFECT OF TURBULENCE ON
SLOT-FED FILM COOLING ADIABATIC EFFECTIVENESS AND DOWNSTREAM
HEAT TRANSFER

by

Mitchell Lee Busche

Bachelor of Science, South Dakota State University, 2009

A Thesis

Submitted to the Graduate Faculty

of the

University of North Dakota

In partial fulfillment of the requirements

for the degree of

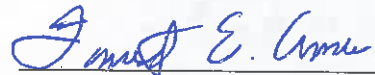
Master of Science

Grand Forks, North Dakota

May

2013

This thesis, submitted by Mitchell L. Busche in partial fulfillment of the requirements for the degree of Master of Science from the University of North Dakota has been read by the Faculty Advisory Committee under whom the work has been done and is hereby approved.



Dr. Forrest Ames

24 April 2013

Date



Dr. Nanak Grewal

April 24, 2013

Date



Dr. Clement Tang

24 April 2013

Date

This thesis meets the standards for appearance, conforms to the style and format requirements of the Graduate School of the University of North Dakota and is hereby approved.



Wayne Swisher

Dean of Graduate School

April 25, 2013

Date

PERMISSION

Title Experimental Investigation of the Effect of Turbulence on Slot-Fed Film Cooling Adiabatic Effectiveness and Downstream Heat Transfer

Department Mechanical Engineering

Degree Master of Science

In presenting this thesis in partial fulfillment of the requirements for a graduate degree from the University of North Dakota, I agree that the library of this University shall make it freely available for inspection. I further agree that permission for extensive copying for scholarly purposes may be granted by the professor who supervised my thesis work or, in his absence, by the chairperson of the department or the dean of the Graduate School. It is understood that any copying or publication or any other use of this thesis or part thereof for financial gain shall not be allowed without my written permission. It is also understood that due recognition shall be given to me and to the University of North Dakota in any scholarly use which may be made of any material in my thesis.

Mitchell L. Busche
23 April 2013

TABLE OF CONTENTS

LIST OF FIGURES	vii
LIST OF TABLES	xii
NOMENCLATURE	xiv
ACKNOWLEDGEMENTS	xvii
ABSTRACT	xviii
CHAPTER	
I. INTRODUCTION	1
II. LITERATURE REVIEW	5
Slot Film Cooling	5
Discrete Hole and Shaped Hole Film Cooling	7
Effects of Turbulence	11
III. EXPERIMENTAL APPROACH	14
Turbine Vane Cascade Wind Tunnel	14
Design and Fabrication of the Cylindrical Test Sections	22
FLUENT	24
Pro/Engineer (Pro/E)	27
Mounting Bracket	30

Test Section After body	34
Data Acquisition Equipment.....	43
Thermocouples and Temperature Measurements.....	44
Pressures	45
Coolant Delivery System.....	46
Data Acquisition	49
Preparation.....	49
Data Acquisition Procedure.....	50
IV. EXPERIMENTAL RESULTS	58
Adiabatic Effectiveness – Large Cylindrical Leading Edge Test Section.....	59
Effects of Blowing.....	59
Effects of Reynolds Number	62
Effects of Turbulence	65
Adiabatic Effectiveness – Small Cylindrical Leading Edge Test Section.....	69
Effects of Blowing.....	69
Effects of Reynolds Number	71
Effects of Turbulence	74
Comparison of Adiabatic Effectiveness Between the Two Test Sections.....	77
Heat Transfer – Large Cylindrical Leading Edge Test Section.....	80
Effects of Blowing.....	80

Effects of Reynolds Number	82
Effects of Turbulence	84
Heat Transfer – Small Cylindrical Leading Edge Test Section.....	88
Effects of Blowing.....	88
Effects of Reynolds Number	90
Effects of Turbulence	92
V. CONCLUSIONS.....	96
Adiabatic Effectiveness	96
Stanton Number	97
APPENDICES	99
A. Analysis of Data Set.....	100
B. Adiabatic Effectiveness and Stanton Number Data.....	103
C. Uncertainty Analysis.....	127
Adiabatic Effectiveness Uncertainty.	127
Stanton Number Uncertainty.....	127
D. QuickBasic Program for the Big Cylindrical Leading Edge Test Section.....	129
REFERENCES	152

LIST OF FIGURES

Figure	Page
1. Turbine Vane with film cooling [2].	2
2. Turbine vane without film cooling [2].	3
3. Boundary layer development over a flat plate [3].	4
4. Schematic of test surface from Bunker.	6
5. Slot parameters investigated by Bruce-Black et al.	6
6. Typical film-cooling blade design [10].	8
7. Schematic of holes used in [13].	9
8. Hole layout for Ligrani et al. [14].	11
9. UND's large scale turbine vane cascade wind tunnel with large cylinder test section [2].	15
10. Blower used by UND.	16
11. Heat Exchanger schematic [33].	17
12. External view of heat exchanger, pump, and tank [33].	17
13. Flow conditioning section.	18
14. Mock aero-combustor and laminar flow nozzle, front view.	19
15. Laminar flow nozzle and mock aero-combustor, rear view.	19
16. Schematic of the mock aero-combustor.	20
17. Grid schematic [38].	22
18. Leading edge profiles [2].	23

19. Big and small cylinder acceleration profiles [2].	24
20. Static pressure contours around the big cylindrical test section from FLUENT.	25
21. Static pressure contours around the small cylindrical test section from FLUENT.	25
22. Static temperature contours around the big cylindrical test section from FLUENT.	26
23. Static temperature contours around the small cylindrical test section from FLUENT.	26
24. Pin layout and dimensions for the large cylindrical test section leading edge from Pro/E.	28
25. Pro/E wireframes of the large cylindrical test section leading edge.	29
26. Pro/E wireframes of the small cylinder leading edge.	30
27. Pro/E model of big cylindrical leading edge mounting bracket.	31
28. Pro/E model of small cylindrical leading edge mounting bracket.	31
29. Dimension 1200es 3-D printer at UND.	33
30. Small cylinder leading edge and mounting bracket.	34
31. Cool air injection pipe and baffle with quick disconnect PVC coupling.	35
32. Inconel heat foil geometry.	37
33. Large and small cylindrical leading edge test section router jigs.	39
34. Glued, cut, and drilled small test section with leading edge and mounting bracket.	40
35. Small test section with mounting bracket and leading edge attached for alignment.	40
36. Small test section with mounting bracket attached and weights applied.	41
37. Epoxy board with contact cement. Thermocouple locations can be seen.	42
38. Small cylindrical test section with inconel foil and acrylic window attached.	43
39. Thermocouple welder, materials, and completed thermocouple.	44

40. Stand containing the computer, HP unit, transducers, solenoids, and thermocouple jack panel.	46
41. Blower, ac unit, thermal inertia box, orifice plate, and power supply.	49
42. Small cylindrical leading edge test section with slot taped.	51
43. Small cylindrical leading edge test section at low turbulence, no blowing.	52
44. Small cylindrical test section, small grid - far position.	55
45. Small cylindrical test section, small grid - near position.	56
46. Small cylindrical test section, large grid.	56
47. Large cylindrical test section, mock aero-combustor with spool.	57
48. Effects of blowing ratio on adiabatic effectiveness for the large cyl. at low Tu.	61
49. Effects of blowing ratio on adiabatic effectiveness for the large cyl. at small grid-near Tu.	61
50. Effects of blowing ratio on adiabatic effectiveness for the large cyl. at aero combustor Tu.	62
51. Effects of Reynolds number on adiabatic effectiveness for the large cyl. at low Tu.	64
52. Effects of Reynolds number on adiabatic effectiveness for the large cyl. at large grid Tu.	64
53. Effects of Reynolds number on adiabatic effectiveness for the large cyl. at aero combustor-spool Tu.	65
54. Effects of turbulence on adiabatic effectiveness for the large cyl. at $ReD=250k$ and $M=0.45$	66
55. Effects of turbulence on adiabatic effectiveness for the large cyl. at $ReD=250k$ and $M=0.80$	67
56. Effects of turbulence on adiabatic effectiveness for the large cyl. at $ReD=250k$ and $M=1.15$	67
57. Effects of turbulence on adiabatic effectiveness for the large cyl. at $ReD=500k$ and $M=0.46$	68
58. Effects of turbulence on adiabatic effectiveness for the large cyl. at $ReD=500k$ and $M=0.80$	68

59. Effects of blowing ratio on adiabatic effectiveness for the small cyl. at low Tu.....	70
60. Effects of blowing ratio on adiabatic effectiveness for the small cyl. at small grid-near Tu.	70
61. Effects of blowing ratio on adiabatic effectiveness for the small cyl. at aero combustor Tu.	71
62. Effects of Reynolds number on adiabatic effectiveness for the small cyl. at low Tu	72
63. Effects of Reynolds number on adiabatic effectiveness for the small cyl. at large grid Tu.....	73
64. Effects of Reynolds number on adiabatic effectiveness for the small cyl. at aero combustor Tu	73
65. Effects of turbulence on adiabatic effectiveness for the small cyl. at ReD=62.5k and M=0.46.	75
66. Effects of turbulence on adiabatic effectiveness for the small cyl. at ReD=62.5k and M=0.80.	75
67. Effects of turbulence on adiabatic effectiveness for the small cyl. at ReD=62.5k and M=1.12.	76
68. Effects of turbulence on adiabatic effectiveness for the small cyl. at ReD=125k and M=0.45.	76
69. Effects of turbulence on adiabatic effectiveness for the small cyl. at ReD=125k and M=0.80.	77
70. Comparison of test section adiabatic effectiveness at low ReD and M=0.46.....	78
71. Comparison of test section adiabatic effectiveness at high ReD and M=0.46.....	79
72. Comparison of test section adiabatic effectiveness at low ReD and M=0.80.....	79
73. Comparison of test section adiabatic effectiveness at high ReD and M=0.80.....	80
74. Effects of blowing ratio on Stanton number at low Tu and ReD=250k.	81
75. Effects of blowing on Stanton number at small grid-far Tu and ReD=250k.....	81
76. Effects of blowing on Stanton number at aero combustor Tu and ReD=250k.	82
77. Effects of ReD on Stanton number at low Tu.....	83

78. Effects of ReD on Stanton number at small grid-near Tu.	83
79. Effects of ReD on Stanton number at aero combustor-spool Tu.	84
80. Effects of turbulence intensity on Stanton number at ReD=250k and M=0.46.....	85
81. Effects of turbulence intensity on Stanton number at ReD=250k and M=0.80.....	86
82. Effects of turbulence intensity on Stanton number at ReD=250k and M=1.14.....	86
83. Effects of turbulence intensity on Stanton number at ReD=500k and M=0.46.....	87
84. Effects of turbulence intensity on Stanton number at ReD=500k and M=0.80.....	87
85. Effects of blowing ratio on Stanton number at low Tu and ReD=62.5k.	88
86. Effects of blowing ratio on Stanton number at small grid-far and ReD=62.5k.....	89
87. Effects of blowing ratio on Stanton number at aero combustor and ReD=62.5k.	89
88. Effects of ReD on Stanton number at low Tu.....	90
89. Effects of ReD on Stanton number at small grid-near Tu.	91
90. Effects of ReD on Stanton number at aero combustor Tu.	91
91. Effects of turbulence intensity on Stanton number at ReD=62.5k and M=0.46.....	93
92. Effects of turbulence intensity on Stanton number at ReD=62.5k and M=0.80.....	93
93. Effects of turbulence intensity on Stanton number at ReD=62.5k and M=1.12.....	94
94. Effects of turbulence intensity on Stanton number at ReD=125k and M=0.46.....	94
95. Effects of turbulence intensity on Stanton number at ReD=125k and M=0.80.....	95

LIST OF TABLES

Table	Page
1. Thermocouple location.	36
2. Heated and ambient data.	100
3. Change in temperature between heated and ambient conditions.	101
4. Average Stanton number for each row of thermocouples.	102
5. Effectiveness data for the large test section at low T_u	103
6. Effectiveness data for the large test section at small grid far T_u	104
7. Effectiveness data for the large test section at small grid near T_u	105
8. Effectiveness data for the large test section at large grid T_u	106
9. Effectiveness data for the large test section at aero-combustor T_u	107
10. Effectiveness data for the large test section at aero-combustor with spool T_u	108
11. Effectiveness data for the small test section at low T_u	109
12. Effectiveness data for the small test section at small grid far T_u	110
13. Effectiveness data for the small test section at small grid near T_u	111
14. Effectiveness data for the small test section at large grid T_u	112
15. Effectiveness data for the small test section at aero-combustor T_u	113
16. Effectiveness data for the small test section at aero-combustor with spool T_u	114
17. Stanton number data for the large test section at low T_u	115
18. Stanton number data for the large test section at small grid far T_u	116

19.	Stanton number data for the large test section at small grid near Tu.....	117
20.	Stanton number data for the large test section at large grid Tu.	118
21.	Stanton number data for the large test section at aero-combustor Tu.	119
22.	Stanton number data for the large test section at aero-combustor with spool Tu.....	120
23.	Stanton number data for the small test section at low Tu.	121
24.	Stanton number data for the small test section at small grid far Tu.	122
25.	Stanton number data for the small test section at small grid near Tu.	123
26.	Stanton number data for the small test section at large grid Tu.	124
27.	Stanton number data for the small test section at aero-combustor Tu.....	125
28.	Stanton number data for the small test section at aero-combustor with spool Tu.....	126

NOMENCLATURE

English Letter Symbols

D	diameter, m
h	convective heat transfer coefficient, $W/(m^2K)$
I	electrical current, amps
k	thermal conductivity, $W/m/K$
M	blowing ratio based on the slot exit area, $\rho_c U_c / \rho_\infty U_\infty$
Nu	Nusselt number; dimensionless number, ratio of convective heat transfer to conductive heat transfer, $Nu = \frac{hD}{k}$
P	pressure, Pa
Pr	Prandtl number; dimensionless number, ratio of viscous diffusion rate to thermal diffusion rate, $Pr = \frac{c_p \mu}{k}$
q"	heat flux, kJ per unit time per unit area
R	resistance; ohms, Ω
Re	Reynolds number; dimensionless number, ratio of inertial forces to viscous forces, $Re = \frac{\rho v D}{\mu}$
St	Stanton number; dimensionless number, ratio of heat transferred to a fluid over the thermal capacity of the fluid, $St = \frac{h}{c_p \rho U}$
T	Temperature, K
Tu	turbulence intensity, $Tu = u' /U_\infty$
U	velocity, m/s
x	streamwise hole spacing, m

z spanwise hole spacing, m

Greek Letter Symbols

Δ Delta, difference

η Eta; adiabatic effectiveness

μ Mu; absolute viscosity, Pa*s

ν Nu; kinematic viscosity, m²/s

ρ Rho; fluid density, mass per unit of volume, kg/m³

Subscripts

a refers to ambient conditions

ac refers to the air conditioner

atm refers to atmospheric conditions

aw adiabatic wall

brkt refers to the mounting bracket

c coolant

co coolant out

D diameter

corr corrected

ex refers to exit conditions

in refers to inlet conditions

orf refers to the orifice

out refers to outlet conditions

plen refers to the plenum

r recovery

s	refers to static conditions
sl	refers to slot conditions
surf	refers to the surface of the test cylinder
t	refers to total conditions
∞	evaluated in the free stream

ACKNOWLEDGEMENTS

This project could not have been completed without the assistance of many people. I would like to thank the University of North Dakota, specifically the Mechanical Engineering department for accepting me in the graduate program, and providing me with a valuable education. I would also like to thank Dr. Ames, my advisor, for giving me the opportunity to work on this project. His knowledge and assistance were invaluable and much appreciated. Thanks to my advisory committee, Dr. Nanak Grewal and Dr. Clement Tang. I would also like to thank the National Energy Technology Laboratory (NETL), the Department of Energy, and the University Turbine Systems Research (UTSR) program for providing the funding necessary for this project.

Many thanks to my fellow graduate students for their knowledge, advice, and assistance: Nafiz Chowdhury, Jon Long, Matt Mihelish, and Leo Moualeu. Special thanks to the two undergraduate assistants I had on this project: Joe Kingery and Jay Wagamon. I would also like to thank Gary Dubuque and Jay Evenstad. Their knowledge and experience with equipment and manufacturing processes was extremely valuable and much appreciated. Many thanks to Teri Salwey for her all of her help.

ABSTRACT

Modern turbine designers are greatly concerned with power out and the efficiency of their engines. One way to increase the power output and effectiveness of the engine is to increase the hot gas temperature inside the combustion chamber. The hot gas can reach a temperature that exceeds the physical limitations of parts inside the engine, causing the parts to fail prematurely. One possible method to cool the parts is with the use film cooling. Film cooling takes cool air from the compressor, bypasses the combustor, and ducts the air to internal chambers of parts, and then ejects the cool air onto the surface of the part. This provides both cooling and protection from deposition.

Due to the large number of turbine engines in service today, it is impossible to know what the perfect film cooling package is. Different turbines have different inlet conditions, burn at different temperatures, have different turbulence intensities in the flow, and require different amount of cooling. Research has been done in the past to determine some of the parameters that affect film cooling performance. The purpose of this research was to determine the effects of turbulence, Reynolds number, and blowing ratio on the adiabatic effectiveness of film cooling and the downstream heat transfer. This research utilized the large scale, low speed cascade wind tunnel facility at the University of North Dakota. The effectiveness of two different cylindrical leading edge test surfaces was investigated.

For this project, a unique pin fin array was developed and integrated in the two cylindrical leading edge test sections. The test sections were designed, fabricated, and

instrumented to be able to acquire temperature measurements and pressure measurements at different locations along the test surface. A way to produce and deliver coolant air was designed, fabricated, and instrumented. Data was acquired for each of the cylinders at the different test conditions. The turbulence intensities were acquired by another student.

In the future, additional data will be taken with the cylindrical test sections. Temperature data while film cooling will be measured via infrared camera. Shaped coolant ejection holes are being designed and will be tested. A leading edge with deposition will also be tested. All of the future data will be compared to this baseline data. Hopefully, the data from this research will be used by turbine designers to better understand the effects on film cooling, and produce a better, more efficient engine.

CHAPTER I

INTRODUCTION

Efficiency and power output are primary concerns for today's industrial gas turbine manufacturers. One of the earliest gas turbine engines had an inlet temperature of 1040°F and an estimated thermal efficiency of just 3% [1]. Modern gas turbine engines can have temperatures in excess of 2600°F with thermal efficiencies over 40%. One proven way to increase efficiency and the power output of a gas turbine engine is to increase the combustion gas temperature. Such high temperatures exceed the physical properties of the materials used. This can cause oxidation, low cycle fatigue and premature failure. Designers have implemented a few ways to counteract the harmful effects of the increased temperatures, including the addition of a thermal barrier coating (TBC) and film cooling.

A TBC is a thin layer of ceramic applied over a part that is exposed to the increased temperature. The TBC utilizes the low thermal conductivity of the ceramic, insulating the metal part. Film cooling in a gas turbine engine is a process of cooling a part that is exposed to the high temperatures by taking cool air from the compressor and bypassing the combustor. The cool air is then ducted to internal chambers of a blade or vane, where it is then discharged through openings on the blade or vane surface in a full coverage film. Film cooling has multiple benefits. The cool air not only provides internal cooling to the part, but the film that is discharged provides a protective layer of cool air. This film inhibits the hot gas of the combustion chamber from melting the part

and also prevents deposition of contaminants on the surface of the part, see Figure 1. These contaminants, if left unchecked, can build up overtime, reducing the aerodynamic efficiency and creating “hot spots” on the surface, which can also lead to premature failure. This build up can be seen in Figure 2.



Figure 1. Turbine Vane with film cooling [2].



Figure 2. Turbine vane without film cooling [2].

There are three different attached flow regimes: laminar, transitional, and turbulent. Laminar flow is characterized by steady, uniform flow. Turbulent flow is characterized by randomness or having changing properties in magnitude and direction. Some properties that can be affected are: momentum, pressure, velocity, and diffusion. Transitional flow occurs when the flow changes from laminar to turbulent, or turbulent to laminar. Laminar flow will push the film of cool air onto the part that is being cooled, helping to provide good protection. However, any disturbance in the flow field upstream or on the surface of the part can cause the flow to transition. This transition can mix away the film cooling and the protection provided. The purpose of this project is to investigate the effects of turbulence on slot film cooling effectiveness and downstream heat transfer. A depiction of boundary layer development can be seen in Figure 3.

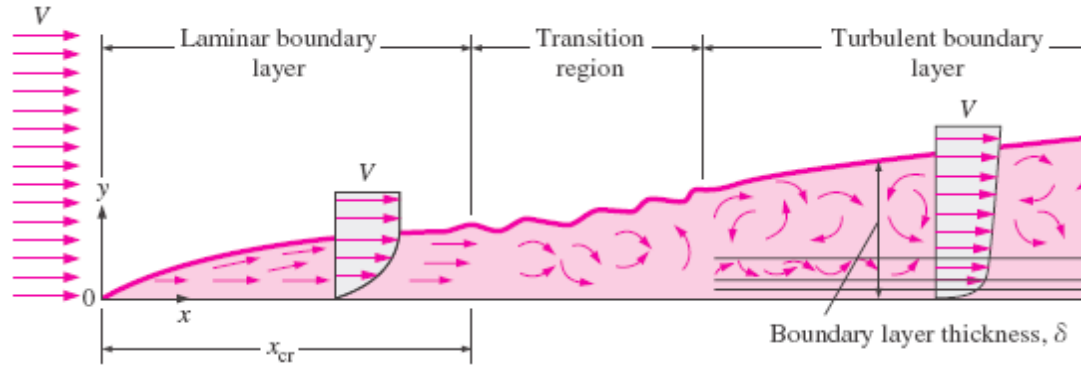


Figure 3. Boundary layer development over a flat plate [3].

Film cooling also has three different flow regimes: mass addition, mixing, and penetration. In the mass addition regime, film cooling effectiveness is increased due to the addition of coolant on the surface and an increase in thermal capacity. The mixing regime has some benefits of the mass addition as well as added mixing of the coolant with the freestream. The penetration regime is characterized by excessive coolant addition to a point where the coolant penetrates into the freestream. This flow regime sees mostly turbulent mixing of the coolant and the freestream flow [4].

CHAPTER II

LITERATURE REVIEW

There are many different research papers on the topic of film cooling. This chapter will focus on the basics of slot cooling, discrete and shaped hole film cooling, as well as turbulence effects.

Slot Film Cooling

The ideal film cooling profile comes from a two dimensional continuous slot with a uniformly distributed cooling supply [5]. Continuous slot film cooling is unpractical from the standpoint of loss of structural integrity due to having the slot. Also, continuous slots provide a low resistance to coolant flow, which would make it difficult to control coolant flow rates [6]. Common applications for slot fed film cooling are: end wall interfaces, combustor liner walls, and airfoil trailing edge regions. A tradeoff occurs between keeping the trailing edge thin to increase aerodynamic performance, and thickening up the trailing edge to allow for sufficient cooling. Bunker [5] offers two different ways of cooling the trailing edge: have film cooling on both the pressure and suction sides of the airfoil, and have a slot fed film cooling that is made by cutting back some material on the pressure side. He also suggests that using mesh-fed slot film cooling can increase the film effectiveness by as much as 100% over shaped holes in the downstream region. The mesh is a network of pedestals between the walls of the airfoil that aids in cooling and also increases the structural integrity of the airfoil. Figure 4 shows a diagram of the test setup used by Bunker.

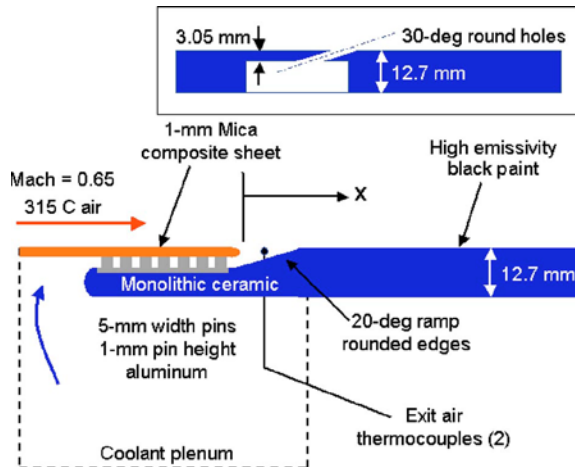


Figure 4. Schematic of test surface from Bunker.

Bruce-Black et al. [6] investigated different geometries for slot fed film cooling. They varied such parameters as slot depth, width, length of slot to the ejection surface, as well as continuous or discrete slots. Their research showed that adiabatic effectiveness was increased by decreasing the width of the film cooling slots. An internal cooling package was also implemented that was able to maintain the cooling performance levels while potentially increasing the structural integrity of the airfoil. Figure 5 shows some different parameters that can be altered to change the effectiveness of film cooling.

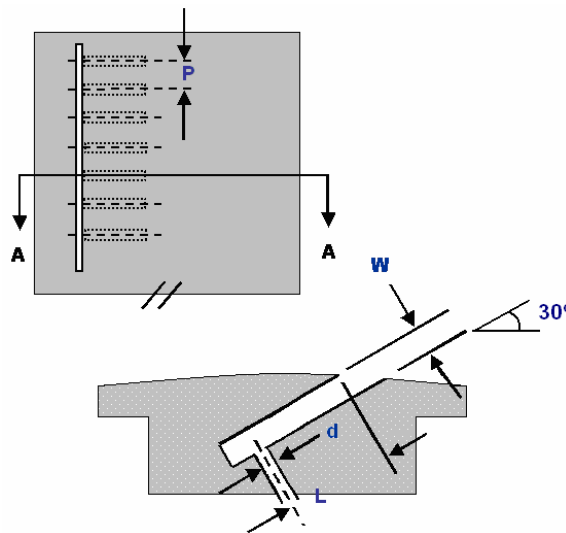


Figure 5. Slot parameters investigated by Bruce-Black et al.

The ejection angle also has an effect on film cooling. Smith et al. [7] set up an experiment that compared normal film cooling slots and 30° angled slots at similar blowing ratios. At similar ratios, the angled slot effectiveness was much higher than the normal holes due to the mixing out of the film, as well as the slot geometry. They also noticed that increasing the blowing ratio did not increase the effectiveness with the normal slot as it did with the angled slot. They attributed the lack of increase in effectiveness to the coolant being ejected farther into the free stream, bypassing the surface entirely. Brauckmann and Wolfersdorf [8] obtained similar results with rows of shaped holes at different injection angles.

Knost and Thole [9] suggest that an interface slot between the combustor and turbine could be used as a source for slot film cooling. This combustor-turbine interface slot is in most turbines, and cooler gases already leak through. They suggest that this slot could be designed to provide a film cooling source for the end wall.

Discrete Hole and Shaped Hole Film Cooling

A more popular method of film cooling is to use discrete holes or shaped holes. Due to the high heat load, these holes are often used on the leading edge and stagnation region of blades or vanes, although cooling holes are commonly used elsewhere. Figure 6 shows a typical film cooled blade utilizing both discrete holes and slot film cooling on the trailing edge.

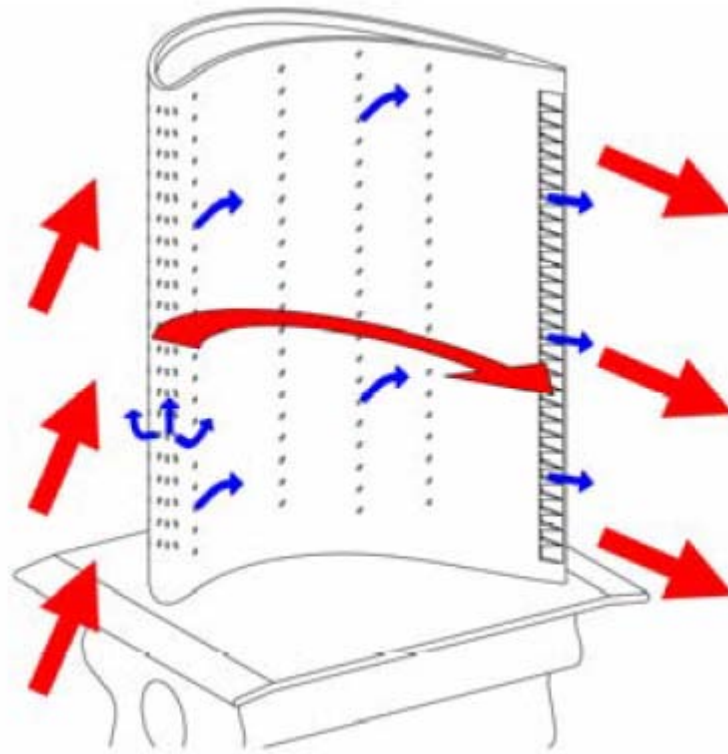


Figure 6. Typical film-cooling blade design [10].

Some modern film cooling applications use shaped holes instead of discrete holes. The shaped holes have a few benefits versus discrete holes, but there are trade-offs. The shaped holes can be used to improve the cooling performance, as well as reduce the cooling air flow required. The down side is that many times, shaped holes require complex hole geometry that can greatly increase the difficulty in manufacturing, and as a result, increase costs. Costs for fan shaped holes can be around four to eight times more expensive, depending on the technique [11]. Often, multiple discrete holes are used in rows to achieve a full coverage cooling film. It has been determined that staggered film cooling holes perform better than film cooling holes that have an inline arrangement. This performance increase is due to an increased area covered by the cooling film, and a lower penetration of the cooling film into the free stream [12]. The lower penetration

keeps the jet attached to the surface. A decrease in effectiveness is observed if the distance between the film cooling rows is increased.

Dittmar, Schulz, and Witting [13] investigated the effectiveness of different film cooling hole configurations using both discrete holes and shaped holes, and a double row of cylindrical holes. They determined that all configurations showed similar effectiveness values at low blowing ratios, and that the shaped holes outperformed the cylindrical holes for both medium and high blowing ratios. A schematic of the holes used can be seen in Figure 7. It is believed that the effectiveness is decreased for the cylindrical holes due to the separation of the coolant jet from the test surface. However, the double row of cylindrical holes showed the best effectiveness downstream at high blowing ratios. Mhetras et al [10] investigated film cooling effectiveness and the effect of flow parameter variations. They concluded that effectiveness magnitudes were largely unaffected by variations in blowing ratios for the suction surface of a blade, and that the suction side effectiveness is comparable to the pressure side effectiveness even when the suction side has fewer film cooling rows.

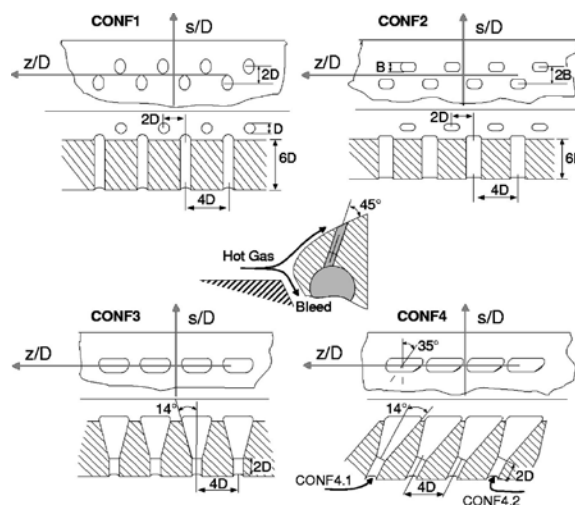


Figure 7. Schematic of holes used in [13].

Ligrani, Goodro, Fox, and Moon [14] also investigated film cooling effectiveness at different blowing ratios and with both sparsely and densely packed hole arrays. They found that there was only a slight increase in effectiveness when the blowing ratio was increased from 2.0 to 5.0 and no significant change in effectiveness when the blowing ratio was changed from 5.0 to 10.0. However, increasing the blowing ratio for the sparsely packed hole array increased the effectiveness as well. Ligrani et al attribute the insensitivity of the densely packed hole array to changes in blowing ratio to an overcooled flow, which can be found in situations where the simplicity of the design is dictated by cost constraints. This overcooling prevents the mainstream flow from interacting with the test surface. A sample hole array used in [14] can be found in Figure 8. Nasir et al [15] performed similar research and obtained similar results. They witnessed an increase in effectiveness with increasing blowing ratio up to a certain point, and then the coolant jet lifted off the test surface, proving ineffective.

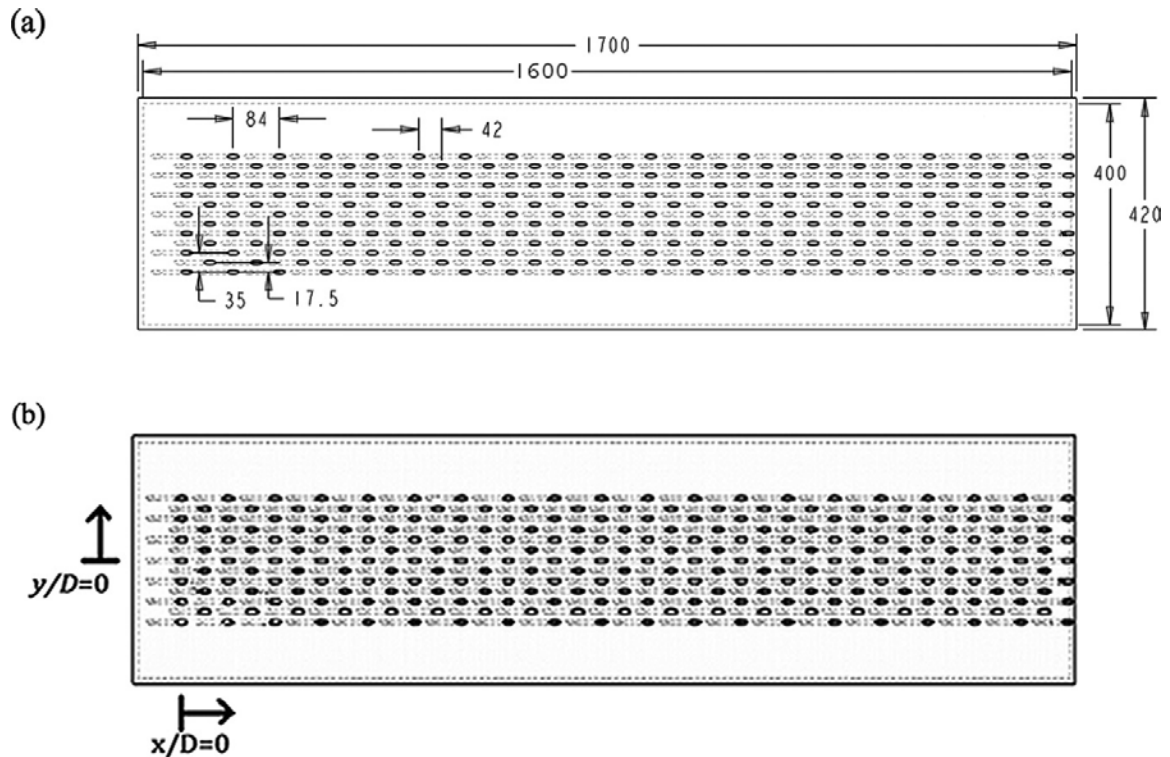


Figure 8. Hole layout for Ligrani et al. [14].

Effects of Turbulence

Turbulence intensities vary within the combustor of a turbine engine, due to the large variety of engines and operating conditions. The highest area of turbulence intensities occurs at the combustor exit, by the near wall regions. Turbulence intensities here can reach up to 20%. Turbulence intensities in the core flow range from around 7-15% [16, 17, 18, 19, and 23]. Research on the effects of turbulence on film cooled turbine blades has been done in the past. Turbulence was found to reduce the effectiveness of the film cooling, while at the same time, increasing the heat transfer coefficient [21, 22, 23, and 24].

Ligrani et al [14] also studied the effects of mainstream acceleration on film cooling hole arrays. Effectiveness changes significantly with the presence of acceleration for the sparsely packed array, but remains largely ineffective on the densely packed array.

This is also attributed to the amount of excess coolant in the mainstream flow. Saumweber and Schulz investigated turbulence on cylindrical and fan shaped cooling holes [25]. They found that higher turbulence intensity and Mach numbers increase the cooling performance of the cylindrical holes, but are detrimental to the fan shaped holes. Wright et al. found that increased turbulence intensity spreads the film cooling jet over a larger area [26]. Mayhew et al. [20] found that turbulence increases the adiabatic effectiveness at high blowing rates and decreases the adiabatic effectiveness at low blowing rates. They also determined that there is only one vortex behind the film cooling hole for high free stream turbulence, while there are two asymmetric counter-rotating vortices for the low free stream turbulence case.

Bons et al. [27] investigated the effect of freestream turbulence on the adiabatic effectiveness of a row of film cooling holes. Multiple levels of turbulence intensity, up to 17.4% were used. They found that for higher levels of freestream turbulence, the adiabatic effectiveness directly behind the injection hole is decreased by as much as seventy percent. However, they also noticed an increase in the film cooling effectiveness between the holes. This increase is thought to have been the result of increased diffusion of the film cooling jets in the spanwise direction (between the holes).

Mayhew et al. [28 and 29] also investigated the effects of freestream turbulence on film cooling effectiveness and heat transfer. For their experiment, they used different turbulence intensities in flow over a flat plate with straight film cooling holes and three blowing ratios. They found that at a low blowing ratio, any type of turbulence decreases the effectiveness of the film cooling jet, due to the increased mixing with the freestream. At the high blowing ratio, however, high freestream turbulence seemed to have increased

the effectiveness. This was because the film cooling jet at the high blowing ratio and low turbulence intensity had lifted off the flat plate, and was blowing into the freestream. With the increased turbulence intensity, some of the coolant that penetrated into the freestream was forced back onto the flat plate, increasing the effectiveness. They also investigated the heat transfer with the same experimental setup. Mayhew et al. found that any increase in turbulence intensity produced an increase in heat transfer.

Freestream turbulence also has an effect on the boundary layer development. Dees et al. [30] conducted research on the momentum and thermal boundary layer development. They discuss how many different parameters affect the development of the boundary layer including: curvature, pressure gradients, and freestream turbulence. They tested a scaled C3X vane in a closed loop with tunnel, with the desired outcome of simulating the flow conditions of a real engine. When the freestream turbulence intensity was increased from 0.5% to 20%, the thermal boundary layer was found to be two to four times thicker. Turbulence also increases the growth rate of the boundary layer. High turbulence intensities show increased growth rates over the more modest growth rates of laminar or transitional boundary layers. This thicker boundary layer can have a negative effect on the adiabatic effectiveness. A thicker boundary layer would not push the film cooling air down onto the surface, reducing the effectiveness.

A similar experiment was performed by Simon [31]. He developed a new way to model the effects turbulence and blowing on a slot fed film cooling. His model was able to predict efficiency with twenty percent accuracy. He also noted an increase in effectiveness at higher blowing ratios and a decrease in effectiveness at increased turbulence intensities.

CHAPTER III

EXPERIMENTAL APPROACH

This chapter provides an in depth description of the test facility at UND and the experimental procedure used to acquire temperature and pressure data. The data were obtained using a large scale turbine vane cascade wind tunnel. Two leading edge cylinders were developed, each with constant radius stagnation regions and accelerating flow downstream. Six different turbulence conditions were generated using a combination of two separate nozzles and two different sized grids. Two different Reynolds numbers based on the cylinder leading edge and the far field approach flow velocity were investigated. The large cylindrical leading edge test section was used to investigate Reynolds numbers of 250,000 and 500,000, while the small cylindrical test section was used to investigate Reynolds numbers of 62,500 and 125,000. Four different blowing ratios were used in this experiment: 0.45, 0.8, 1.15, and 1.6.

Turbine Vane Cascade Wind Tunnel

The University of North Dakota has a unique large scale turbine vane cascade wind tunnel that can be seen in Figure 9. It is comprised of many different components, including: a filter box, a large centrifugal blower, a series of diffusers, an air-water heat exchanger, a screen flow conditioning section, interchangeable nozzles, and then the test section which houses the cylinder and instrumentation.

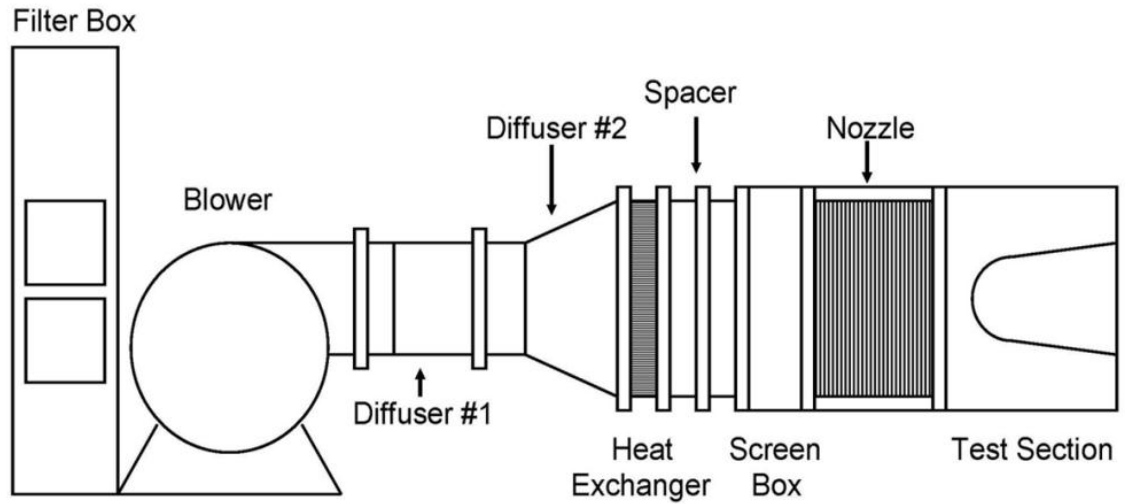


Figure 9. UND's large scale turbine vane cascade wind tunnel with large cylinder test section [2].

Air is drawn into the blower through a large plenum that houses eight filters. Each filter has a filtering efficiency of about 95%. The air is filtered to try to prevent particle deposition on the test cylinder and instrumentation, and as a result, give erroneous data readings. The air is then drawn by a large centrifugal blower. The blower is manufactured by New York Blower, and is model AF-Forty size 274 and can be seen in Figure 10. It is capable of moving $6.6 \text{ m}^3/\text{s}$ of air at a static pressure rise of 5000Pa. Powering the blower is a 45kW induction motor. The motor speed is controlled by a variable frequency drive. This allows the velocity to be fine tuned in order to achieve the desired Reynolds number.



Figure 10. Blower used by UND.

The drawn air from the blower is then discharged into two multi-vane diffusers. The diffusers are utilized to increase the flow area, first in the x-direction, then in the z-direction, decreasing the velocity of the air, thereby recovering some static pressure. The diffusers increased the flow area from 41.91 cm x 61.60 cm (2581.66 cm²) to 91.44 cm x 127 cm (11,612.88 cm²) in two stages [32].

Air then leaves the diffusers and then passes through an air-to-water heat exchanger. This heat exchanger allows for better control of the free stream temperature. Cool water is piped into a 100 gallon storage tank. The water is then circulated through the heating exchanger using a one half horsepower Jacuzzi centrifugal pump. The heat from the air is transferred to the water, which is then returned to the storage tank. Additional cold water is added as needed to maintain the water at the desired temperature. The overflow water is piped directly to a floor drain. Figure 11 is of a schematic of the heat exchanger while Figure 12 is a picture of the system installed.

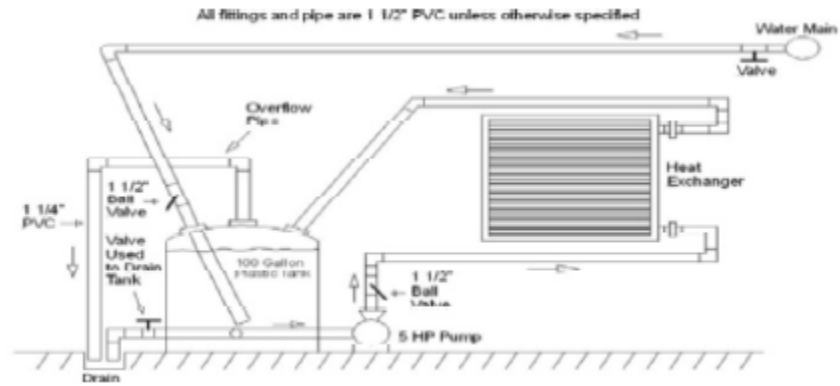


Figure 11. Heat Exchanger schematic [33].



Figure 12. External view of heat exchanger, pump, and tank [33].

After the heat exchanger, the air flows through a flow conditioning section. This section contains four small nylon mesh screens that are spaced at 5 cm (2 in) apart. The screens help to promote uniformity in the flow and reduce variations in the velocity. The screen mesh can be seen in Figure 13.



Figure 13. Flow conditioning section.

Attached to the flow conditioning section is either a nozzle or a mock aero combustor. Both served two purposes. First, they changed the flow area from the 91.44 cm x 127.00 cm inlet to 25.40 cm x 127.00 cm outlet that is required for the test section. Second, they helped to determine the turbulence intensity of the flow. Figure 14 shows the exit of the mock aero-combustor and laminar flow nozzle. Figure 15 shows the internal layout of both the laminar flow nozzle and the mock aero-combustor.



Figure 14. Mock aero-combustor and laminar flow nozzle, front view.

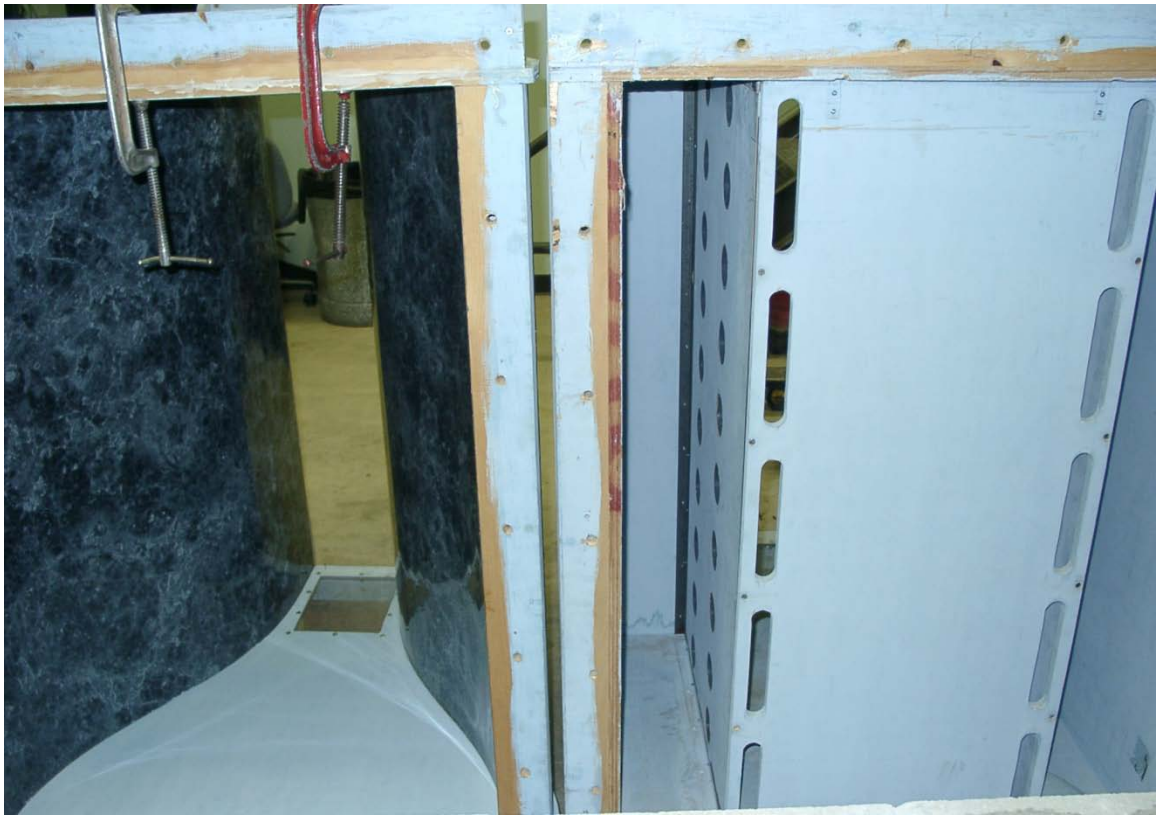


Figure 15. Laminar flow nozzle and mock aero-combustor, rear view.

The nozzle produces a very low turbulence intensity level of approximately 0.7%. The mock aero-combustor section was developed to mimic combustors used in gas turbine engines today [33]. It produces a large scale, high intensity turbulence intensity of approximately 14%. This is accomplished by having flow pass through a back panel as well as two side panels. The back panel has a series of five slots in each of two rows. The rows are spaced 45.7 cm from centerline to centerline and the centerline of each slot is located 3.81 cm in from the edge of the back panel. Each slot has a width of 3.175 cm and is 20.32 cm long and there is a spacing of 6.1 cm between each slot. The side panels consist of two rows, each with ten 6.35 cm ID holes spaced 12.7 cm apart. The first row of holes is 25.4 cm from the edge of the wall, while the second row is in line from the first and is 50.8 cm from the edge of the wall.. Each hole has a 0.55 cm wall thickness tube attached that extends 6.35 cm into the mock aero combustor. The tube is thought to better direct the airflow. Using large c-clamps, either the spool or the test section was attached to one of the nozzles. A schematic of the mock combustor can be seen in Figure 16.

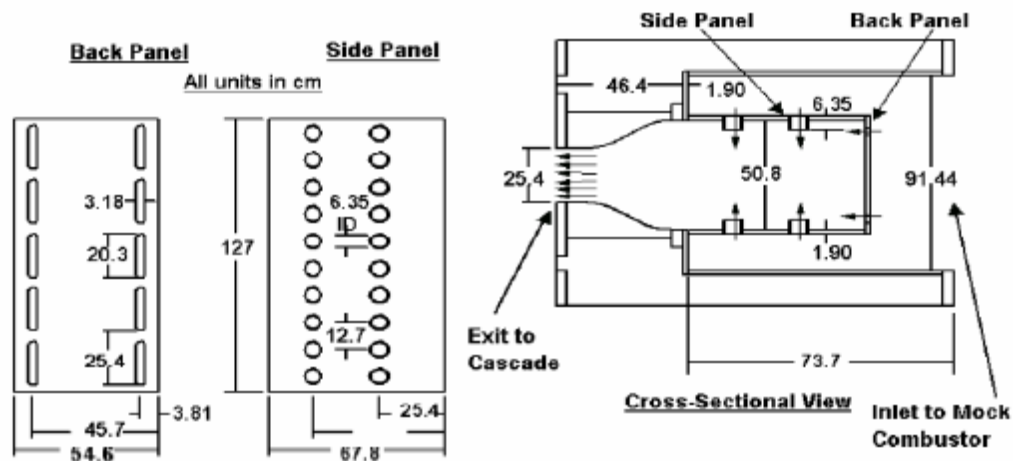


Figure 16. Schematic of the mock aero-combustor.

An acrylic rectangular spool section can be attached after the nozzle or mock aero combustor. The spool serves as a way to change the turbulence intensity of the flow. It can be used on its own, or it can hold a turbulence generating grid in several different places. This experiment used a small grid and a large grid. The small grid was constructed of 0.635 cm square aluminum bar stock arranged in a grid with a spacing of 3.175 cm. The small grid was used at two different locations: ten grid lengths and thirty two grid lengths, or 31.75 cm and 101.6 cm from the cylinder leading edge respectively. The small grid in the near position produces a turbulence intensity of approximately 9.2% while the small grid in the far position produces a turbulence intensity of approximately 3.1%. A large grid was also used in this experiment. The large grid was constructed of 1.27 cm square aluminum bar stock and arranged in a grid with a spacing of 6.35 cm. The large grid was used at a single location: ten grid lengths, or 63.5 cm from the cylinder leading edge. The large grid produces a turbulence intensity of approximately 8.5%. The mock aero-combustor when used with the spool alone produces a turbulence intensity of approximately 9.5%. The large grid turbulence generator and aero-combustor have been extensively studied by [35, 36, and 37]. A schematic of the grid used can be seen in Figure 17.

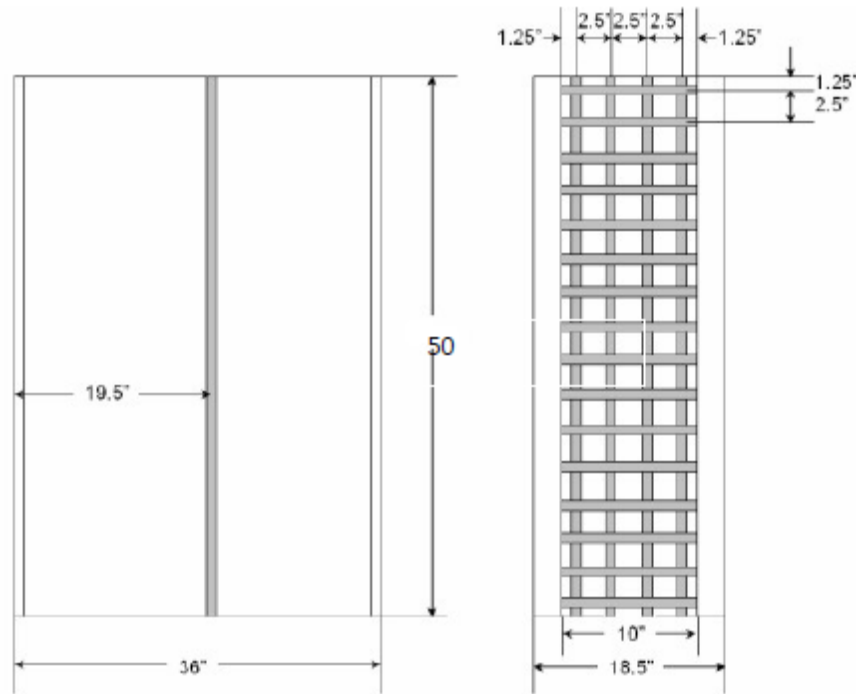


Figure 17. Grid schematic [38].

The test section was made of 1.91 cm (0.75 in) thick acrylic sheets, and housed either of the test cylinders. Holes were drilled in the side of the test section to allow for the coolant air, as well as: total pressure probes, thermocouples for measuring the free stream temperature, and exit static pressure probes.

Design and Fabrication of the Cylindrical Test Sections

The large cylindrical leading edge test section was designed with a 40.64 cm (16 in) leading edge and an after body that provided continued acceleration. The body of the test surface was designed by incrementally increasing the diameter of the leading edge. The velocity around the large section is larger than the small section, but tapers off at the end, whereas the small section continually increases in velocity as the flow travels along the test section. This shape has been used in past experiments at UND and can be seen in Figure 18. Figure 19 displays the velocity profiles of both test sections. Both cylinders

were designed in English units, but both metric and English units will be given for clarity. The slot location for the large cylindrical leading edge was at a surface distance of 12.3 cm (4.83 in) while the slot location for the small cylindrical leading edge was at a surface distance of 10.3 cm (4.05 in).

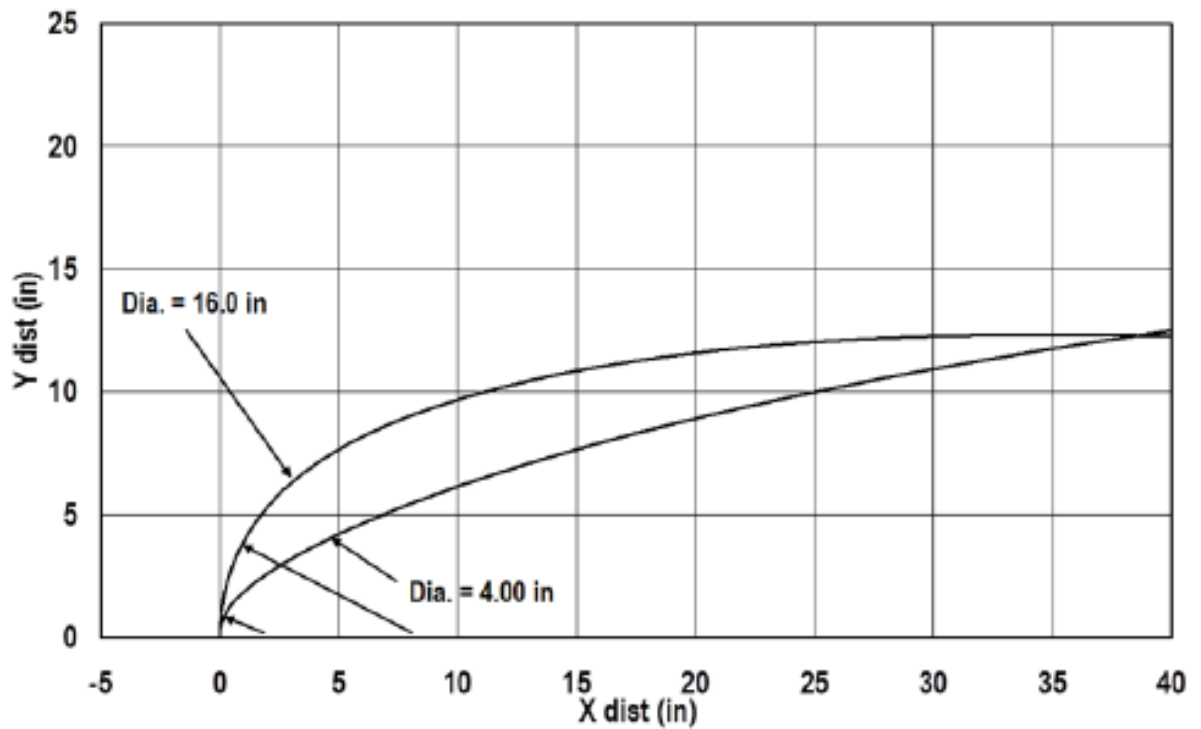


Figure 18. Leading edge profiles [2].

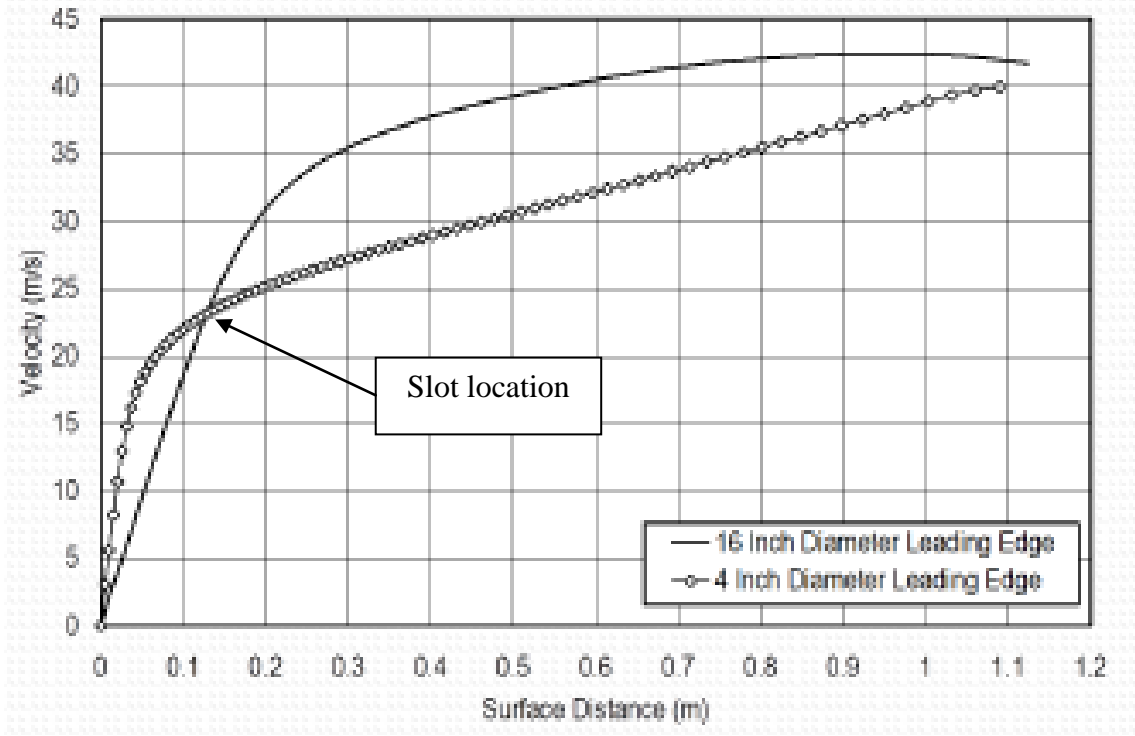


Figure 19. Big and small cylinder acceleration profiles [2].

FLUENT

The entire test section profile with the ejection slot was tested in FLUENT for both the big and small cylindrical test section. Figure 20 and Figure 21 display the static pressure contours around each test section. While Figure 22 and Figure 23 show the contours of static temperature coming from and downstream of the ejection slot. For clarity, the FLUENT model was made using warmer air coming out of the ejection slot than the free stream air, when in reality, the ejection slot would have cooler air. The model also shows some effects of the end walls on the ejection flow. The results shown are only for one blowing ratio condition, one Reynolds number, and one turbulence intensity. The results from the FLUENT simulation allowed a close estimation of what could be expected from the experiment.



Figure 20. Static pressure contours around the big cylindrical test section from FLUENT.

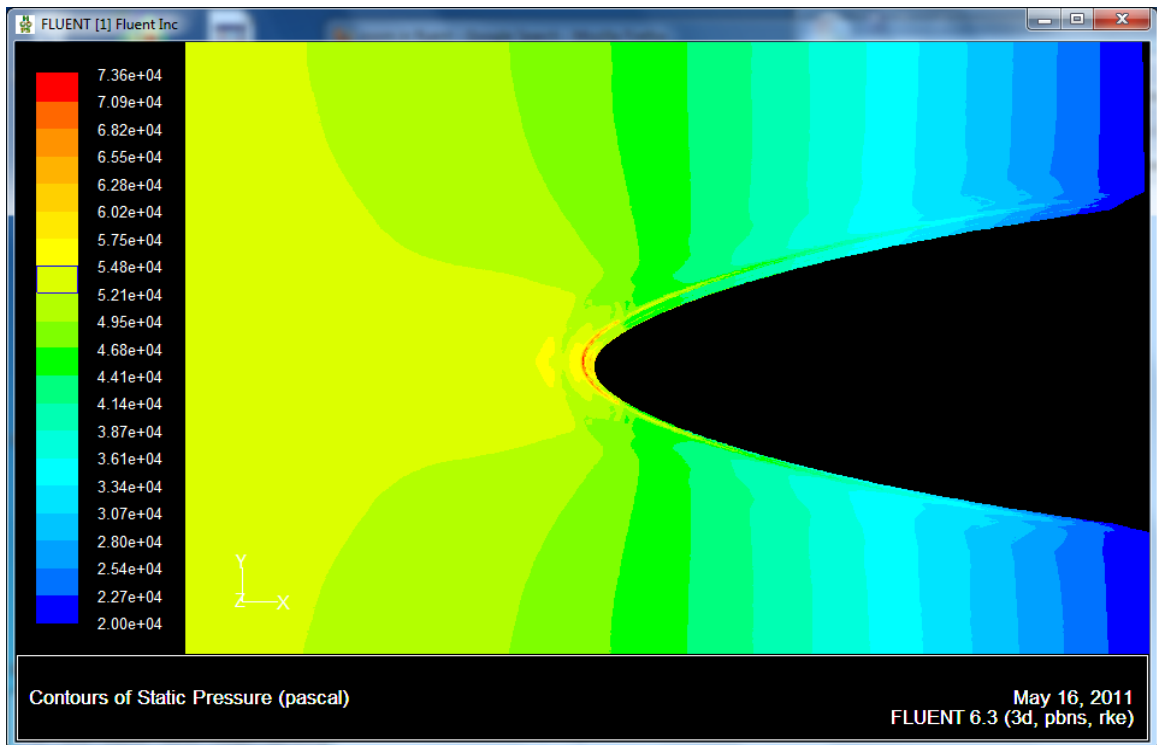


Figure 21. Static pressure contours around the small cylindrical test section from FLUENT.

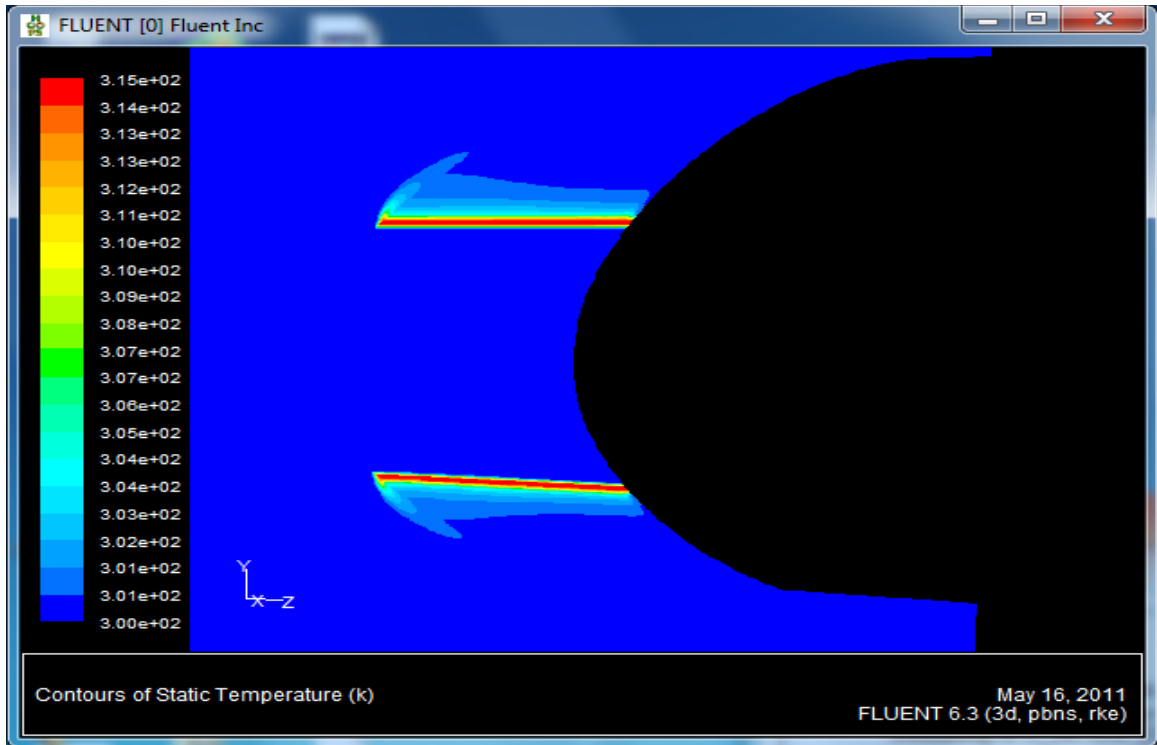


Figure 22. Static temperature contours around the big cylindrical test section from FLUENT.

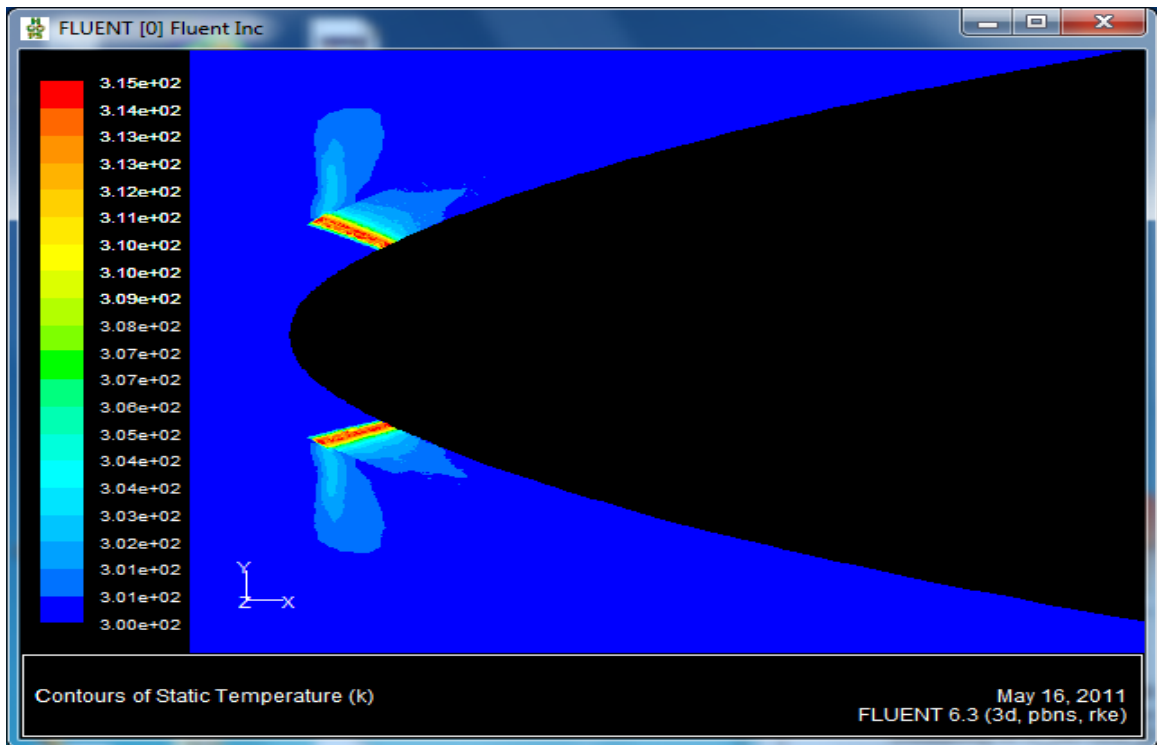


Figure 23. Static temperature contours around the small cylindrical test section from FLUENT.

Pro/Engineer (Pro/E)

The leading edge was designed using the solid modeling software, Pro/E. The objective was to make a leading edge with complex internal cooling features, such as double wall construction with a pin fin array and a 30° ejection slot. The pin fin array used in this experiment was modeled after an array used in [39]. Air would be injected into the side of the leading edge, where it would fill a hollow space. The air would then travel between the double walls and around the pedestals of the pin fin array. Both walls were 0.84 cm (0.33 in) thick. Each pin was 1.68 cm (0.66 in) in diameter, 1.27 cm (0.5 in) tall and spaced 2.725 cm (1.073 in) apart, center to center, in the span-wise direction, with nine pedestals in each row. There were three rows of pins in the bottom section of the leading edge, and three rows in the top section, for a total of six rows of pins. The rows in each section are staggered and spaced 1.801 cm (0.709 in) apart, center to center. After the pin fin array, the air would discharge out of a slot that was at an angle of 30° from the surface. The area of the ejection slot was 0.363 cm (0.143 in) by 21.679 cm (8.535 in). A gap of 2.11 cm (0.83 in) was left before the first row of pins and the entrance, and after the last row of pins before the ejection slot. Figure 24 is a screenshot from Pro/E that shows the pin fin array layout and dimensions.

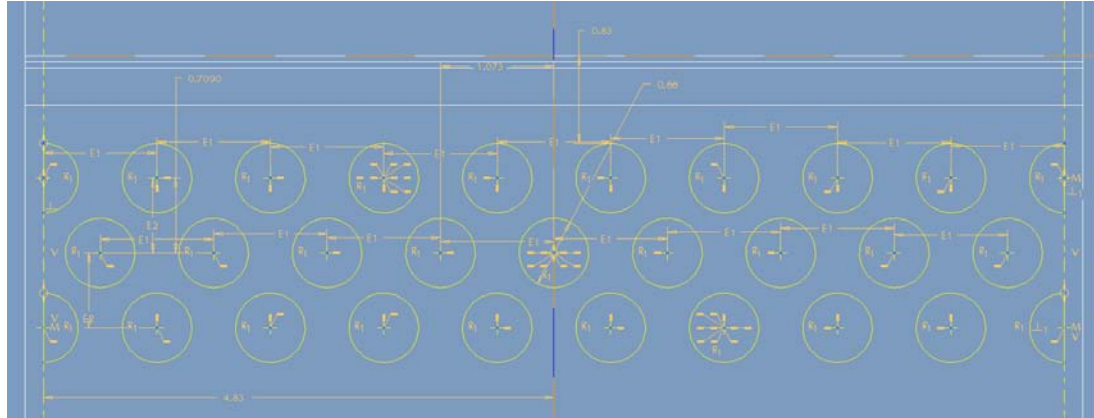


Figure 24. Pin layout and dimensions for the large cylindrical test section leading edge from Pro/E.

Three type-k thermocouples were installed in the flow field of the ejection slot in order to correctly record the ejection slot temperature. The thermocouples were located at the midspan of the leading edge and \pm two inches from the midspan. The thermocouple unions were half way between the walls of the ejection slot to ensure an accurate temperature of the flow and not the temperature of the walls. Each thermocouple was held in place by using a strong two part epoxy. Two static pressure taps were also installed in the ejection slot, located \pm one inch from the midspan. Special care was made when installing the static pressure taps to ensure they were not interfering with the flow. The design was supposed to mimic a pin fin array inside of a real vane, as well as, provide some turbulence in the ejection flow to aid in heat transfer. Figure 25 shows a wireframe Pro/E screenshot of the large cylindrical leading edge.

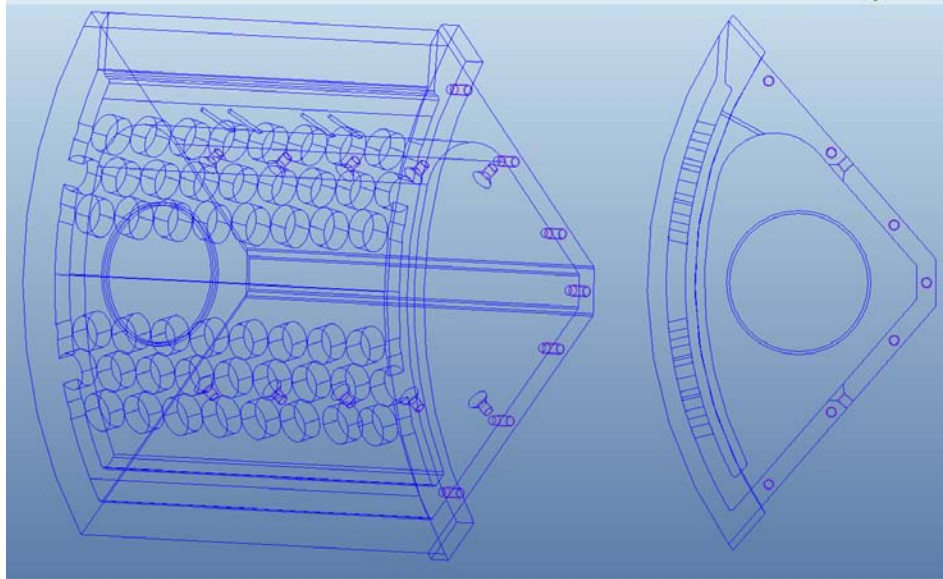


Figure 25. Pro/E wireframes of the large cylindrical test section leading edge.

The small cylindrical test section was designed to have a 10.16 cm (4.00 in) leading edge. The shape and body of the test section was designed in the same way as the large cylindrical leading edge test section, by incrementally increasing the radius after thirty degrees along the leading edge. The after body that provided continued acceleration. Once again, Pro/E was used to design the small cylindrical leading edge test surface. It had much of the same geometries that the large cylindrical leading test surface had. The main difference was the smaller size, which made the design more difficult. The small size prevented the use of six rows of pins in the internal pin fin array. Only four rows of pins could be used, two rows on the top section and two rows on the bottom section. It was also difficult to design a route for the instrumentation of static pressure taps and thermocouples due to interference between parts. The ejection slot was also slightly different at 0.373 cm (0.147 in) by 21.747 cm (8.562 in). A wireframe view of the small cylindrical leading edge can be seen in Figure 26. For both cylindrical sections, the ejection slot was designed to fit the overall cylindrical test section profile.

This design feature helped to minimize any turbulence generated by the test section due to parts disrupting the flow around the test section.

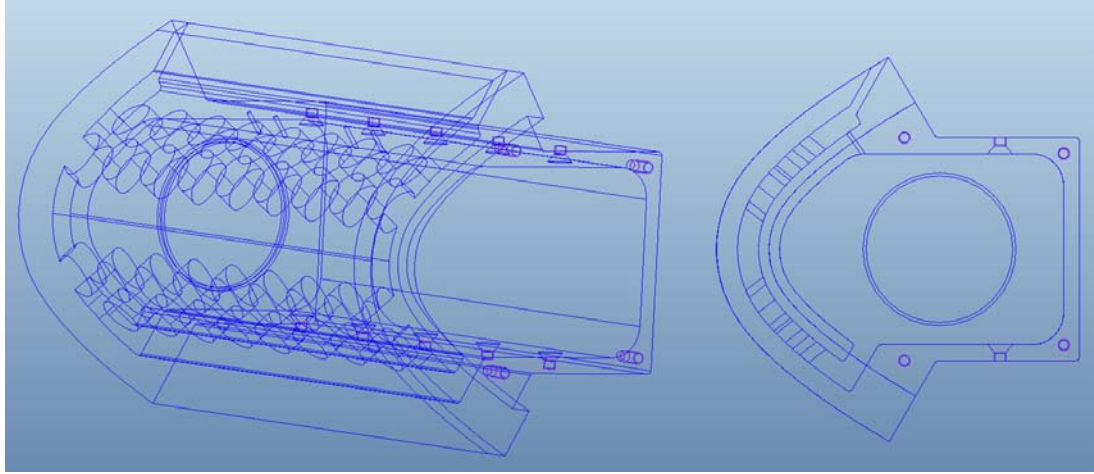


Figure 26. Pro/E wireframes of the small cylinder leading edge.

Mounting Bracket

The leading edge was designed to be removable, which meant that a permanent mounting bracket needed to be designed. The mounting bracket was designed to fit inside of the cylindrical test section with tabs that would be part of the cylindrical test surface. These tabs would provide a surface to begin when attaching the epoxy board, as well as, provide a good place to install instrumentation. Three type-k thermocouples would be installed in addition to two static pressure taps. The thermocouples were located at the midspan of leading edge and \pm two inches from the midspan, and were held in place using OmegaBond 101, a high thermal conductivity epoxy. The thermocouples were embedded in the surface of the mounting bracket, out of the flow field. The epoxy had a thermal conductivity of 1.038 W/(m*K). This allowed for adequate heat transfer between the flow and the thermocouple. The pressure taps were located \pm one inch from the midspan. Special attention was given to ensure the static pressure probes were not infringing on the flow. A groove was designed into the mounting bracket for the Inconel

foil bus bar to rest in. This groove would allow the bus bar to not obstruct the flow around the test section, possibly producing bad data. The instrumentation was the same for the large cylindrical leading edge test section. Figures 27 and 28 are of the mounting brackets for the large leading edge test section and small leading edge test section respectively.

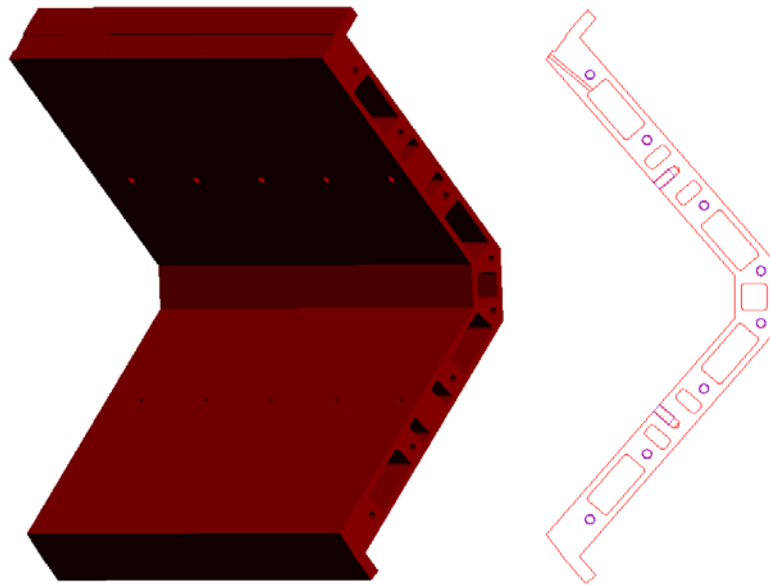


Figure 27. Pro/E model of big cylindrical leading edge mounting bracket.

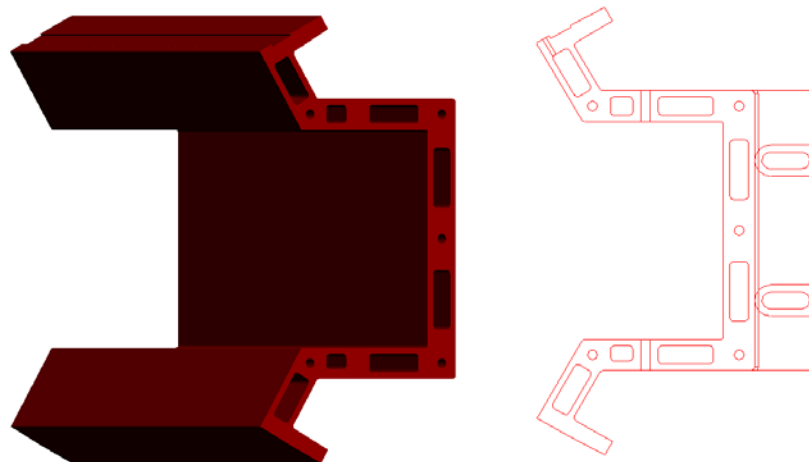


Figure 28. Pro/E model of small cylindrical leading edge mounting bracket.

Due to the complex geometry of the leading edge and the mounting bracket, both parts were made using UND's rapid prototype machine. The machine is a Dimension SST 1200es 3-D printer and can be seen in Figure 29. The parts were made by pulling plastic from a spool, melting it in the writing tool, and drawing the part one line at a time. Both leading edges were made solid because there would be forces acting on them during data acquisition. However, in an effort to save material, some sections of the mounting bracket were removed. Each line is .254 mm (0.010 in) thick. This process of manufacturing left small ridges or lines on the surface of the part, where the writing head deposited material. This experiment required the surfaces that were in the flow field to be smooth to prevent any disturbances to the flow. So the leading edge of both cylindrical test sections, and the tabs on both mounting brackets were lightly sanded to remove the ridges. After the parts were sanded, each part was polished using a polishing wheel. Figure 30 shows the small cylindrical leading edge and mounting bracket after being sanded and polished.



Figure 29. Dimension 1200es 3-D printer at UND.

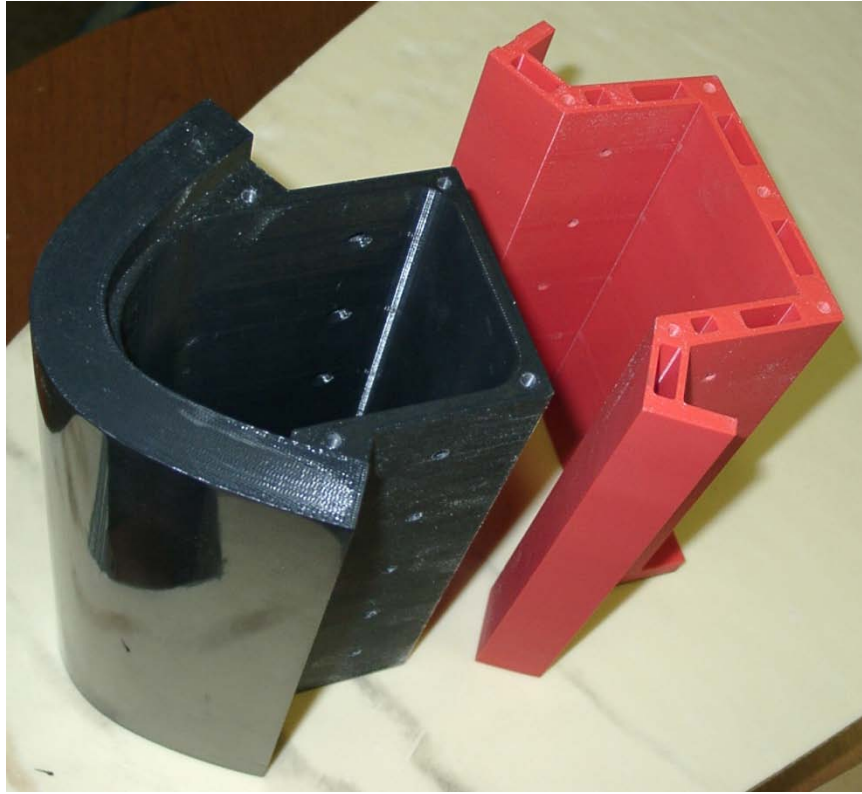


Figure 30. Small cylinder leading edge and mounting bracket.

Test Section After body

Because of the large opening in each leading edge, a cover had to be designed to seal the inlet plenum. The cover followed the contours of the leading edge and had a hole for a two inch PVC pipe to be inserted into the cover. The window was made with help from Jay Evenstad using the CNC machine out of a small piece of 1.91 cm (0.75 in) thick acrylic. The PVC pipe delivered the cool air to the leading edge. The pipe had nine 1.27 cm (0.50 in) holes spaced 2.54 cm (1.00 in) apart. There was also a baffle installed in the pipe to help make the flow exiting the holes more uniform. Figure 31 shows the injection pipe with holes and quick disconnect coupling.



Figure 31. Cool air injection pipe and baffle with quick disconnect PVC coupling.

In order to ensure the flow path around the test surface is as smooth as possible, the surface of the cylindrical test section are covered using a thin epoxy board, one on the top and one on the bottom of the test surface. The epoxy board helps to smooth out any ridges that were formed due to miss-alignment of the foam board and/or plywood sections. Each piece of epoxy board was made to cover the tabs of the mounting bracket and cover the rest of the cylinder downstream, or 24.89 cm (9.80 in) tall by 97.54 cm (38.40 in) long. The bottom epoxy board had no modifications. The top epoxy board, however, required the installation of sixty thermocouples. The exact location of the thermocouples can be seen in Table 1.

First, locations were marked and 0.159 cm (1/16 in) holes were drilled. Then each thermocouple was taped into position. Once all of the thermocouples were in place, the epoxy board was flipped over. Special attention was given to ensure that the union of each thermocouple was located in a hole. Each thermocouple was held in position using Omegabond 101 high thermal conductivity epoxy. After the epoxy had cured, each thermocouple location was sanded down to remove any bumps that may negatively impact the flow.

Table 1. Thermocouple location.

Distance from Slot to Start of Epoxy Board (from Pro/E)					
0.585726 in			1.487744 cm		
Distance from Start of Epoxy Board to:			Distance from Slot to:		
Row	in	cm	Row	in	cm
0	0.4	1.0	0	1.0	2.5
1	0.8	2.0	1	1.4	3.5
2	1.3	3.3	2	1.9	4.8
3	1.8	4.6	3	2.4	6.1
4	2.3	5.8	4	2.9	7.3
5	2.8	7.1	5	3.4	8.6
6	3.4	8.6	6	4.0	10.1
7	4.4	11.2	7	5.0	12.7
8	5.4	13.7	8	6.0	15.2
9	6.4	16.3	9	7.0	17.7
10	7.4	18.8	10	8.0	20.3
11	9.4	23.9	11	10.0	25.4
12	11.4	29.0	12	12.0	30.4
13	13.4	34.0	13	14.0	35.5
14	15.4	39.1	14	16.0	40.6
15	17.4	44.2	15	18.0	45.7
16	19.4	49.3	16	20.0	50.8
17	21.9	55.6	17	22.5	57.1
18	24.4	62.0	18	25.0	63.5
19	26.9	68.3	19	27.5	69.8

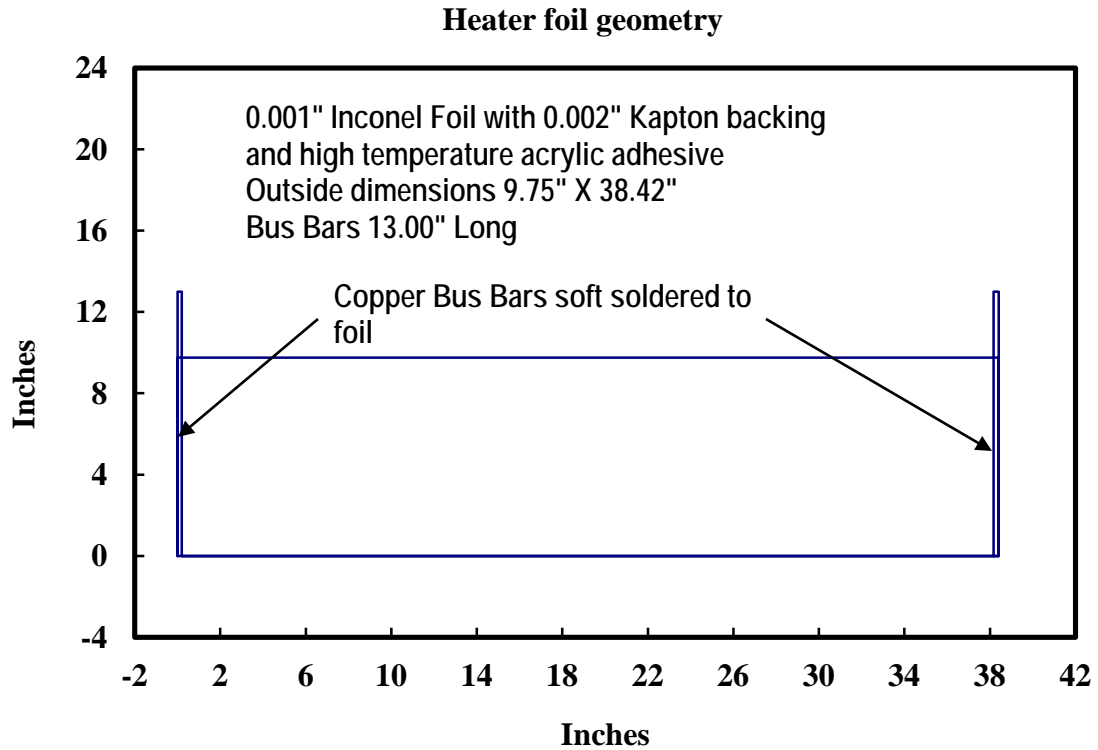


Figure 32. Inconel heat foil geometry.

The top epoxy board also served as a mounting surface for the Inconel foil heater. A schematic of the heater can be seen in Figure 32. Any roughness on the surface would have shown through the foil heater. Inconel is an alloy that is made out of mostly nickel and chromium, with various other elements depending on the alloy. Inconel was designed to be able to withstand high temperatures and be able to resist corrosion. The heater foils were manufactured by Tayco Engineering, Inc and consisted of a sheet of 0.00254 cm (0.001 in) thick sheet of inconel foil with a 0.00508 cm (0.002 in) Kapton backing. The system was adhered to the epoxy board using a high temperature acrylic adhesive. Kapton is a polyimide film that has a wide range of operating temperatures. A copper bus bar was soldered on at each end, with dimensions of 0.0508 cm (0.02 in) thick by 0.635 cm (0.25 in) wide by 33.02 cm (13.00 in) long. The Inconel foil heater generated a constant heat flux by applying a differential DC voltage across the bus bars.

The voltage would travel through the foil, which in turn, heated up the foil. Because the Inconel foil heater did not wrap around the leading edge of the cylindrical test section, it is possible that the flow around the test surface could be disrupted due to this unheated starting length. This unheated starting length will make the thermal and velocity boundary layers start at different positions on the test surface. The Nusselt number of a heated flat plate can be approximated by [40]:

$$Nu = 0.332Pr^{1/3}Re^{1/2} \quad (3.1)$$

However, with the introduction of the unheated starting length, the Nusselt number becomes [40]:

$$Nu = \frac{0.332Pr^{1/3}Re^{1/2}}{[1-(\xi/x)^{3/4}]^{1/3}} \quad (3.2)$$

where ξ is the unheated starting length.

Each cylinder is made of nine layers of 2.54 cm (1.0 in) thick polyisocyanurate foam board between two layers of 1.27 cm (0.5 in) thick paper-lined plywood. Several aluminum plates were made into the shape desired using the CNC machine at UND. Those plates were fastened to a 2.54 cm thick sheet of plywood to make a jig. The sheets of 1.27 cm plywood and 2.54 cm foam board were then cut using the jig and a router with a 0.95 cm (3/8 in) cutting bit. Figure 33 shows both the large leading edge test section and small leading edge test section jigs.



Figure 33. Large and small cylindrical leading edge test section router jigs.

The sheets of foam board were then aligned with and glued to one of the sheets of plywood using PL300 Foam board adhesive. The PL300 adhesive formed a good bond with the wood and the foam without causing corrosion damage to the foam. Weights were applied to the assembly to prevent separation of the layers, as well as prevent buckling and warping of the test section. After the adhesive was dry and the weights were removed, the leading edge and mounting bracket sections were cut away from the foam while only the leading edge section was removed from both sheets of plywood. The sections were left on during the gluing process to aid in alignment. Alignment was checked again, and holes were marked and drilled on both pieces of plywood to fasten the mounting bracket in place. Figure 34 shows the small cylindrical test section with the leading edge removed, while Figure 35 shows the small cylindrical test section with the mounting bracket and leading edge in place for alignment.



Figure 34. Glued, cut, and drilled small test section with leading edge and mounting bracket.

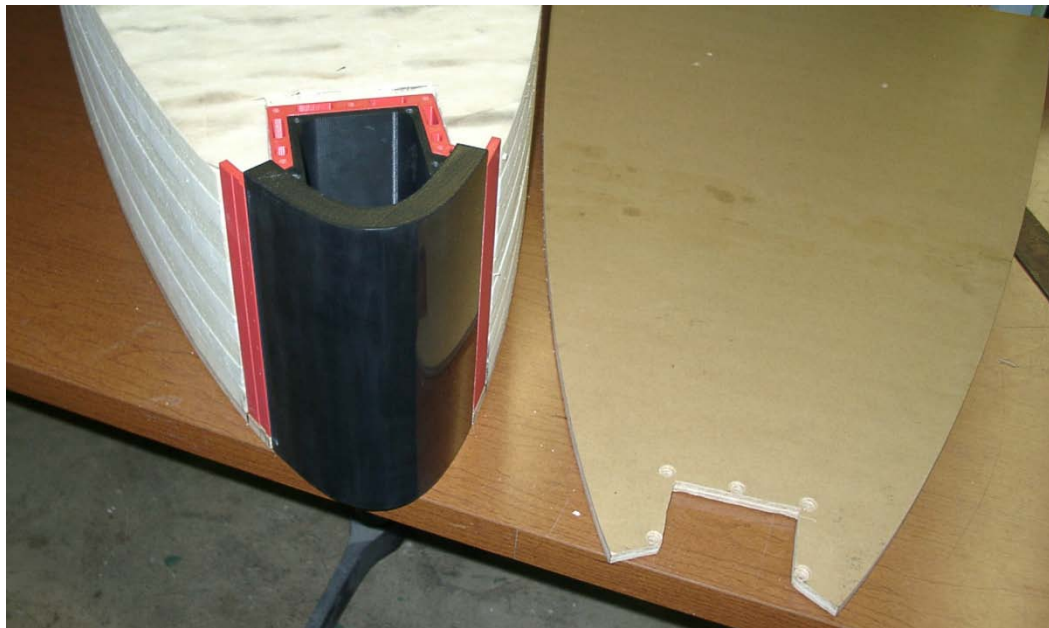


Figure 35. Small test section with mounting bracket and leading edge attached for alignment.

The mounting bracket was then attached and the last section of plywood was aligned and glued into position. Once again, weights were applied to hold everything in place.

Figure 36 shows the top plywood being glued on with the weights applied. At this time, the leading edge assembly was mounted to the bracket.



Figure 36. Small test section with mounting bracket attached and weights applied.

After the glue had dried and the plates were removed, a visual alignment check was made using the epoxy boards. A groove had to be cut into the foam board to accommodate the bundle of thermocouple wires running down the edge of the epoxy board. After the alignment check, Weldwood contact cement was applied to both pieces of epoxy board, as well as both sides of the test section. Figure 37 shows both pieces of epoxy board with the Weldwood contact cement applied.



Figure 37. Epoxy board with contact cement. Thermocouple locations can be seen.

The pieces of epoxy board were then applied to the test surface, with extra effort being made to ensure that the thermocouples remained undamaged and rest in the previously cut groove. Pressure was then applied to activate the adhesive and push out any air bubbles that may have been trapped in the process. After the adhesive cured, the Inconel foil heater was put into position and marks were made for the bus bar. Using the marks and a straight edge as a guide, grooves were cut into the plywood using a router. These grooves allowed the bus bars and wires to lay flat inside the walls of the test section. Next the Inconel foil heater was carefully applied. Starting at the mounting bracket, the backing of the heater was peeled off and light pressure was applied. As the backing was removed, alignment was continually monitored and light pressure was applied. Special care was taken to prevent any wrinkles that would disrupt the flow from forming. After the foil was in place, more pressure was applied to activate the pressure sensitive adhesive and force out any remaining air bubbles that may have been formed, as the air

bubbles would have proven disruptive to the flow. The bus bar was bent down into the previously cut groove so the cylinder would fit in the test section. Multi-strand 10 awg wires were then soldered to the bus bars to deliver current to the heater. Smaller multi-strand wires were also soldered on the bus bars. These smaller wires would attach to the HP data acquisition unit to monitor the voltage across the heater. Figure 38 shows the small test section with leading edge and Inconel foil heater attached.

Next, the acrylic window was attached to the side of the leading edge. Instrumentation from the leading edge was routed through the opening in the window. The cool air discharge pipe was installed next, taking care not to pinch any of the thermocouples or pressure tubes. Silicone sealant was used around the acrylic window and discharge pipe to ensure no coolant was leaking from the leading edge. The cylindrical leading edge test section was ready to be installed in the acrylic housing section.

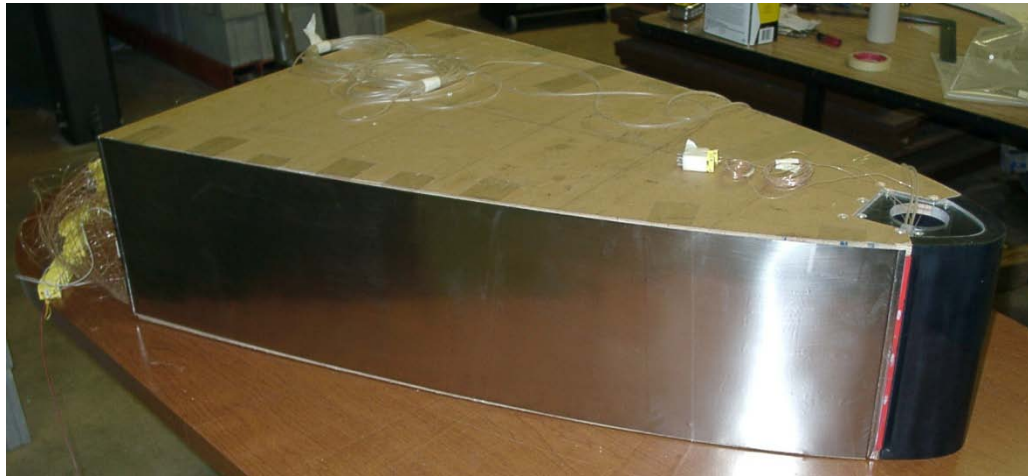


Figure 38. Small cylindrical test section with inconel foil and acrylic window attached.

Data Acquisition Equipment

All of the data was taken using a HP 3497A data acquisition unit capable of reading 100 different channels. The unit housed an integral voltmeter with a sensitivity

of one microvolt. Controlling the HP 3497A data acquisition unit was a Dell OptiPlex GMT-590 computer.

Thermocouples and Temperature Measurements

Temperatures were measured using type-K thermocouples, composed of chromel and alumel. Each thermocouple was made from wire, a male plug, and had a welded junction at one end. The wire was 36gauge with a temperature range of -267°C to 260°C . The chromel and alumel ends of the thermocouple were welded together using a Therm-X 258B thermocouple welder, which can be seen in Figure 39. It is a tungsten-inert gas (TIG) welder that uses argon gas to create an inert environment around the weld, thus preventing corrosion on the weld. The energy from the arc melts the chromel and alumel together to form the junction required.



Figure 39. Thermocouple welder, materials, and completed thermocouple.

All seventy-three thermocouples from the cylinder, test section, and other parts of the experiment were attached to a junction panel, which was then attached to a constant

temperature junction box. The thermocouples were then referenced to an ice bath. The ice bath consisted of a vacuum sealed thermos, which held ice and water. A hole was drilled in the thermos cap and a glass tube filled with mineral oil, and containing the thermocouple was inserted into the hole. The thought behind the mineral oil was to try to obtain an accurate temperature reading every data set, and not have to worry if the thermocouple junction was touching the wall of the glass tube or not. Temperatures measured include: air conditioning in, air conditioning out, orifice, plenum, ejection slot, mounting bracket, free stream, and sixty downstream surfaced temperatures.

Pressures

Pressure tubes from the experimental setup were connected to quick disconnects which were in turn, connected to the solenoids. Pressure measurements were controlled by the computer. It utilized a multiport DI/O board to control the operation of the pressure solenoids. The solenoids were connected to two Rosemount pressure transducers, each with a reported accuracy of ± 0.1 percent. The low pressure measured pressure from up to 250 Pa, while the high pressure transducer measured pressure up to 5000 Pa. The voltages from the Rosemount transducers were read and reported by the HP data acquisition unit. Pressures measured include: atmospheric, total, plenum static, exit static, slot static, bracket static, and the change in pressure across the sharp edged orifice plate. Figure 40 shows the stand that held the computer, HP data acquisition unit, solenoids, pressure transducers, ice bath, and thermocouple jack panel.



Figure 40. Stand containing the computer, HP unit, transducers, solenoids, and thermocouple jack panel.

Coolant Delivery System

Blower and Air Conditioning Unit. The cool air comes from a blower manufactured by New York Blower, pressure blower model 1704A. It is capable of providing a $0.2 \text{ m}^3/\text{s}$ at a static pressure rise of 5400 Pa. Blower speed is controlled by a variable frequency drive. The blower forces air through an air conditioning unit manufactured by GE, model AET05LWL1 and has cooling capacity of 5050 Btu/hr. Some modifications had to be made to allow the rectangular air conditioning unit to accept air from the blower's circular ducting and allow for the cold air to be collected. The blower and air conditioning unit are connected via four inch flex tubing. Air is collected from the tubing by a 15.24 cm (6.0 in) by 30.48 cm (12 in) register. A custom mounting bracket was made and installed on the air conditioning unit to accept the register. A smaller 5.08 cm (2.0 in) by 30.48 cm

(12 in) register was installed to collect the cold air leaving the air conditioning unit. The front panel of the air conditioning unit had to be removed to accommodate the changes made. The cold air then travels via 10.16 cm (4.0 in) flex tubing to a thermal inertia box.

Thermal Inertia Box. The thermal inertia box consisted of thirteen plates of 2.54 cm (1.0 in) by 25.4 cm (10.0 in) by 55.88 cm (22.0 in) aluminum plates, separated by 0.32 cm (1/8 in) thick particle board spacers. The plates are enclosed by 1.27 cm (0.5 in) thick plywood. The idea behind the thermal inertia box is that the cold air from the air conditioning unit would cool down the plates enough to keep the cooling air temperature constant. 2.54 cm (1.0 in) thick polyisocyanurate foam board was used to insulate the thermal inertia box to try and prevent losses. The cool air leaves the thermal inertia box via 5.08cm (2.0in) PVC pipe and approaches a tee fitting. One direction leads to a ball valve, while the other direction leads to a sharp edged orifice plate. The ball valve was used as a way to control the flow by dumping some of the cool air if needed.

Orifice Plate. The sharp edged orifice plate was made with the help of Gary Dubuque out of a 0.64 cm (0.25 in) thick plate of aluminum. It had a hole diameter of 3.175 cm (1.25 in) and was beveled with a 45° angle. With static pressure taps before and after the orifice plate and the known area of the hole in the plate, the cool air mass flow rate could be determined. In an attempt to make sure the flow is fairly uniform before it reaches the orifice plate, a tube length of at least fifteen diameters, or 76.2 cm (30.0 in) was used upstream of the orifice plate. A pipe of six diameters, or 30.48 cm (12.0 in) was used downstream of the orifice plate. The flow then passed through a section of 5.08 cm (2.0 in) diameter flex tubing and then into a quick disconnect attached to cool air injection tube at the leading edge. This quick disconnect allowed for easy removal of flex tubing

from the test section when equipment needed to be moved, and also helped to reduce stress on the test section during the process. In order to deliver the coolest air possible, all sections of pipe and flex tubing were double insulated, including the cold air collection register.

Power Supply. Current was delivered to the Inconel foil heater through the 10 awg wires, by means of a powerful external DC power supply. The output was connected to a 0.001 ohm precision constantan shunt resistor, which was accurate up to \pm two percent. The Inconel foil had a known resistance per unit area. Using that resistance, a total resistance for the foil was calculated. The HP data acquisition unit measured the voltage across the inconel heater foil. The current through the foil was then calculated by measuring the shunt resistor in series with the heat foil resistance. Output from the DC power supply was then calculated, as well as the power being used by the heater. Figure 41 shows the layout of the cool air delivery setup. The small blower, air conditioning unit, thermal inertia box, power supply, ball valve, and orifice plate can be seen in the figure.



Figure 41. Blower, ac unit, thermal inertia box, orifice plate, and power supply.

Data Acquisition

Data for this experiment was acquired with a program made in QuickBasic. This program had both monitoring routines, as well as the data collection routines. In order to obtain a full data set for this experiment, each data point was collected three times, to ensure that the system had reached steady state. A data set is the data acquired from a specific test section, at a specific Reynolds number, at a specific blowing ratio, at a specific turbulence intensity, and measuring one of the five different flow conditions. The five flow conditions are: no blowing-ambient, no blowing-heated, heat transfer-ambient, heat transfer-heated, and film cooled.

Preparation

Prior to starting up the flow rig and taking a new data set, the barometric pressure (in inches mercury) was checked and recorded, and the ice bath was checked and

replenished if needed. To start the flow rig, the circuit breaker for the variable frequency drive and large blower was flipped to the 'on' position. The shutoff valve for the cold water line was slightly opened. Usually only the high Reynolds number required additional cold water to maintain the temperature difference needed. To get water flowing through the heat exchanger, the circulation pump was turned on. The large blower was now turned on, along with the HP data acquisition unit and the Dell computer. One of two QuickBasic programs was used, depending on which test surface was being tested: bigcylfc or medcylfc to test the large cylindrical leading edge test surface and the small cylindrical leading edge test surface, respectively. Once the proper program was selected, barometric pressure was entered, and the pressure transducers were zeroed. The pressure transducers were always zeroed multiple times to make sure they continued to have the same readings.

Data Acquisition Procedure

The first data set taken for any turbulence intensity was the no blowing-ambient condition. This provided values for how the flow acted around the test section under normal conditions, without blowing or heating. No blowing required the ejection slot of the leading edge to be covered or plugged to prevent flow from the free stream from entering the leading edge. Transparent Scotch tape was used to cover the slot, with sections removed that may have covered any static pressure probes on the mounting bracket and can be seen in Figure 42.



Figure 42. Small cylindrical leading edge test section with slot taped.

Blower velocity was controlled using the variable frequency drive, depending on what Reynolds number was being tested. Because the Reynolds number was constantly fluctuating, an allowable value of \pm one percent of the target Reynolds number was accepted. The temperatures were then monitored until they stopped changing, or were within a $0.05\text{ }^{\circ}\text{C}$ temperature range of the previous value after ten minutes. A data set could now be taken. The data set was then checked for accuracy and to make sure steady state was indeed achieved. If the data set appeared acceptable, the DC power supply was turned on to supply current to the heater. The goal was to have at least a six degree Celsius temperature rise on the surface at the mounting bracket, and at most a twenty degree Celsius temperature rise downstream on the surface of the test section when compared to the free stream temperature. Temperatures were monitored and the output of the power supply was adjusted as needed. Once steady state was achieved, another data set was taken. Again, this data set was analyzed for any errors and to check steady state. If the data was acceptable, the power supply was turned off. This no blowing-

heated data set helps describes how the state of the boundary layer, without any film cooling.

This procedure was repeated for both Reynolds numbers. To increase the system to the next Reynolds number, the program had to be switched to a monitoring routine, and the blower speed increased. The increase in blower speed required more thermal dissipation be removed from the system. In order to dissipate the heat, the cold water valve was opened to allow cold water to mix with the water already in the storage tank. The overflow from that tank would dump warm water from the heat exchanger down the drain. Temperatures needed to be monitored depending on the conditions required for the data set. Figure 43 shows the small test section being tested at the no blowing condition.



Figure 43. Small cylindrical leading edge test section at low turbulence, no blowing.

After the no blowing data had been acquired and analyzed, the test section could be removed to allow for the removal of the Scotch tape covering the ejection slot. With the tape removed, and the test section re-attached, the Reynolds number was once again

set. The small blower was then turned on and the blowing ratio was then set. Temperatures were monitored in the same way as in the no blowing condition, with the exception that now the air exiting the slot needed to be within $\pm 0.1^\circ\text{C}$ of the free stream temperature. This was normally achieved by either cooling down the free stream temperature by adding cold water to the reserve tank, or by turning up the speed of the small blower and opening the waste valve. Once steady state was reached, a data set was taken and checked for accuracy. If the data set was acceptable, the power supply was turned on and the heated data were taken in the same way as the no blowing-heated data was. After the heated data was checked and the power supply turned off, data were taken for the next blowing ratio. The blowing ratio was changed by increasing the speed of the small blower. When data have been taken for all of the blowing ratios, the Reynolds number was increased and the process started over again. The heat transfer -ambient and -heated data allows for the determination of the Stanton number. The Stanton number can be expressed by a series of nondimensional heat transfer coefficients from Kays, Crawford, and Weigand [40]. First, the recovery temperature needed to be calculated using a recovery coefficient (r_c), which can be expressed by:

$$r_c \approx Pr^{1/2} \text{ for Laminar flow} \quad (3.3)$$

$$r_c \approx Pr^{1/3} \text{ for Turbulent flow} \quad (3.4)$$

Using the measured values of T_{total} (T_T) and T_{static} , (T_S) a value can be obtained for the following expression:

$$T_T = T_S + \frac{U^2}{2gc c_p} \quad (3.5)$$

The recovery temperature (T_r) could then be expressed by:

$$T_r = T_s + r_c \frac{U^2}{2gc c_p} \quad (3.6)$$

Next, a value for the net heat of the system needed to be calculated. This was done by:

$$\dot{Q}_{net} = \frac{\dot{Q}_F}{A_F} - Q''_{rad} \quad (3.7)$$

where \dot{Q}_F is the heat of the Inconel foil heater, expressed by:

$$\dot{Q}_F = V * I \quad (3.8)$$

where V is the voltage and I is the current of the Inconel foil heater. A_F is the area of the foil heater, minus the bus bars. A heat transfer coefficient, h , could be found using the net heat of the system, the heated wall temperature (T_{HW}), and the recovery temperature.

$$h = \frac{\dot{Q}_{net}}{(T_{HW} - T_R)} \quad (3.9)$$

Finally, the Stanton number can be calculated.

$$St = \frac{Nu}{Pr Re} \quad (3.10)$$

After the heat transfer data has been acquired and analyzed, everything was shut down or turned off except the small blower. The small blower was left on and the air conditioning unit was turned on high. Both pieces of equipment were made to run overnight. This allowed for the plates in the thermal inertia box to begin cooling. Once the plates have been sufficiently cooled, usually by the next morning, the film cooling data was taken.

With the Reynolds number and blowing ratio set in the same method as before, temperatures were monitored. For the film cooling data, the temperatures at the slot needed to be at least ten degrees Celsius less than the free stream temperature. After the desired temperature had been reached and steady state achieved, a data set was taken and reviewed for accuracy. Then the data for the next blowing ratios, and eventually, Reynolds number can be acquired in the same manner. Once a cylindrical test section

had been tested at all Reynolds numbers, blowing ratios, and for ambient, heat transfer, and film cooling conditions, the turbulence intensity could be changed. This variation was done by either adding a turbulence generating grid, a spool section, or changing out the nozzle entirely. Once all data sets for all turbulence conditions, blowing ratios, and Reynolds numbers had been acquired, the test section could be replaced. This required all thermocouples, pressure tubes, and electrical connections of the current cylindrical test section to be disconnected, and replaced with connections from the new cylindrical test section. Figure 44 shows the small cylindrical test section under the small grid far turbulence condition. Figure 45 shows the same test section at the small grid near turbulence condition. The small cylindrical test section at the large turbulence intensity can be seen in Figure 46. Figure 47 is of the large cylindrical test section under the mock aero-combustor with spool turbulence condition.



Figure 44. Small cylindrical test section, small grid - far position.



Figure 45. Small cylindrical test section, small grid - near position.



Figure 46. Small cylindrical test section, large grid.

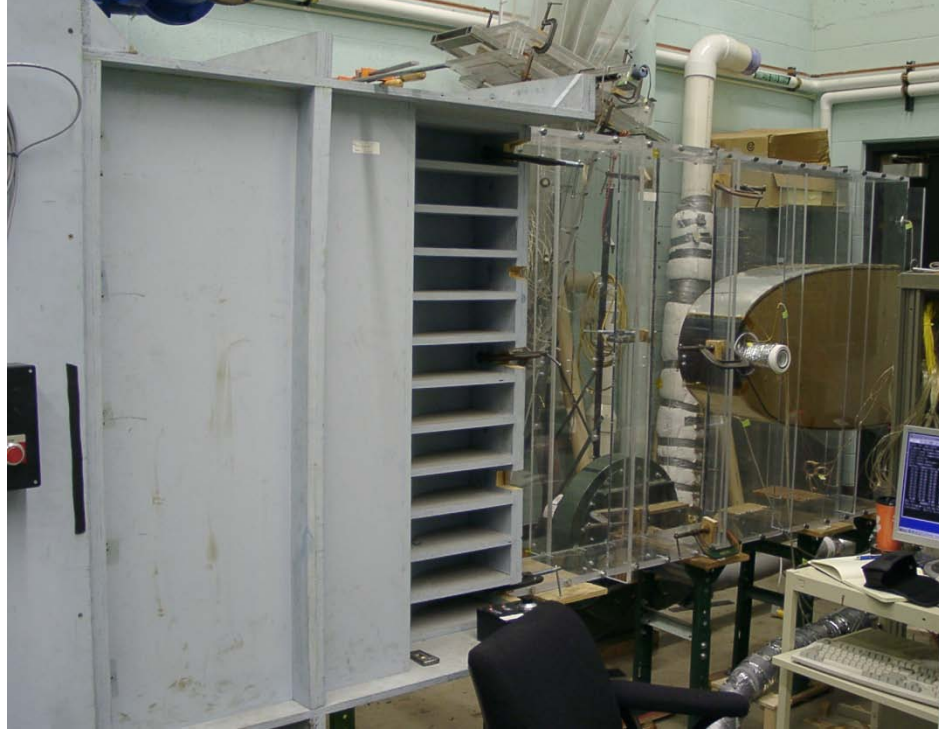


Figure 47. Large cylindrical test section, mock aero-combustor with spool.

An analysis of a data file can be found in the appendix.

CHAPTER IV

EXPERIMENTAL RESULTS

The application of film cooling on turbine surfaces is typically accompanied by a range of flow acceleration, various levels of turbulence, at various surface and slot Reynolds numbers, and it is discharged at various blowing ratios. This complexity increases the difficulty of accurately estimating the benefit of film cooling. Slot film cooling arguably provides the best protection for a given condition due to its two-dimensional nature, which is expected to minimize mixing with the external flow. For that reason, a slot configuration was used in this experiment. This chapter will discuss the results found in terms of the adiabatic effectiveness for both cylindrical leading edge test sections, as well as the heat transfer for both test sections. Each section will discuss the effects of blowing ratio, turbulence, and Reynolds number. For the large leading edge test section, the Reynolds numbers used were $Re_D = 250,000$ and $Re_D = 500,000$. In an attempt to create the same flow conditions around the small cylindrical test section, the Reynolds numbers were quartered to reflect the difference in the leading edge diameter of the test sections. The Reynolds numbers used for the small cylindrical test section were $Re_D = 62,500$, and $Re_D = 125,000$. The thermocouple location distance is given in a dimensionless ratio of the x-direction distance from the slot over the slot height. Effectiveness values are given using the following equation:

$$\eta = \frac{(T_{aw} - T_r)}{(T_{co} - T_r)} \quad (4.1)$$

Understanding the blowing condition for the two cylindrical test sections. The Reynolds number is a dimensionless parameter based on the density, velocity, length, and viscosity. The large cylindrical leading edge test section has a leading edge diameter of sixteen inches while the small cylindrical leading edge test section has a leading edge diameter of four inches. When the large test section was run at a Reynolds number of $Re_D = 500,000$ the small test section was run at a Reynolds number of $Re_D = 125,000$. The reduction in Reynolds number reflects the change in the leading edge diameter. The location of the coolant ejection slot for the large test section was at a surface distance of 12.3 cm (4.83 in) and the location of the coolant ejection slot for the small test section was at a surface distance of 10.3 cm (4.05 in). Due to the shape of the after body and the acceleration profile around both test sections, the free stream velocity at the ejection slot is within ten percent for both test sections. Although the Reynolds numbers that are compared are different, the conditions around the test sections are similar.

Adiabatic Effectiveness – Large Cylindrical Leading Edge Test Section

Effects of Blowing

Blowing ratio has a large effect on the adiabatic effectiveness. Directly behind the ejection slot, the highest blowing ratio has the highest effectiveness. The adiabatic effectiveness of the lowest blowing ratio of $M = 0.46$ drops off rapidly at a distance of approximately ten slot heights, and eventually starts to even off. Increasing the blowing ratio appears to increase the adiabatic effectiveness. In most cases, there is a difference in adiabatic effectiveness between the high blowing ratio of $M = 1.60$ and the low blowing ratio of $M = 0.46$ by twenty percent or more. By the end of the test surface, the difference in effectiveness between the high and low blowing ratio has been reduced to

around ten percent. At the low turbulence intensity, the low blowing ratio has an efficiency of thirty percent at a distance of about eighty that the high blowing ratio has at a distance of 175. Figure 48 shows the blowing ratio effects on the large cylinder at the low turbulence condition. The effectiveness for all of the blowing ratios are very similar up to a distance of twenty five slot heights. At that distance, the effectiveness of the low blowing ratio continues to decrease at the accelerated rate. There was a difference in effectiveness between the highest and lowest blowing ratio of about thirteen percent at the end of the test section. Figure 49 shows how changing the blowing ratio for the small grid near turbulence condition changes the effectiveness. Here, an effectiveness of thirty percent is achieved at the low blowing ratio at a distance of about thirty seven slot heights, where as the high blowing ratio has the same effectiveness at a distance of about seventy four slot heights. A difference of about nine percent exists between the highest and lowest blowing ratio at the end of the test section. Figure 50 shows how changing the blowing ratio changes the efficiency at the aero-combustor turbulence condition. Here, an effectiveness of thirty percent is achieved by the low blowing ratio at a slot height distance of about twenty four and the high blowing ratio has the same effectiveness at a slot height distance of about sixty. The difference in the high and low blowing ratio effectiveness at the end of the cylinder has decreased to about five percent.

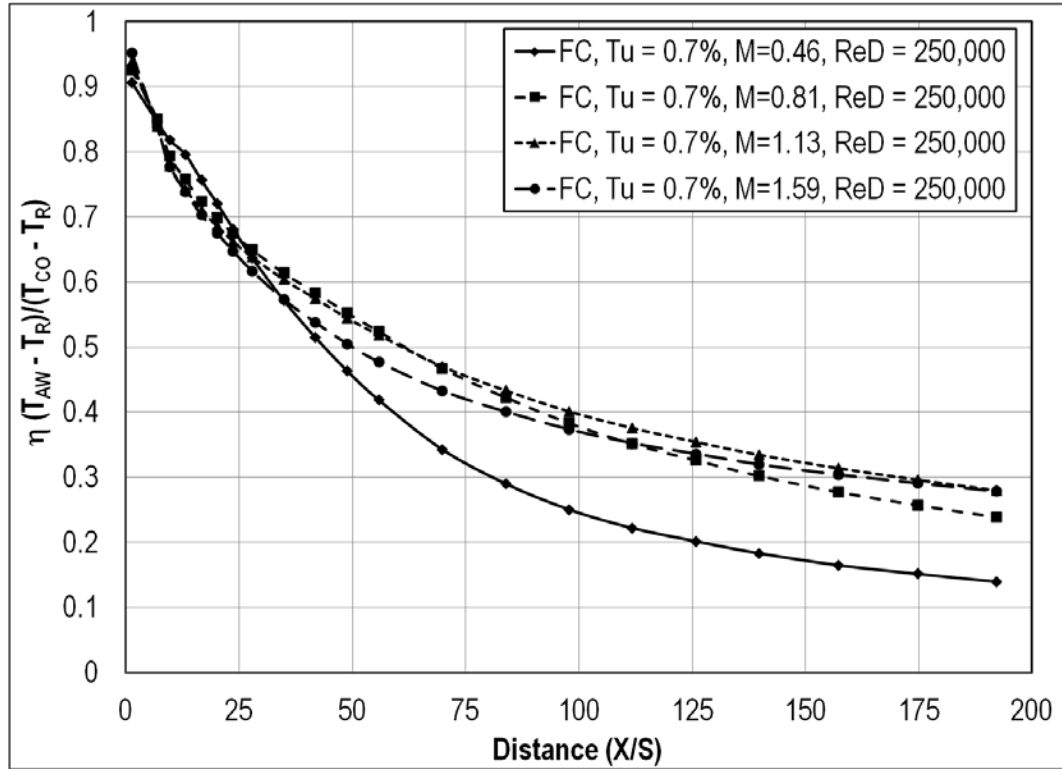


Figure 48. Effects of blowing ratio on adiabatic effectiveness for the large cyl. at low Tu.

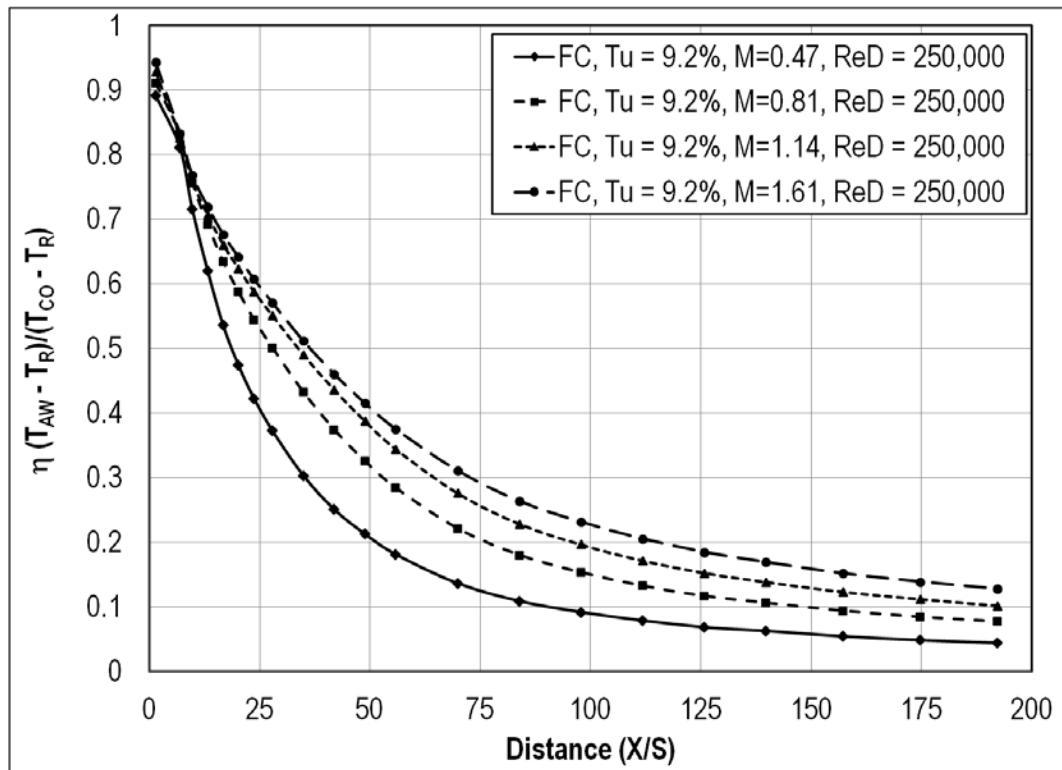


Figure 49. Effects of blowing ratio on adiabatic effectiveness for the large cyl. at small grid-near Tu.

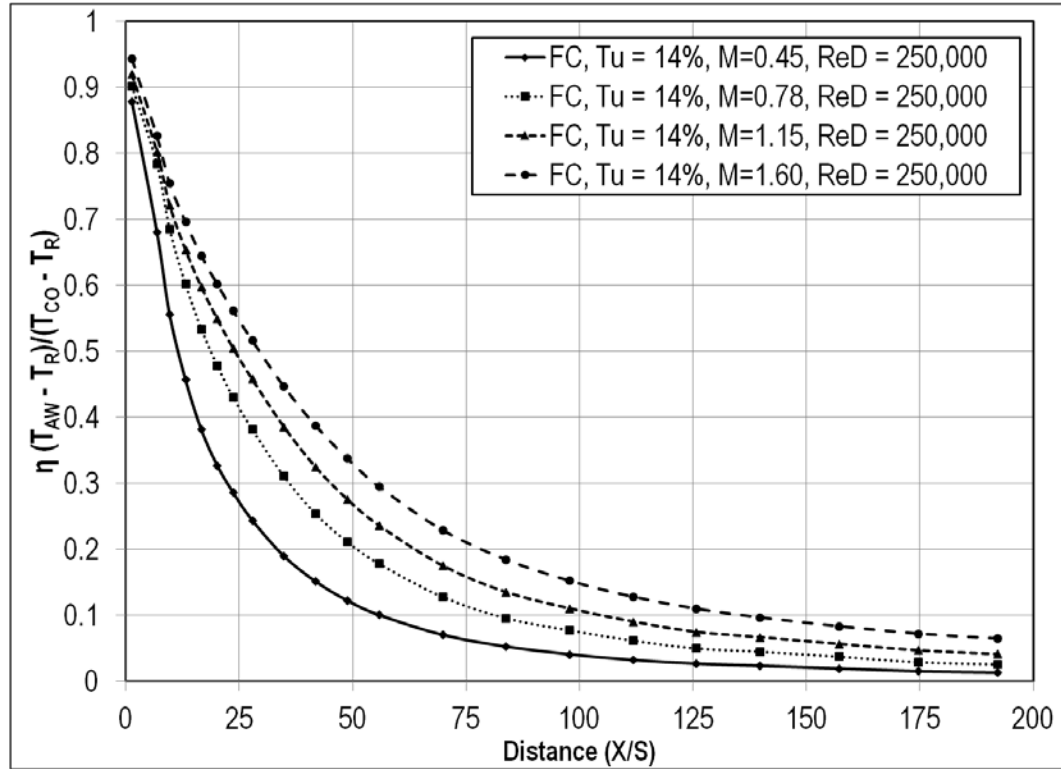


Figure 50. Effects of blowing ratio on adiabatic effectiveness for the large cyl. at aero combustor Tu.

Effects of Reynolds Number

The effects of Reynolds number on the adiabatic effectiveness are not as clear as the effects of blowing ratio. For all cases, the adiabatic effectiveness was greater for the two blowing ratios at the highest Reynolds number, at the start of the test surface.

However, the effectiveness values quickly dropped to a value that was less than that of the lower Reynolds number. By the end of the test section, the effectiveness of the high blowing ratio and high Reynolds number would usually match or be slightly greater than the effectiveness of the high blowing ratio at the low Reynolds number. The low blowing ratio effectiveness at the high Reynolds number was almost always similar or less than at the low Reynolds number and same blowing ratio. An effectiveness of thirty percent is achieved at the high Reynolds number and low blowing ratio at a distance of about sixty

five slot heights, whereas the low Reynolds number and low blowing ratio has the same effectiveness at a distance of eighty. That same effectiveness is achieved at the high Reynolds number and high blowing ratio at a distance of 160, but the low Reynolds number and high blowing ratio achieves this efficiency at a distance of approximately 140. Figure 51 shows a comparison of Reynolds numbers at the two low blowing ratios for the large cylindrical leading edge test section at the low turbulence condition. Here, there is a significant difference in the effectiveness between the two Reynolds numbers at the low blowing ratio up to a slot height distance of about one hundred. The effectiveness between the two Reynolds numbers at the large grid turbulence intensity was very similar and can be seen in Figure 52. Figure 53 shows the effect of Reynolds number on adiabatic effectiveness at the aero-combustor with spool turbulence intensity. Here, the high Reynolds numbers start with higher effectiveness values, but they quickly mix out to a value very close to that of the low Reynolds number.

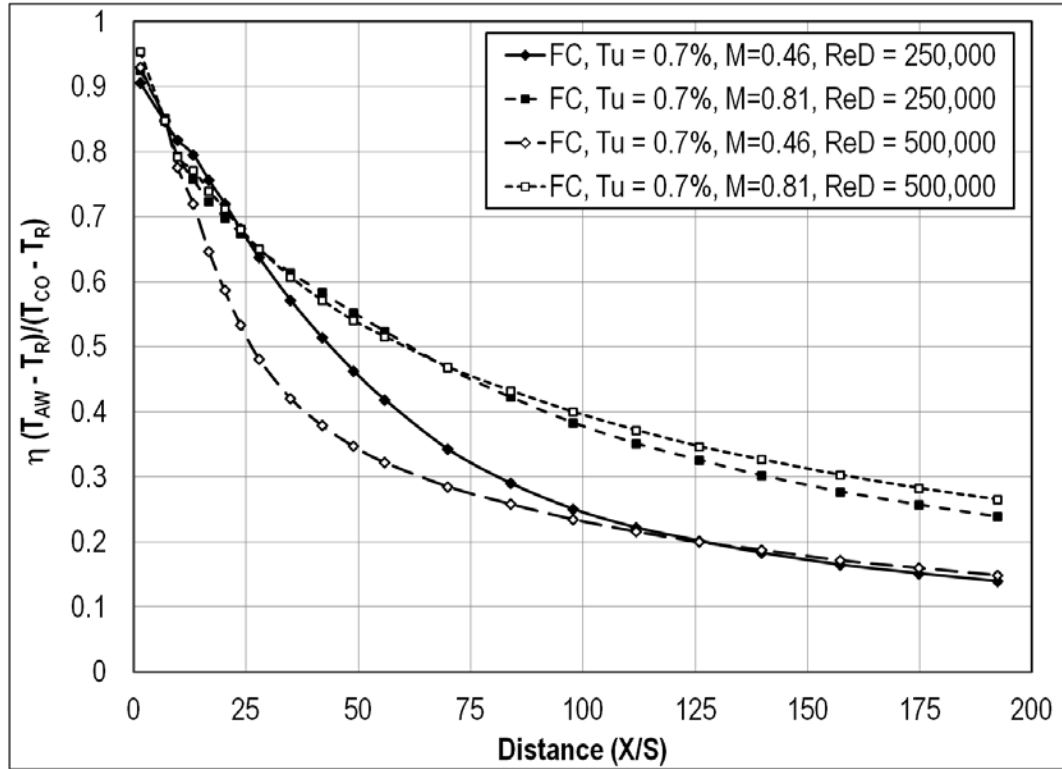


Figure 51. Effects of Reynolds number on adiabatic effectiveness for the large cyl. at low Tu.

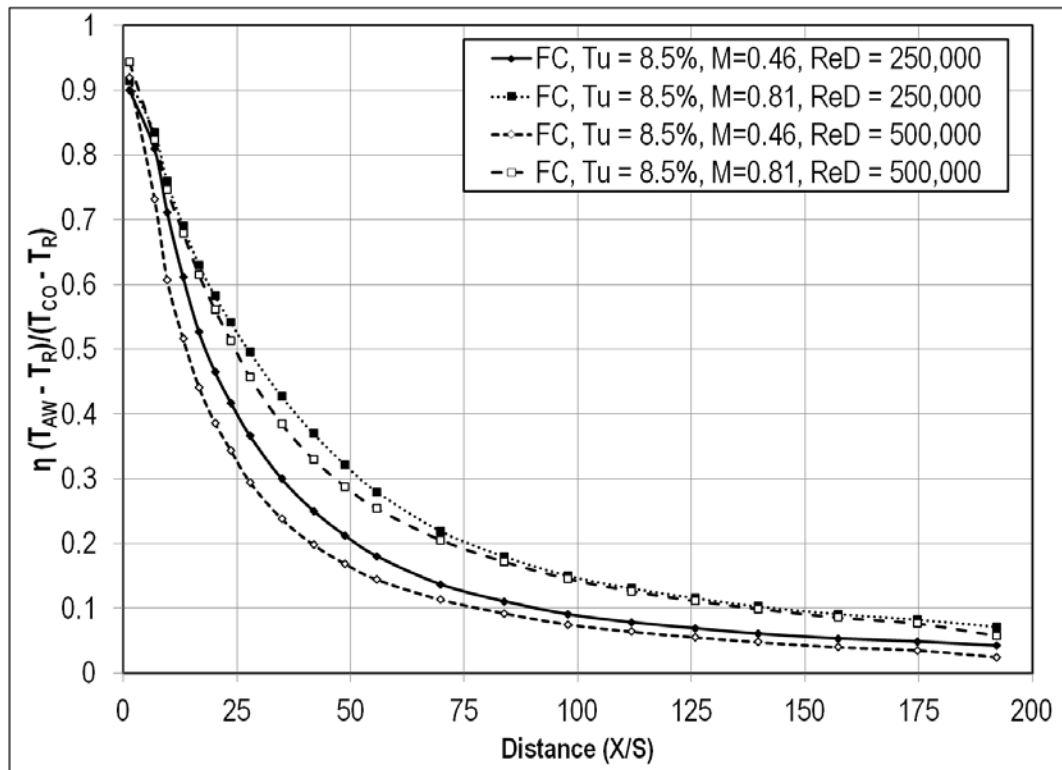


Figure 52. Effects of Reynolds number on adiabatic effectiveness for the large cyl. at large grid Tu.

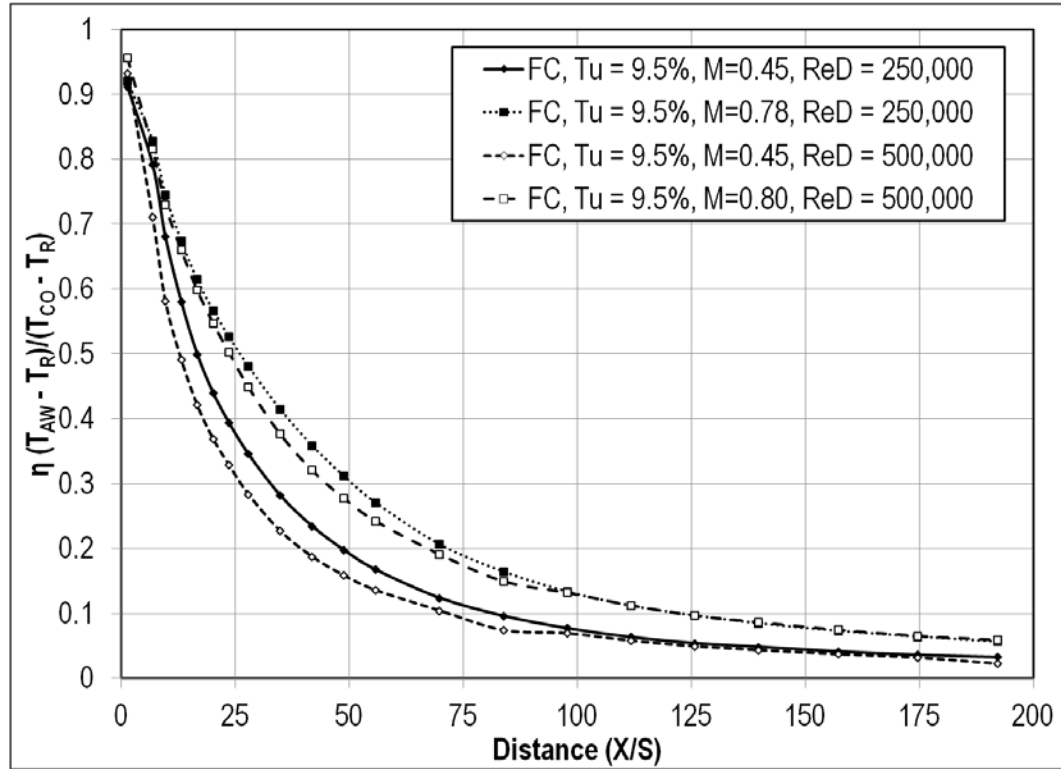


Figure 53. Effects of Reynolds number on adiabatic effectiveness for the large cyl. at aero combustor-spool Tu.

Effects of Turbulence

Turbulence has a very pronounced effect on the adiabatic effectiveness of film cooling. Increasing the turbulence decreases the effectiveness. At a distance of fifty slot heights, there exists an effectiveness difference of about thirty percent between the low turbulence intensity and the aero combustor turbulence intensity. This can be seen graphically in Figures 54 and 55. Turbulence appears to shift the graph down and to the left, meaning that the effectiveness is lower, earlier on the test surface. Figure 56 shows the effect of turbulence intensity at the second highest blowing ratio. Here, there is a very large distance in effectiveness downstream between the low turbulence and mock aero-combustor. The shift in the effectiveness is also seen at $Re_D = 500,000$. At $M = 0.46$ and $Re_D = 500,000$, an effectiveness of thirty percent is achieved for the low

turbulence intensity at a distance of eighty slot heights, whereas the same effectiveness is achieved for the aero combustor at a distance of twenty three slot heights. This can be seen in Figure 57. Figure 58 shows the effect of turbulence intensity at the high Reynolds number and high blowing ratio. Once again, there is a very large difference in effectiveness between the highest and lowest turbulence intensity. At a slot height distance of seventy five, there exists a thirty five percent difference between low turbulence conditions and mock aero-combustor conditions.

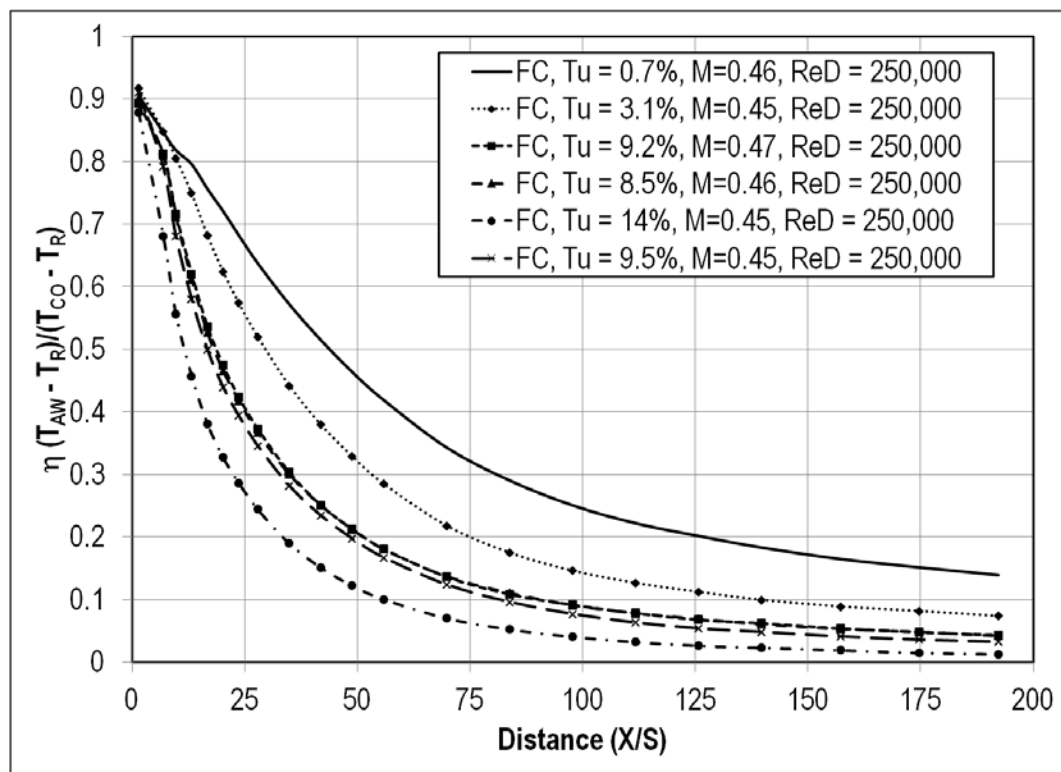


Figure 54. Effects of turbulence on adiabatic effectiveness for the large cyl. at ReD=250k and M=0.45.

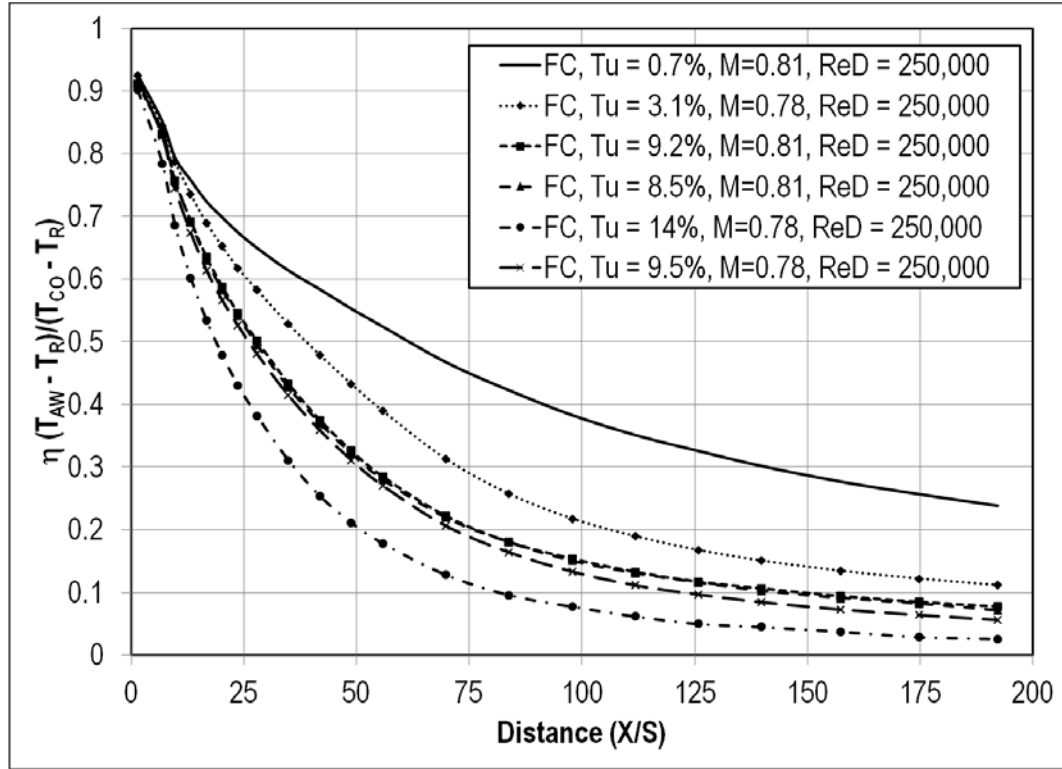


Figure 55. Effects of turbulence on adiabatic effectiveness for the large cyl. at $ReD=250k$ and $M=0.80$.

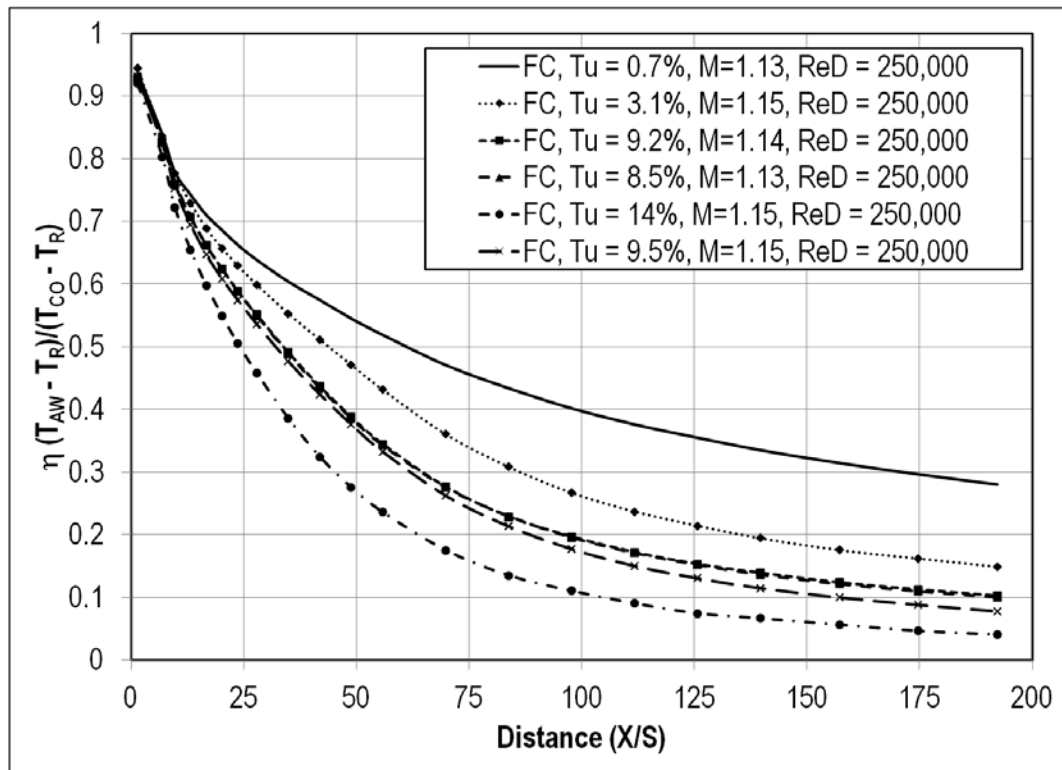


Figure 56. Effects of turbulence on adiabatic effectiveness for the large cyl. at $ReD=250k$ and $M=1.15$.

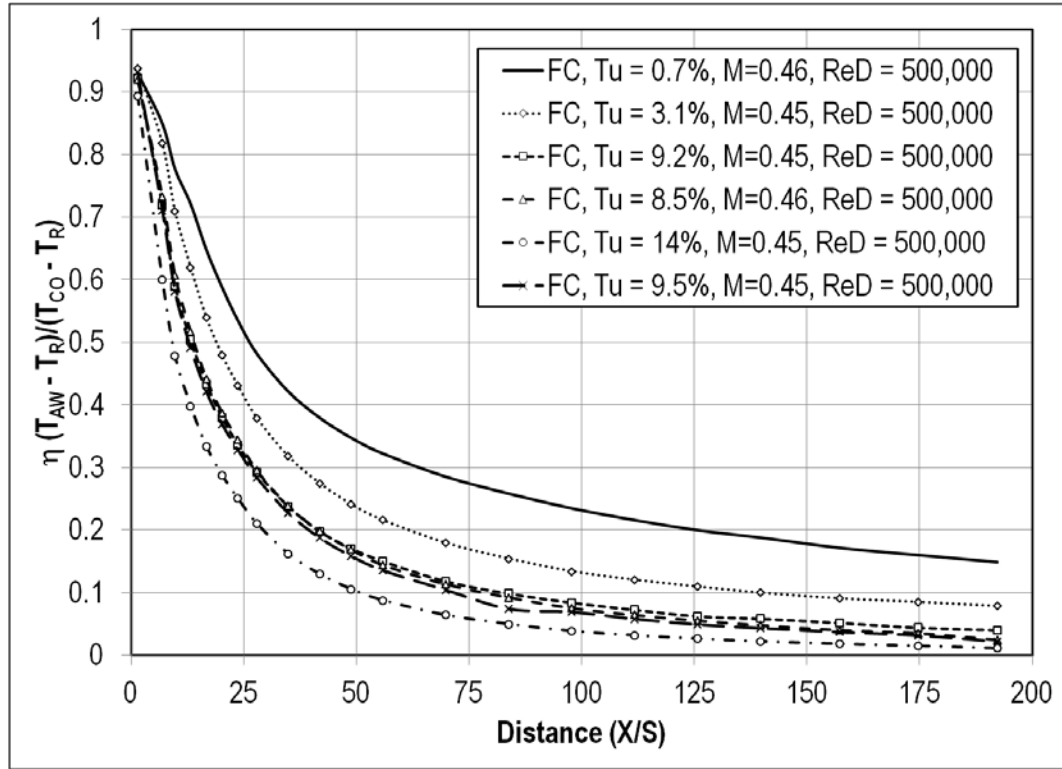


Figure 57. Effects of turbulence on adiabatic effectiveness for the large cyl. at $ReD=500k$ and $M=0.46$.

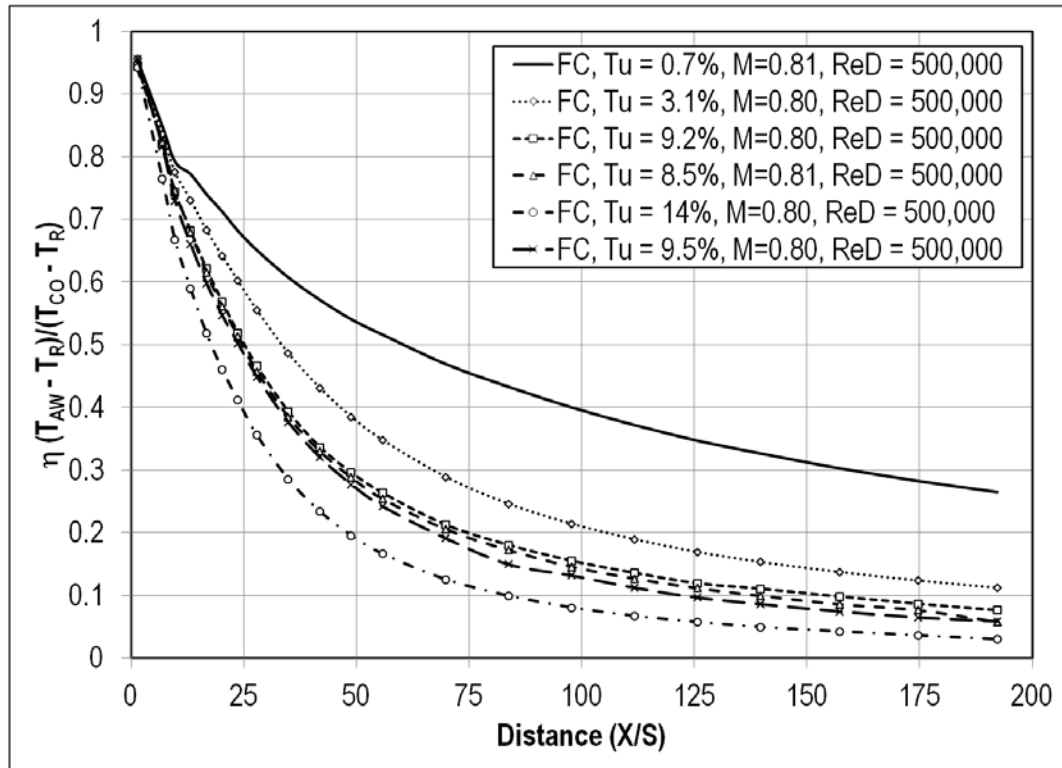


Figure 58. Effects of turbulence on adiabatic effectiveness for the large cyl. at $ReD=500k$ and $M=0.80$.

Adiabatic Effectiveness – Small Cylindrical Leading Edge Test Section

Effects of Blowing

Blowing ratio has a similar effect on the small cylindrical leading edge test section that was seen on the large cylindrical leading edge test section. The adiabatic effectiveness is increased with a larger blowing ratio. Once again, the highest blowing ratio has the highest effectiveness directly behind the ejection slot. The adiabatic effectiveness of the lowest blowing ratio of $M = 0.46$ drops off rapidly at a distance of approximately ten slot heights, and eventually starts to even off. This can be seen in Figure 59. In most cases, there is a difference in adiabatic effectiveness between the high blowing ratio of $M = 1.60$ and the low blowing ratio of $M = 0.46$ by twenty percent or more, as seen in Figure 60. By the end of the test surface, the difference in effectiveness between the high and low blowing ratio has been reduced to around ten percent. At the low turbulence intensity, the low blowing ratio has an efficiency of thirty percent at a slot height distance of about forty that the high blowing ratio has at a slot height distance of 185. At the small grid near turbulence intensity and effectiveness of thirty percent is achieved by the low blowing ratio at a slot height distance of about thirty, whereas the high blowing ratio has the same effectiveness at a slot height distance of about 115. Figure 61 shows the effects of blowing at the aero-combustor turbulence intensity. Here, the effectiveness behaves in a similar way as the small grid near turbulence condition, except that it has slightly smaller effectiveness values, especially downstream.

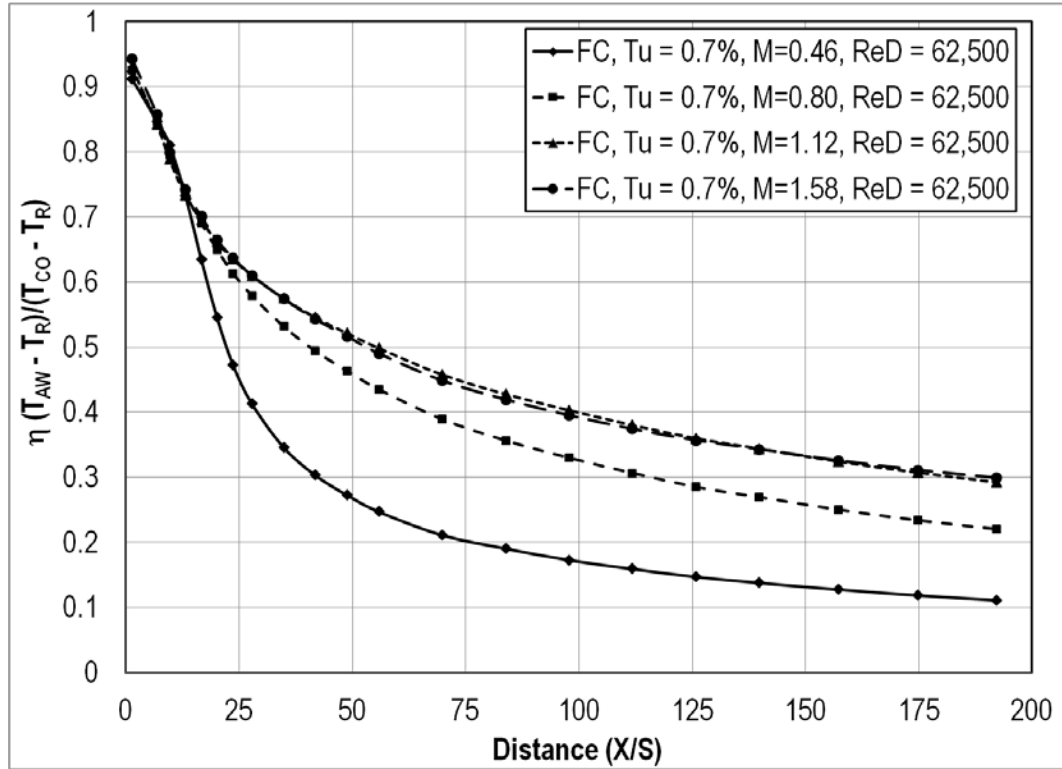


Figure 59. Effects of blowing ratio on adiabatic effectiveness for the small cyl. at low Tu.

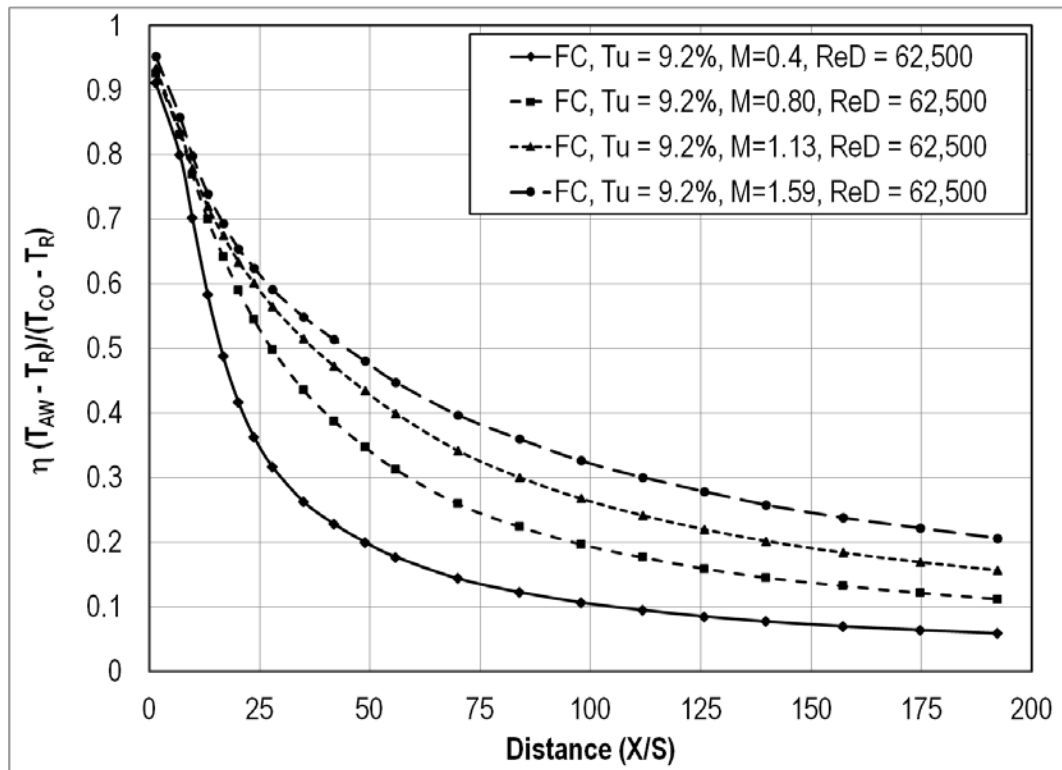


Figure 60. Effects of blowing ratio on adiabatic effectiveness for the small cyl. at small grid-near Tu.

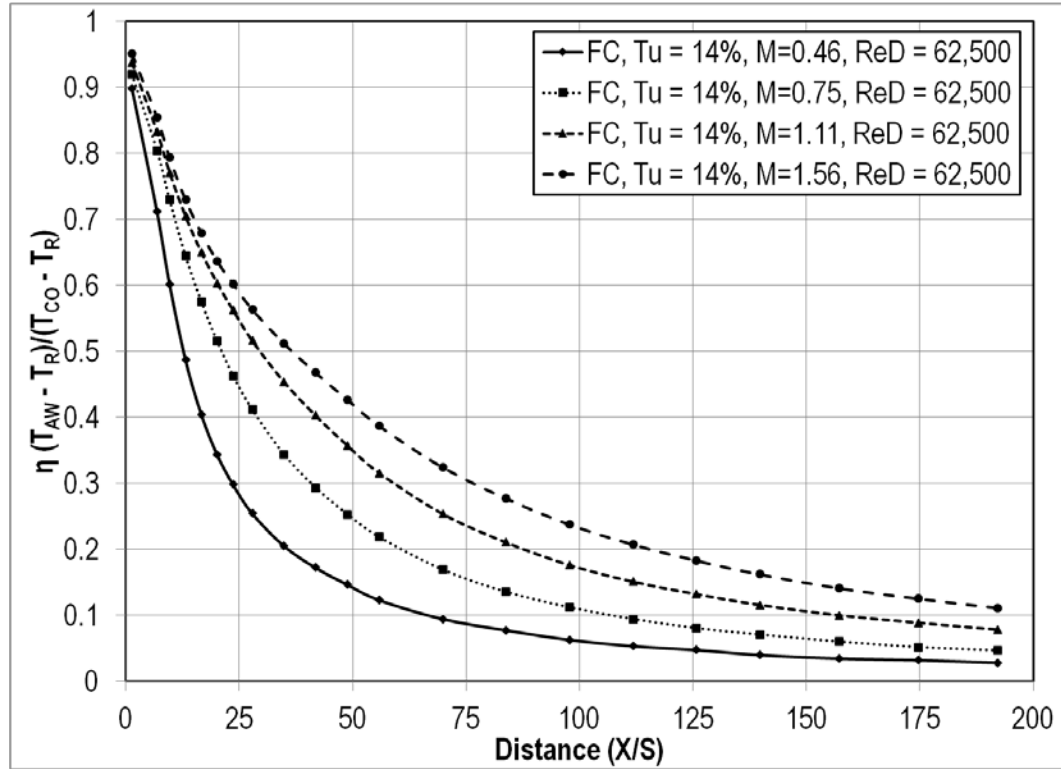


Figure 61. Effects of blowing ratio on adiabatic effectiveness for the small cyl. at aero combustor Tu.

Effects of Reynolds Number

The effects of Reynolds number on the adiabatic effectiveness for the small cylindrical leading edge were very similar to the effects of Reynolds number on the large cylindrical leading edge. For all cases, the adiabatic effectiveness was greater for the two blowing ratios at the highest Reynolds number, right behind the ejection slot. The low blowing ratio effectiveness at the high Reynolds number was almost always less than, or similar to the low Reynolds number at the same blowing ratio. In contrast, the effectiveness of the high blowing ratio at the high Reynolds number would usually match or be slightly greater than the effectiveness of the high blowing ratio at the low Reynolds number. This can be seen in Figures 62, 63, and 64. The difference between the two Reynolds numbers was greater for the low turbulence condition, as seen in Figure 62. For the large grid turbulence condition, an effectiveness of forty percent is achieved at

the high Reynolds number and low blowing ratio at a slot height distance of about twenty three, whereas the low Reynolds number and low blowing ratio has the same effectiveness at a slot height distance of twenty seven. That same effectiveness is achieved at the high Reynolds number and both blowing ratios at a distance of about fifty three. This can be seen in Figure 63. Figure 64 shows the effects of Reynolds number on effectiveness at the aero-combustor turbulence condition. There, there is very little difference between the two Reynolds numbers throughout the test section.

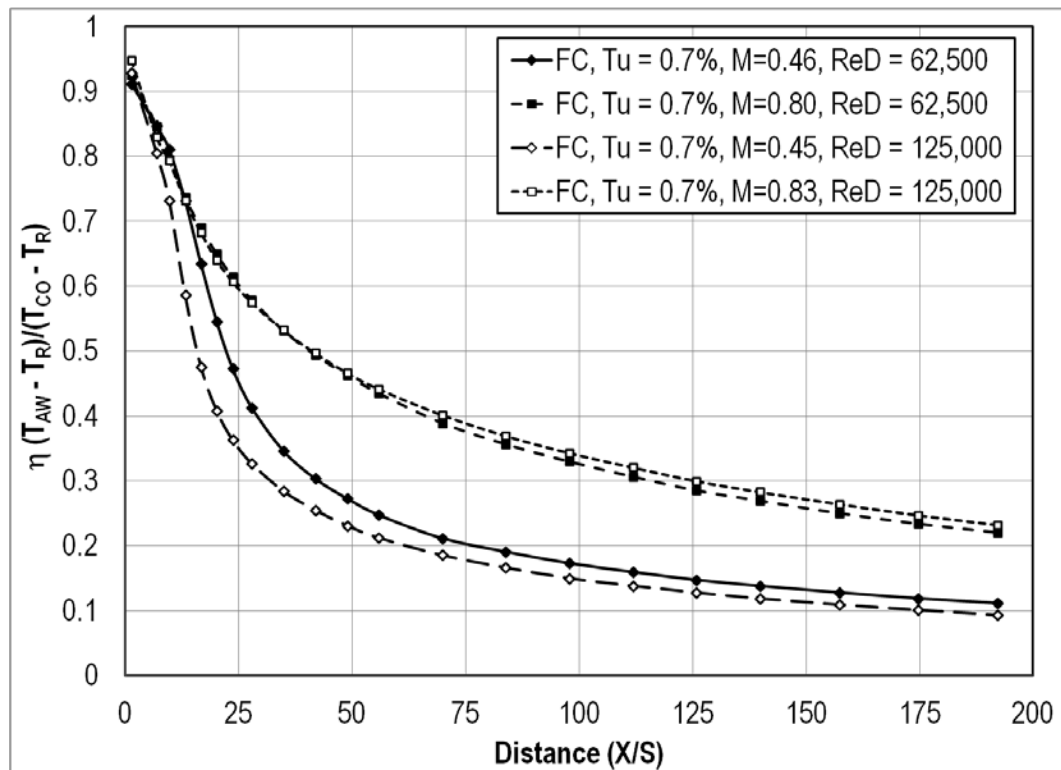


Figure 62. Effects of Reynolds number on adiabatic effectiveness for the small cyl. at low Tu

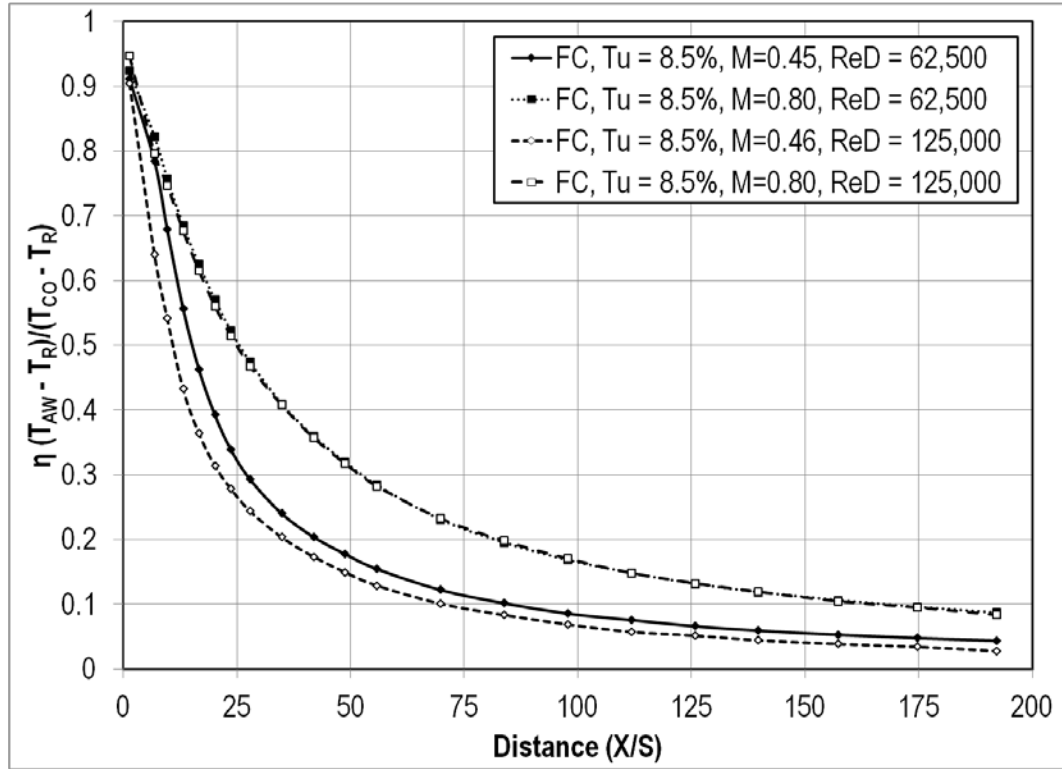


Figure 63. Effects of Reynolds number on adiabatic effectiveness for the small cyl. at large grid Tu

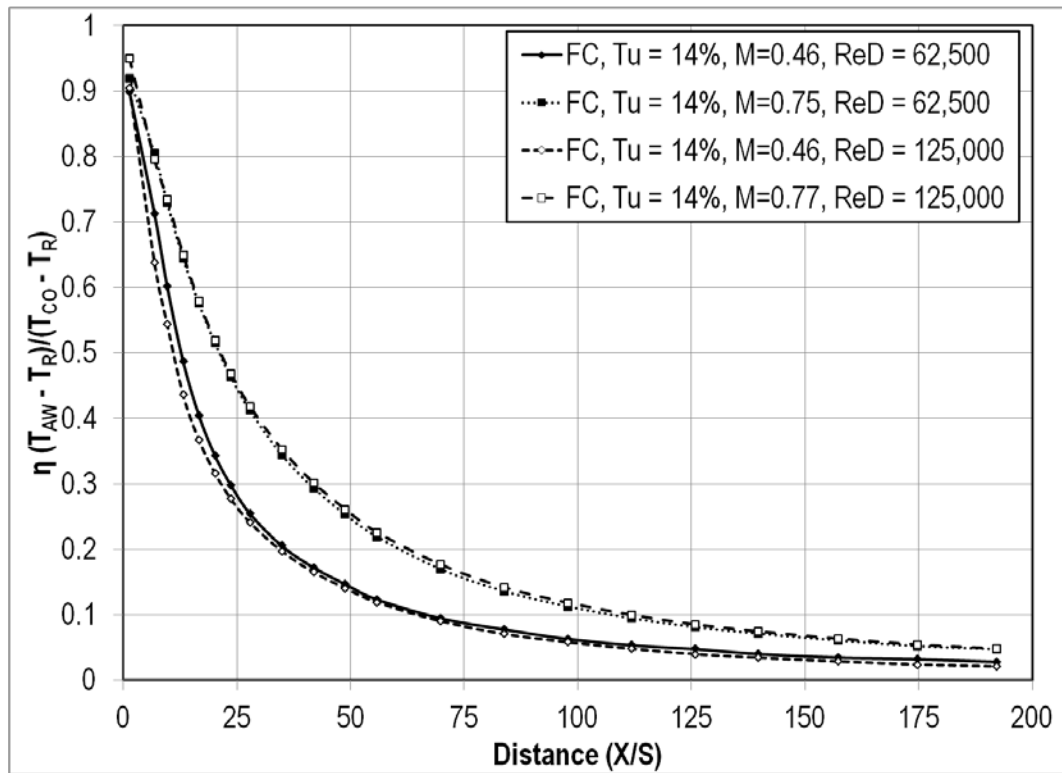


Figure 64. Effects of Reynolds number on adiabatic effectiveness for the small cyl. at aero combustor Tu

Effects of Turbulence

Film cooling adiabatic effectiveness is largely influenced by free stream turbulence intensity. A decrease in effectiveness was the result of an increase in turbulence intensity. At $M = 0.46$, $Re_D = 62,500$, and a slot height distance of fifty, there exists an effectiveness difference of about twenty percent between the low turbulence intensity and the aero combustor turbulence intensity as seen in Figure 65. Again, turbulence appears to shift the graph down and to the left, meaning that the effectiveness is lower, earlier on the test surface. Figure 66 shows how turbulence alters effectiveness at low Reynolds number and the second lowest blowing ratio. Here, effectiveness values are higher than in Figure 65, at the lowest blowing ratio. Figure 67 shows similar results for the second highest blowing ratio. Here, there is a ten percent difference in effectiveness between the highest and lowest turbulence intensity at a slot height distance of fifty. This shift in the effectiveness is also seen at $Re_D = 125,000$. At $M = 1.12$ and $Re_D = 12,500$, an effectiveness of thirty percent is achieved for the low turbulence intensity at a slot height distance of approximately 185, whereas the same effectiveness is achieved for the aero combustor at a slot height distance of sixty, as seen in Figure 68. Figure 69 show similar results for the high blowing ratio at the high Reynolds number. Once again, there exists a difference in effectiveness of about ten percent at a slot height distance of fifty.

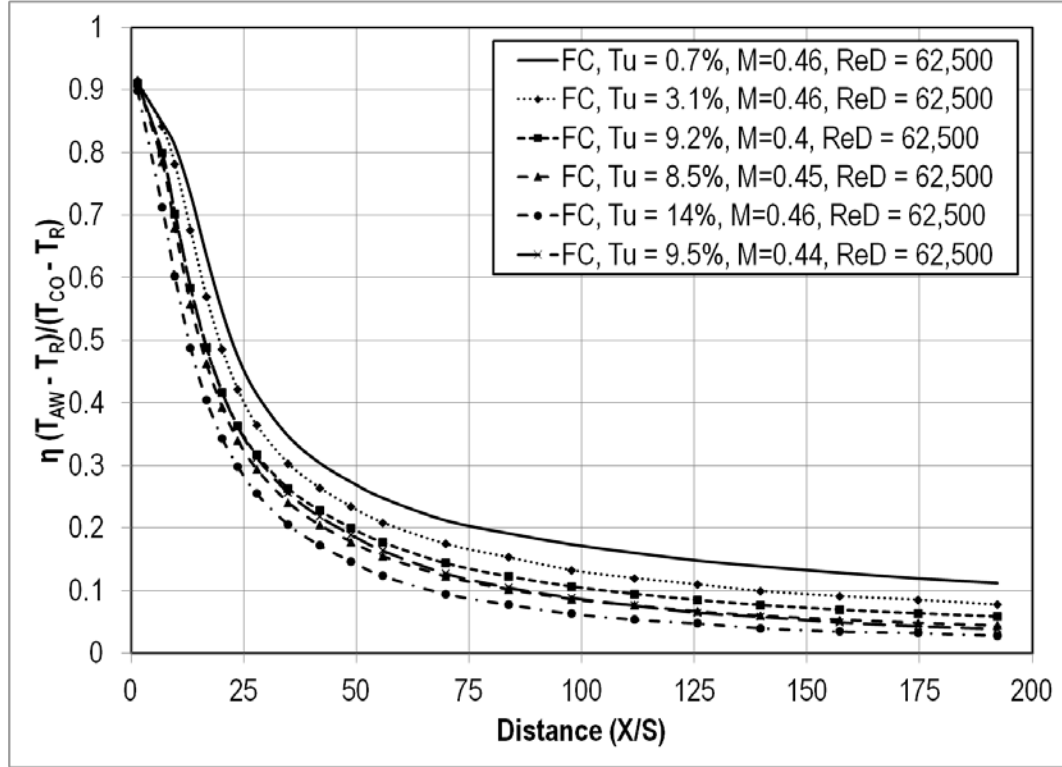


Figure 65. Effects of turbulence on adiabatic effectiveness for the small cyl. at ReD=62.5k and M=0.46.

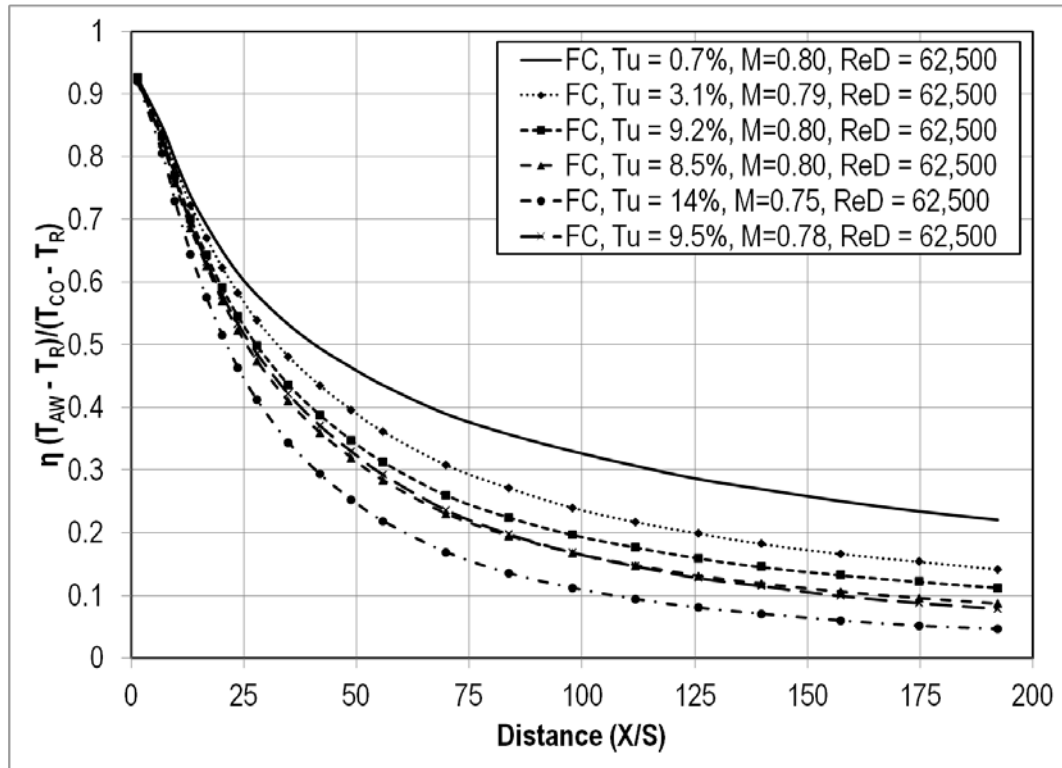


Figure 66. Effects of turbulence on adiabatic effectiveness for the small cyl. at ReD=62.5k and M=0.80.

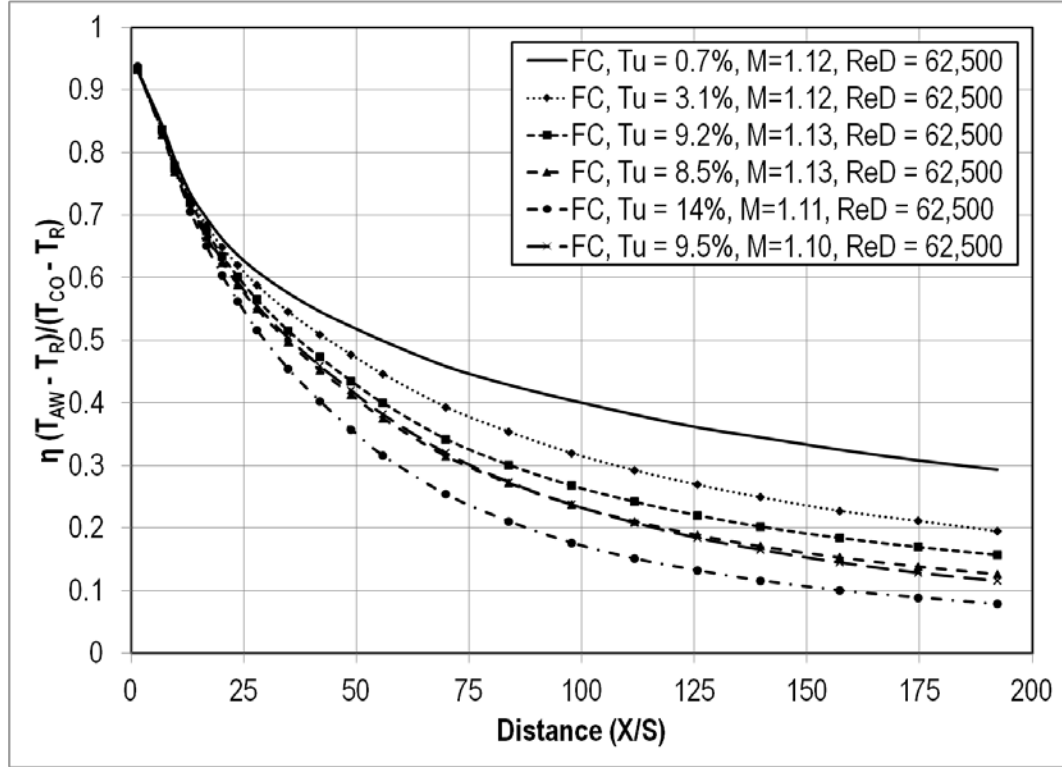


Figure 67. Effects of turbulence on adiabatic effectiveness for the small cyl. at $ReD=62.5k$ and $M=1.12$.

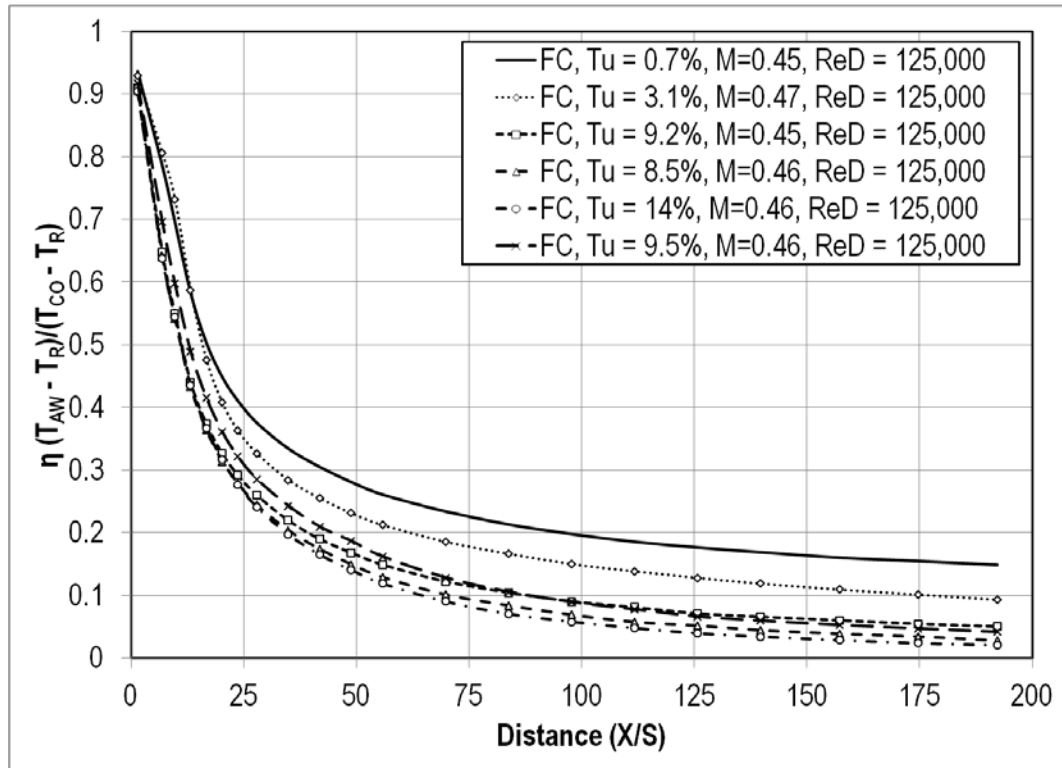


Figure 68. Effects of turbulence on adiabatic effectiveness for the small cyl. at $ReD=125k$ and $M=0.45$.

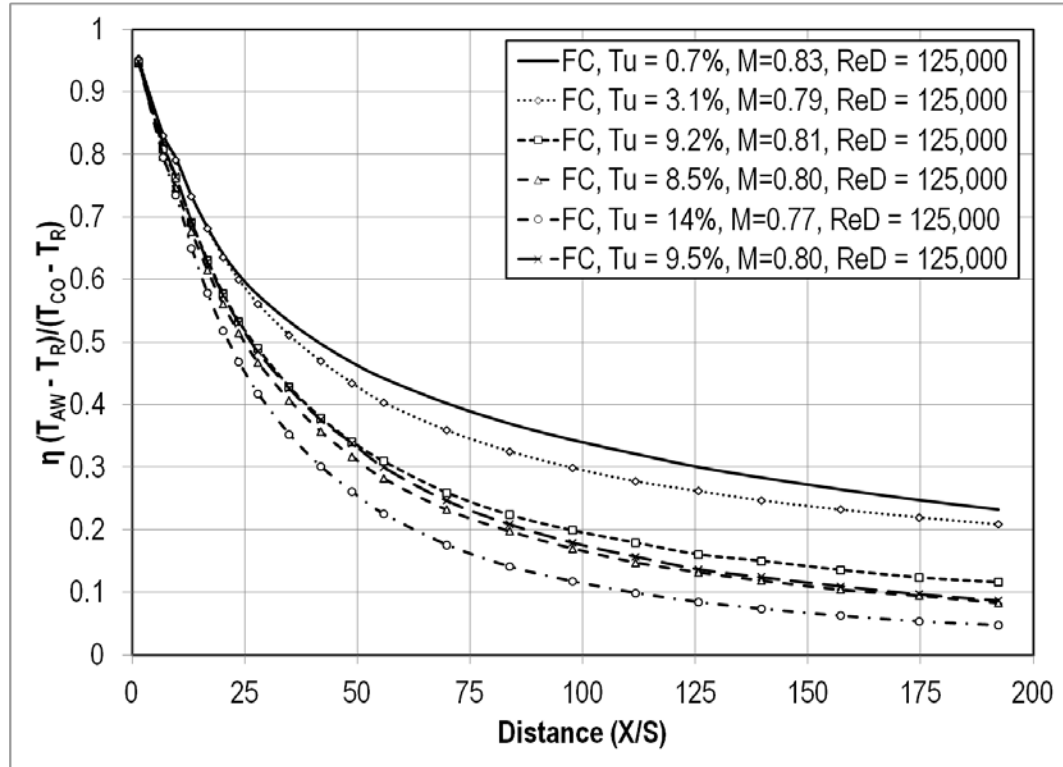


Figure 69. Effects of turbulence on adiabatic effectiveness for the small cyl. at ReD=125k and M=0.80.

Comparison of Adiabatic Effectiveness Between the Two Test Sections

A direct comparison between the adiabatic effectiveness of the two cylindrical leading edge test sections reveals that the large test section has both the highest and lowest effectiveness at low blowing ratios. Figure 70 shows the different turbulence intensities at the low blowing ratio and low Reynolds number of both test sections. Here, the effectiveness values for the small test section are generally higher after a slot height distance of about one hundred. Figure 71 is the same plot, but at the high Reynolds number. This plot is shifted slightly to the left of Figure 70, meaning that the effectiveness values are small earlier on. Figure 72 is a plot that shows turbulence intensities for both test sections at the low Reynolds number and second lowest blowing ratio. This plot is shifted up and to the left of Figure 70, meaning that the values for

effectiveness are higher farther downstream. Figure 73 shows turbulence intensities for both test sections at the high Reynolds number and second lowest blowing ratio. This graph shows effectiveness values for the small cylindrical leading edge test section higher than those of the larger test section for many of the turbulence intensities. This suggests that at higher blowing ratios and Reynolds numbers, the smaller test section could be more effective than the large test section. This may be due to the acceleration around the cylinder. The continued acceleration of the flow around the small cylindrical leading edge test section could help to keep the coolant film attached to the surface, increasing effectiveness. In the following figures, the solid lines represent values for the large cylindrical test section while the dashed lines represent values for the small cylindrical test section.

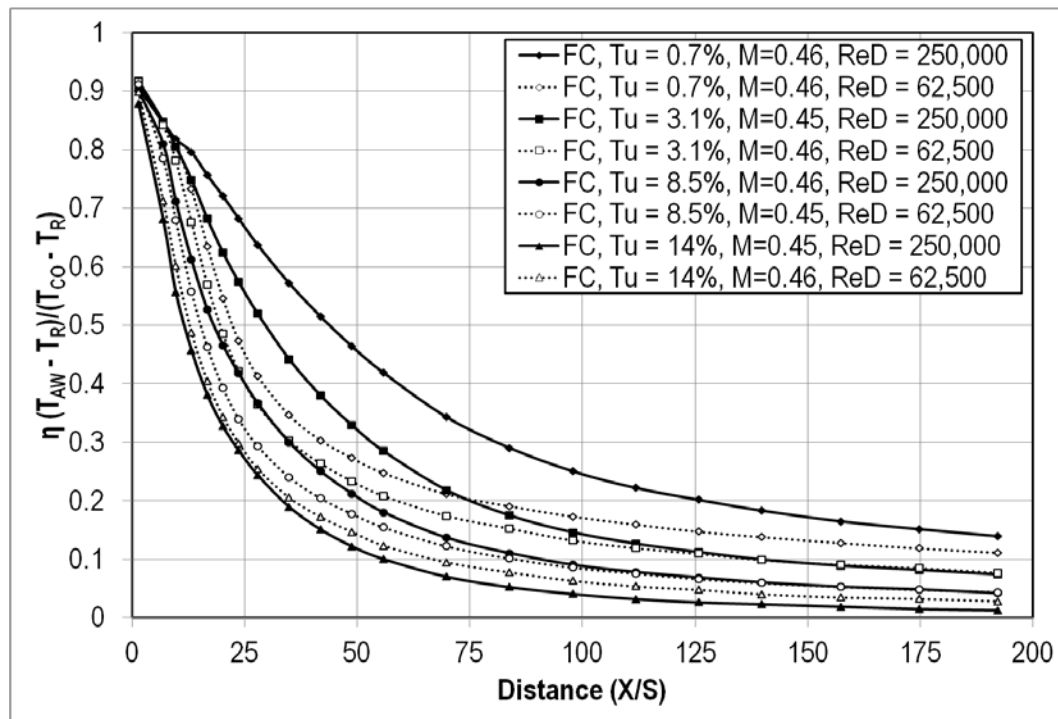


Figure 70. Comparison of test section adiabatic effectiveness at low ReD and M=0.46.

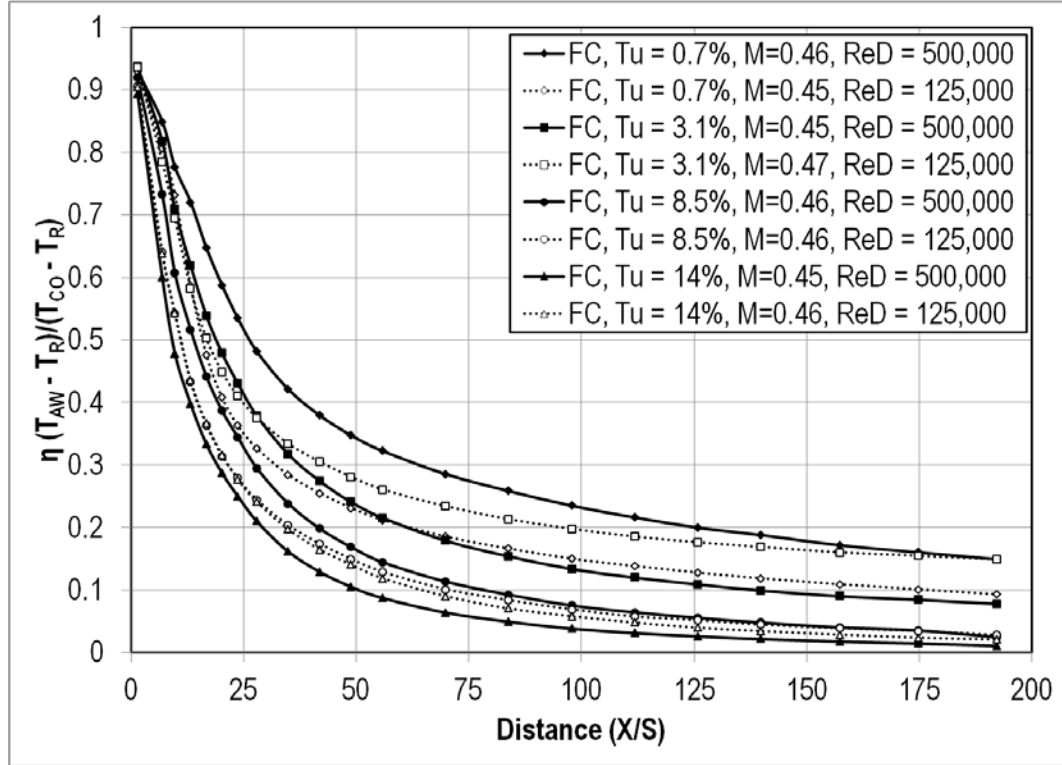


Figure 71. Comparison of test section adiabatic effectiveness at high ReD and $M=0.46$.

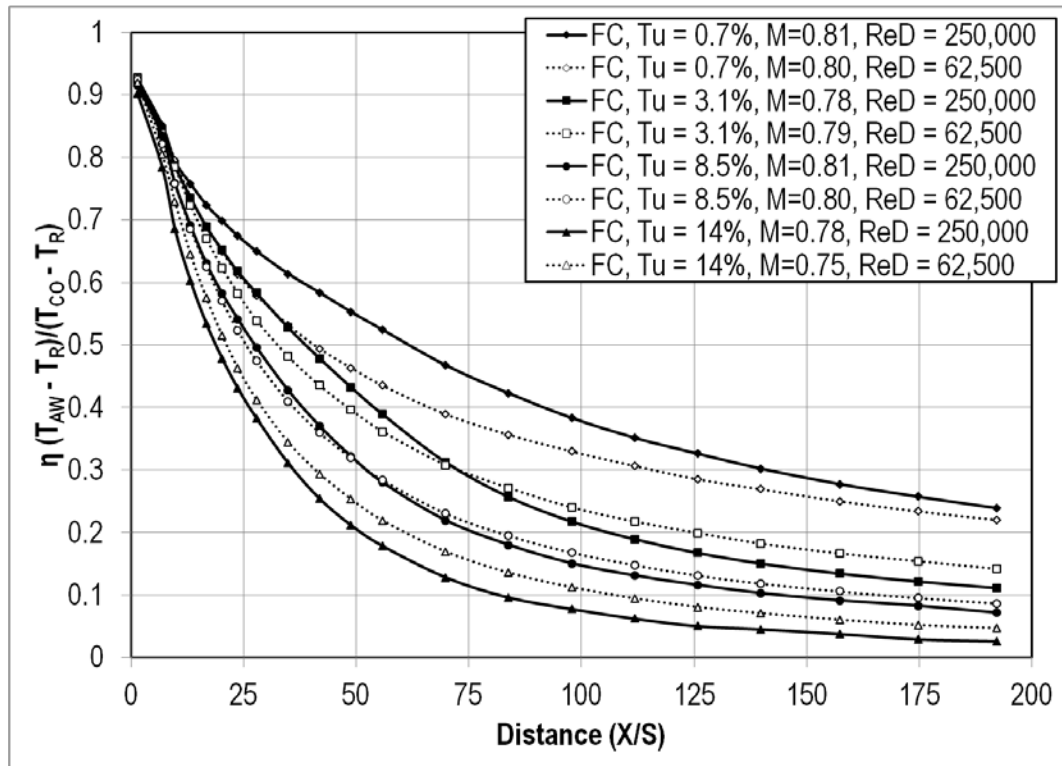


Figure 72. Comparison of test section adiabatic effectiveness at low ReD and $M=0.80$.

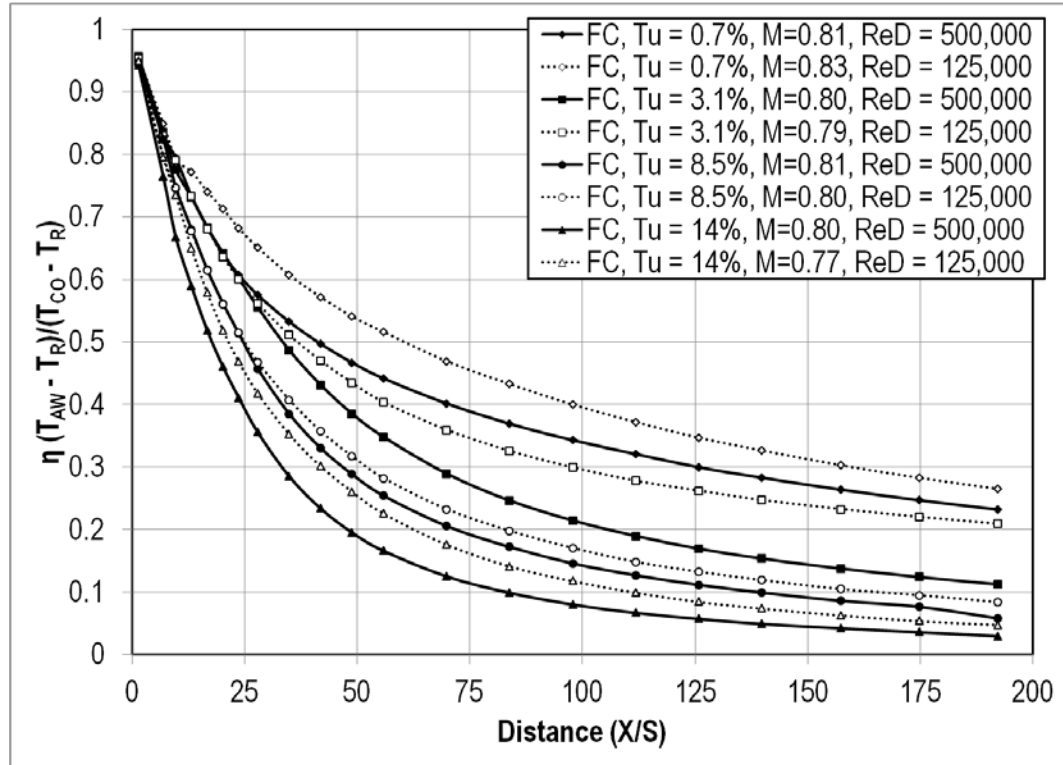


Figure 73. Comparison of test section adiabatic effectiveness at high ReD and M=0.80.

Heat Transfer – Large Cylindrical Leading Edge Test Section

Effects of Blowing

An increase in blowing ratio correlates to an increase in the Stanton number. The highest values of Stanton number were achieved by the data sets with the highest blowing ratio of $M = 1.60$. The lowest Stanton number values were achieved by the no blowing cases. This can be seen in Figure 74. In most cases, the Stanton number would reach a minimum at a slot height distance of around fifty, and then recover some before leveling off, as seen in Figure 75. The Stanton number at the end of the large cylindrical test section was around 0.0022 for the small grid far turbulence condition. Figure 76 shows the effects of blowing ratio on Stanton number for the mock aero-combustor. Here, the values for Stanton number level off sooner, at a value of about 0.0025.

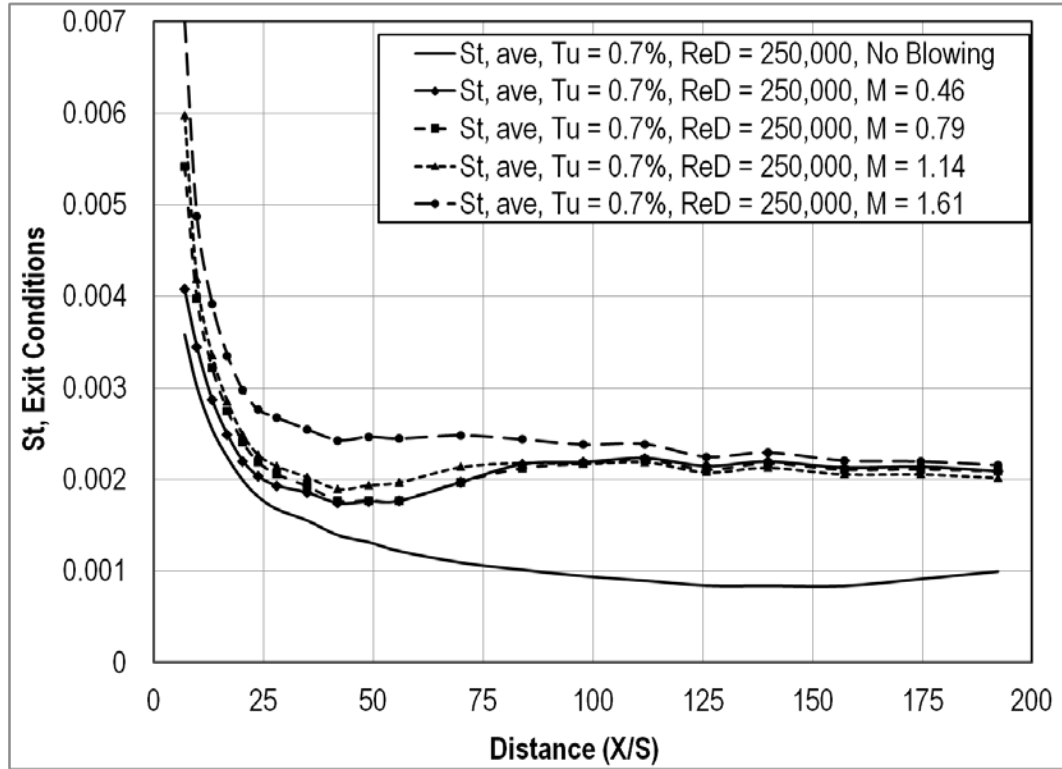


Figure 74. Effects of blowing ratio on Stanton number at low Tu and $ReD=250k$.

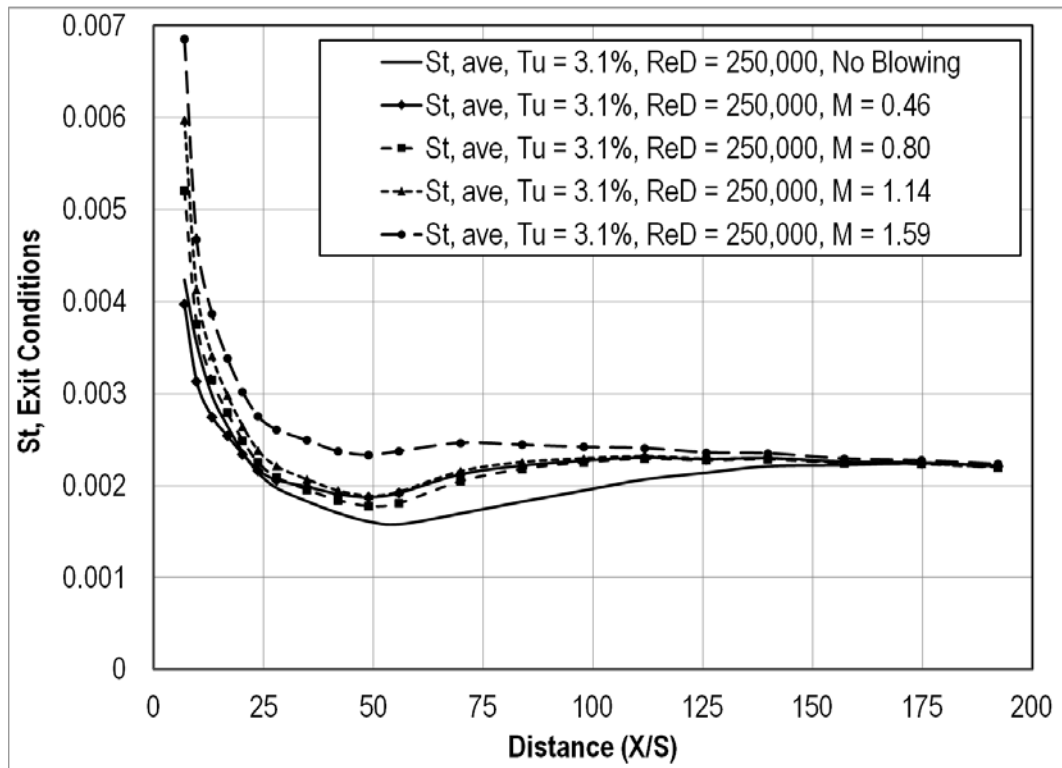


Figure 75. Effects of blowing on Stanton number at small grid-far Tu and $ReD=250k$.

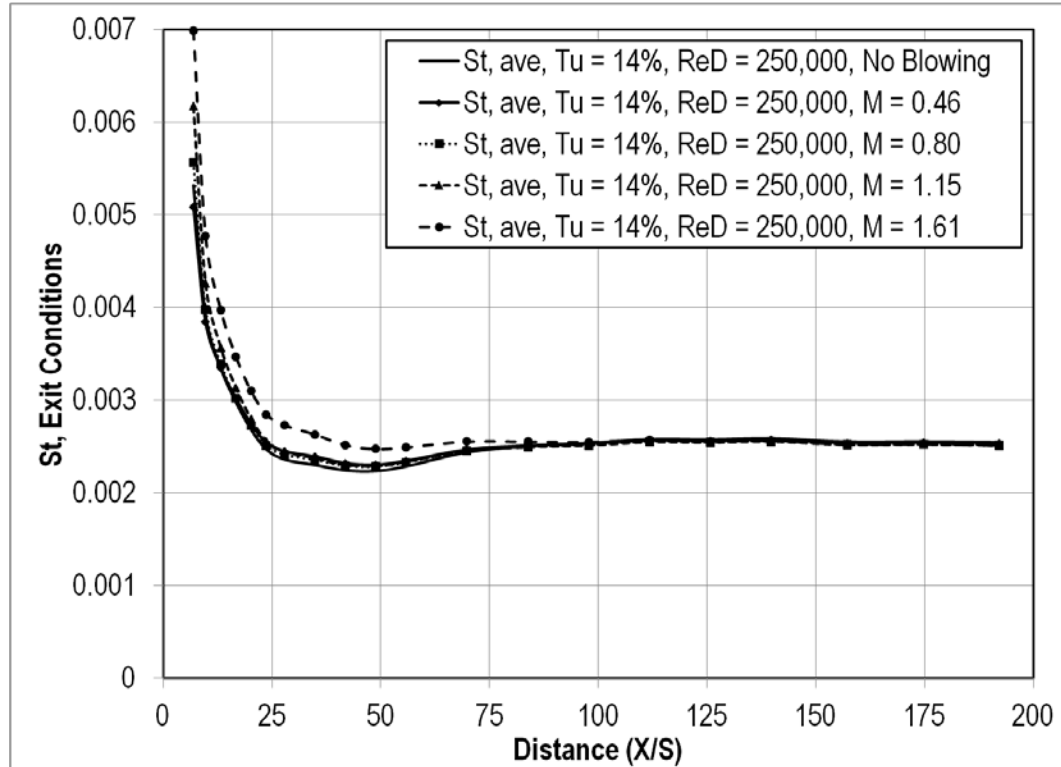


Figure 76. Effects of blowing on Stanton number at aero combustor T_u and $ReD=250k$.

Effects of Reynolds Number

Increasing from $ReD = 250,000$ to $ReD = 500,000$ generally decreased the Stanton number. This can be seen close to the ejection slot and farther downstream. But at a slot height distance of around fifty, the higher Reynolds number has a higher Stanton number. The higher Reynolds numbers also tend to reach their minimum Stanton number sooner, and level off faster. This behavior can be seen in Figures 77, 78, and 79. The minimum Stanton number at the high Reynolds number occurs at a slot height distance of less than twenty five, where the low Reynolds number reaches a minimum around a slot height of fifty.

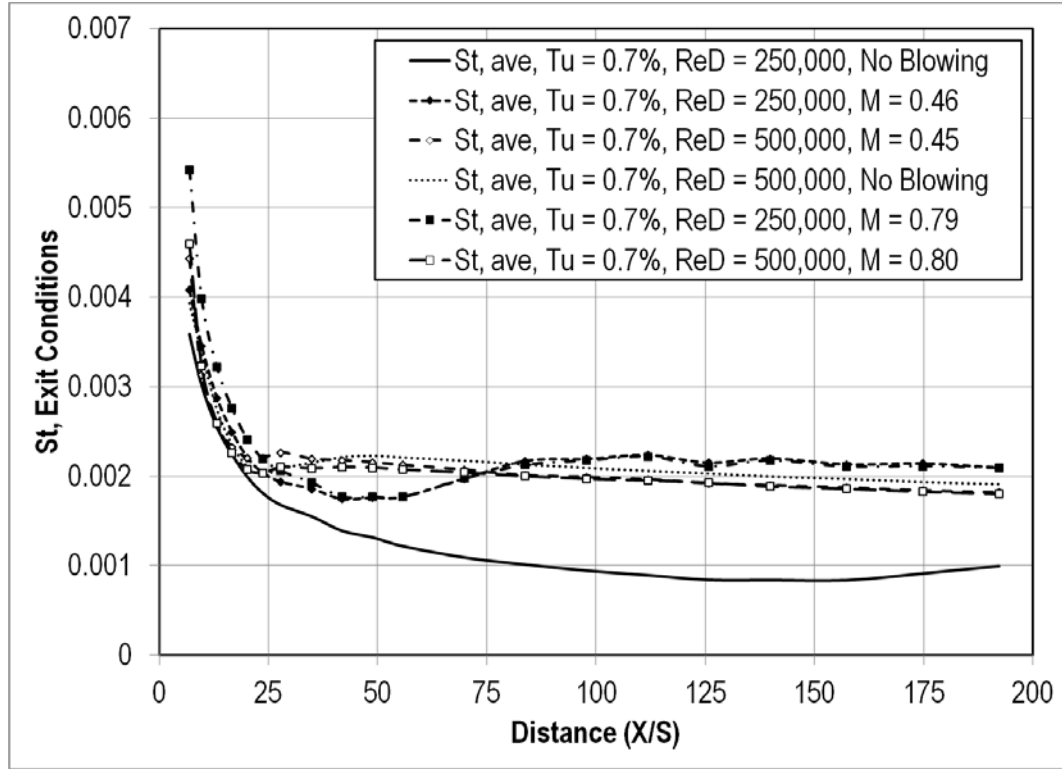


Figure 77. Effects of ReD on Stanton number at low Tu .

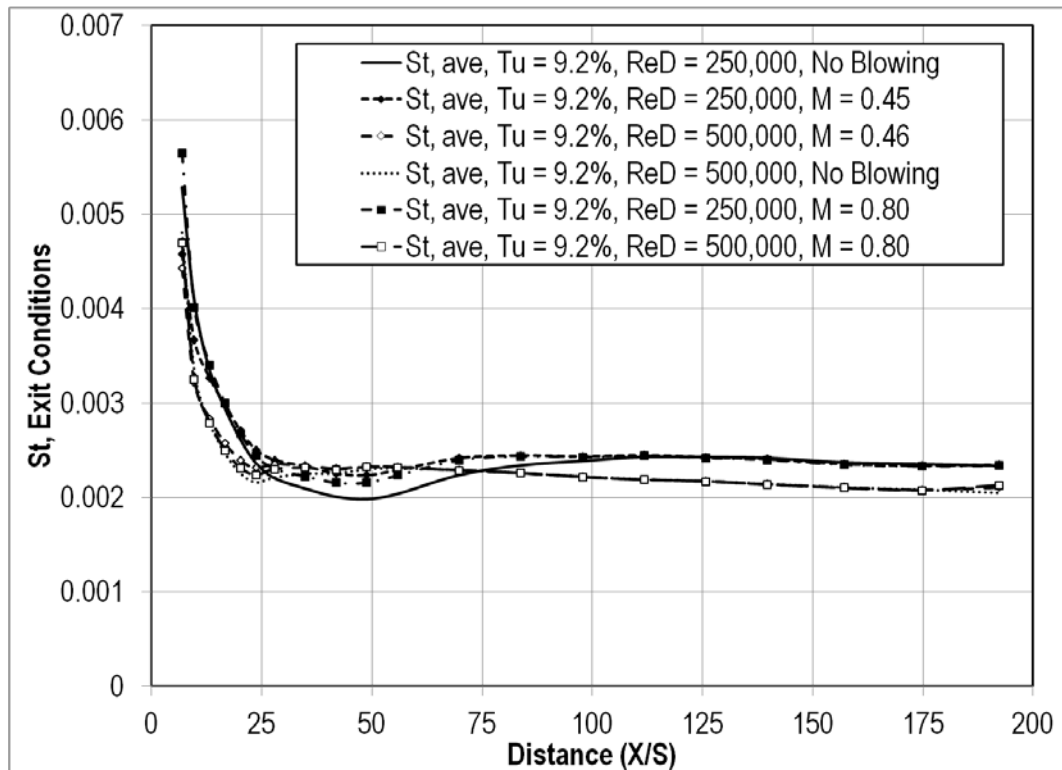


Figure 78. Effects of ReD on Stanton number at small grid-near Tu .

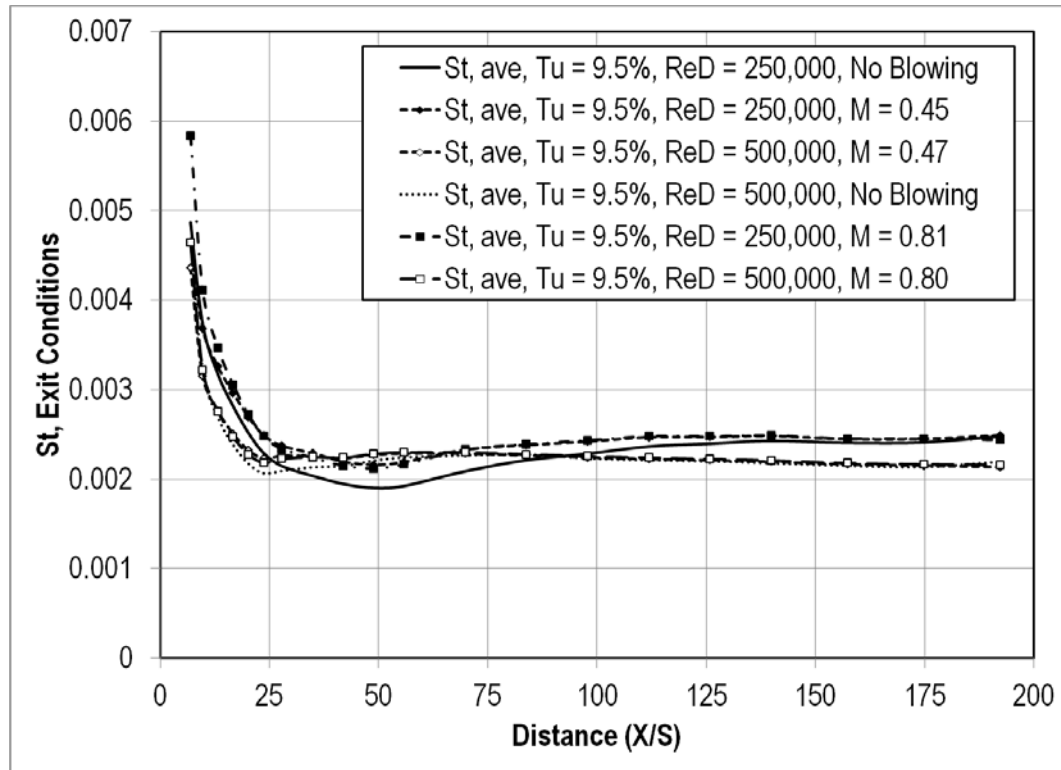


Figure 79. Effects of ReD on Stanton number at aero combustor-spool Tu.

Effects of Turbulence

Larger turbulence intensities appear to have larger Stanton numbers. The mock aero combustor turbulence intensity has about a twenty two percent increase in Stanton number over the no blowing case, and approximately a fourteen percent increase over the low turbulence intensity, as seen in Figures 80, 81, and 82. Figure 80 shows the Stanton number at low Reynolds number and the lowest blowing ratio. When the blowing ratio is increased in Figure 81, the Stanton number has a higher maximum value directly behind the ejection slot. Figure 82 shows the same plot but at the second highest blowing ratio. Again, the higher turbulence conditions have the higher values for Stanton number downstream, whereas the low turbulence condition as the smaller value for Stanton number. The increased Stanton number due to turbulence appears to be true for the increased Reynolds number as seen in Figures 83 and 84. Figure 83 shows the effects of

turbulence intensity on Stanton number at the high Reynolds number and low blowing ratio, while Figure 84 shows similar effects at the high Reynolds number and high blowing ratio. Here, the mock aero combustor has a twenty three percent increase in Stanton number over the no blowing case, and about a twelve percent increase over the low turbulence intensity near the end of the measured test section. At the increased Reynolds numbers, the higher turbulence conditions have a higher minimum value for Stanton number than the low turbulence conditions.

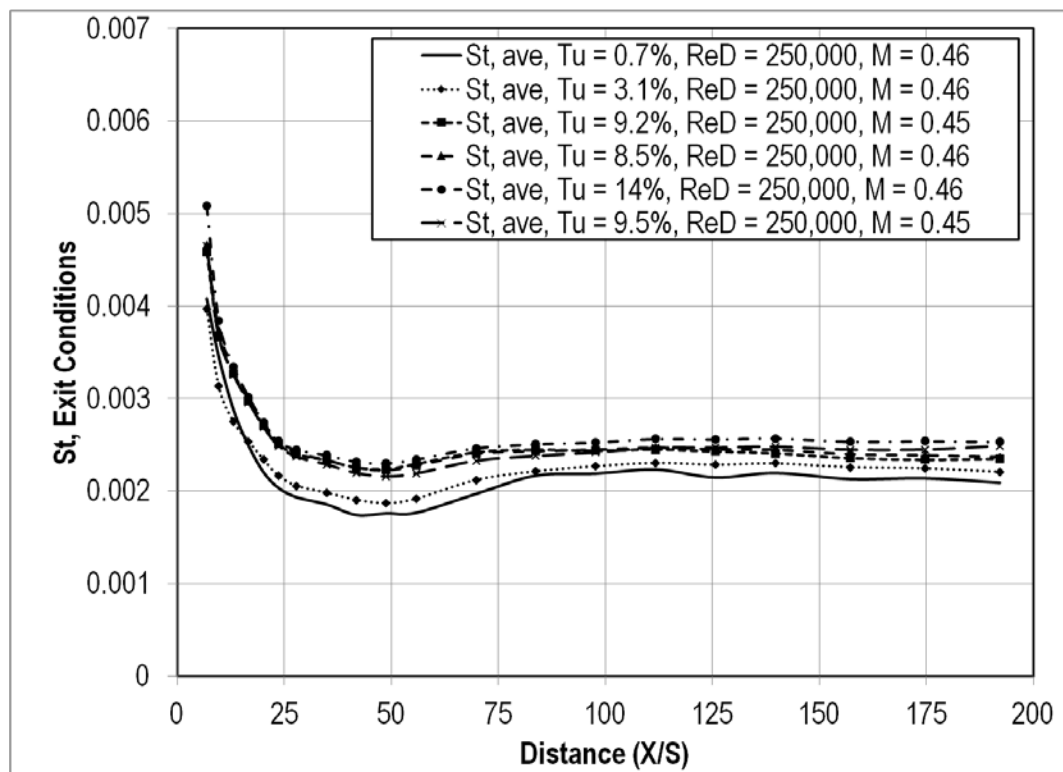


Figure 80. Effects of turbulence intensity on Stanton number at $ReD=250k$ and $M=0.46$.

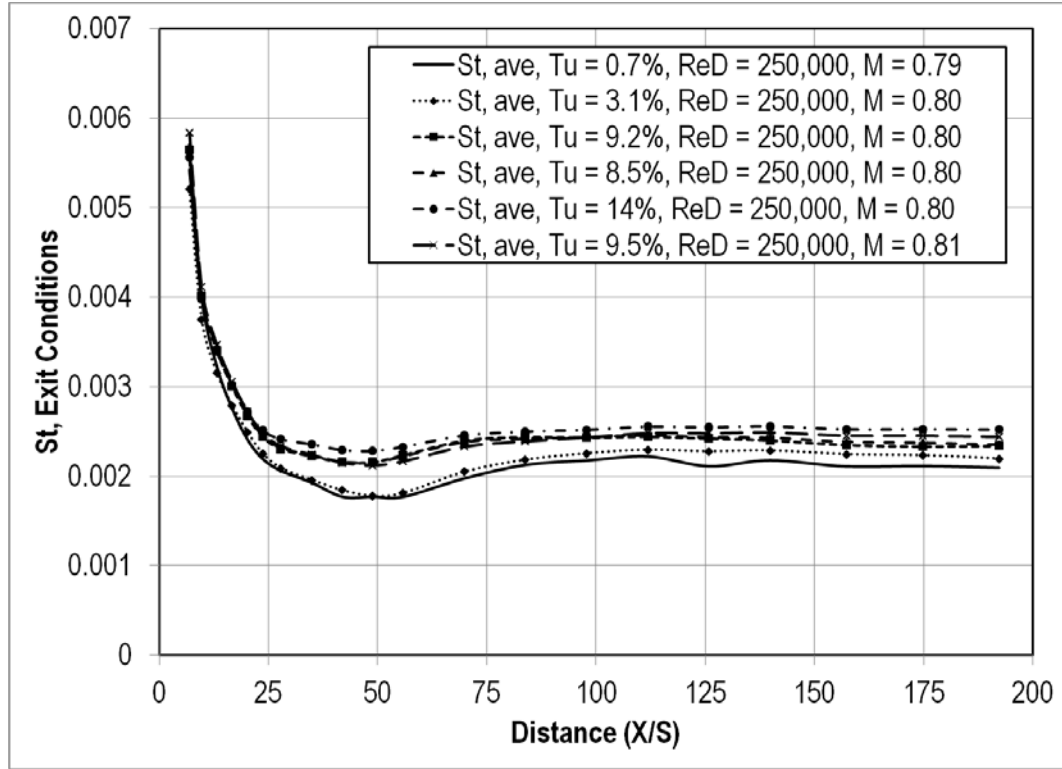


Figure 81. Effects of turbulence intensity on Stanton number at $ReD=250k$ and $M=0.80$.

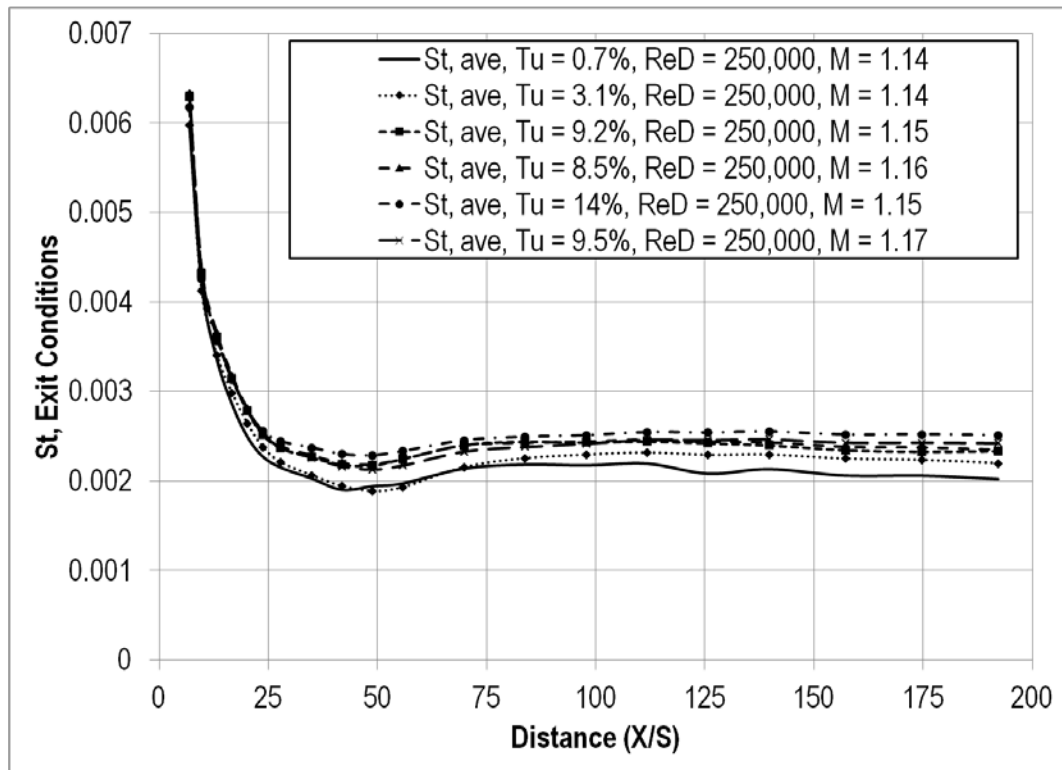


Figure 82. Effects of turbulence intensity on Stanton number at $ReD=250k$ and $M=1.14$.

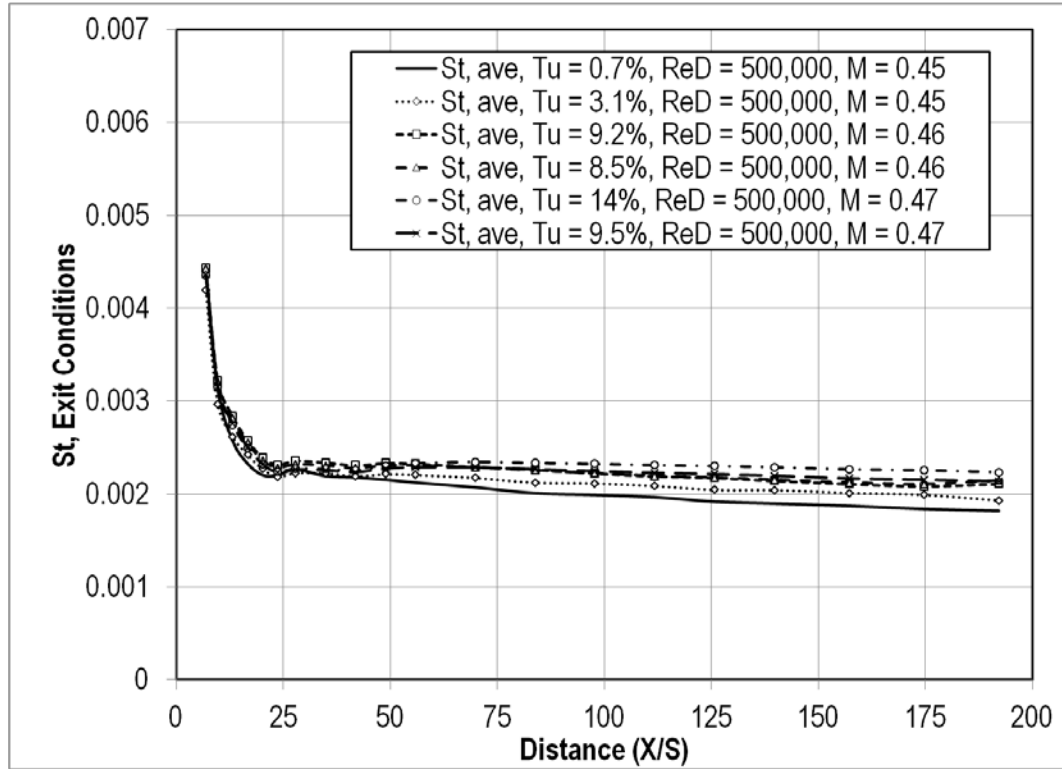


Figure 83. Effects of turbulence intensity on Stanton number at $ReD=500k$ and $M=0.46$.

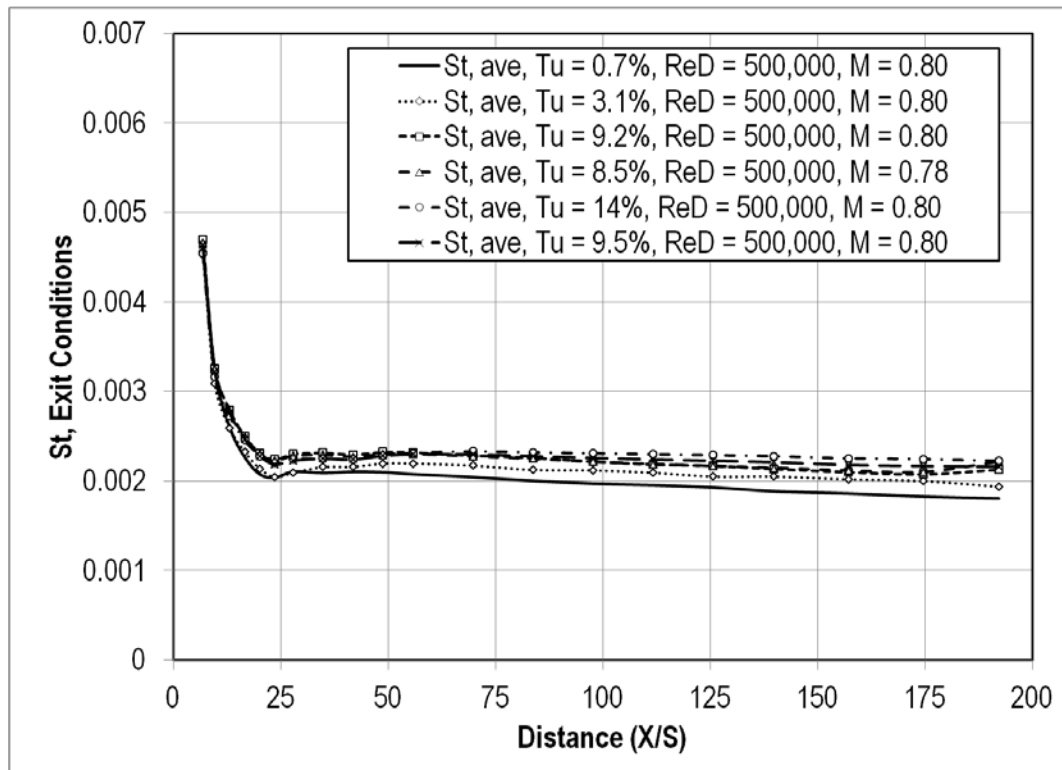


Figure 84. Effects of turbulence intensity on Stanton number at $ReD=500k$ and $M=0.80$.

Heat Transfer – Small Cylindrical Leading Edge Test Section

Effects of Blowing

For the small cylindrical leading edge test section, it has been shown that increasing the blowing ratio increases the Stanton number. The effect of the increase is determined by the slot height distance from the ejection slot. There exists a large increase in Stanton number right behind the ejection slot, almost doubling in some cases as seen in Figure 85. But farther downstream, the effects of blowing aren't as noticeable. This change in Stanton number between the blowing ratios happens at a slot height distance of approximately seventy five for most cases. Figure 86 shows the effects of blowing on Stanton number at the second lowest turbulence intensity, while Figure 87 shows similar effects at the highest turbulence intensity. The similarities of the blowing ratios downstream could mean that the film cooling has mixed into the freestream.

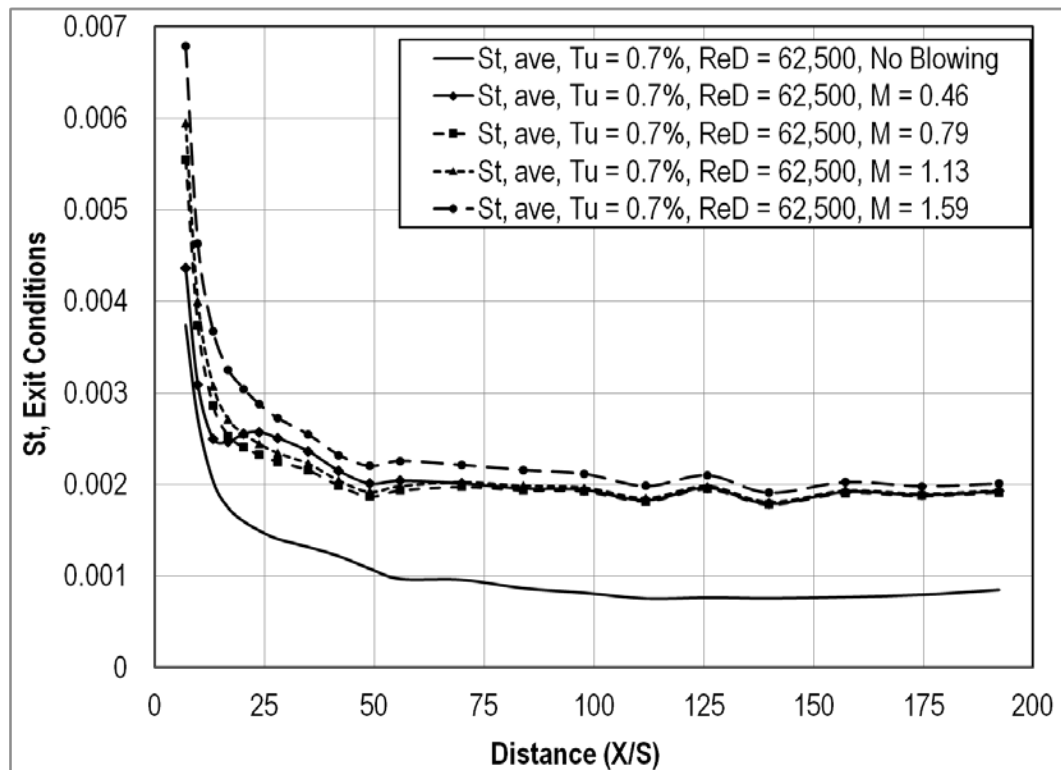


Figure 85. Effects of blowing ratio on Stanton number at low Tu and ReD=62.5k.

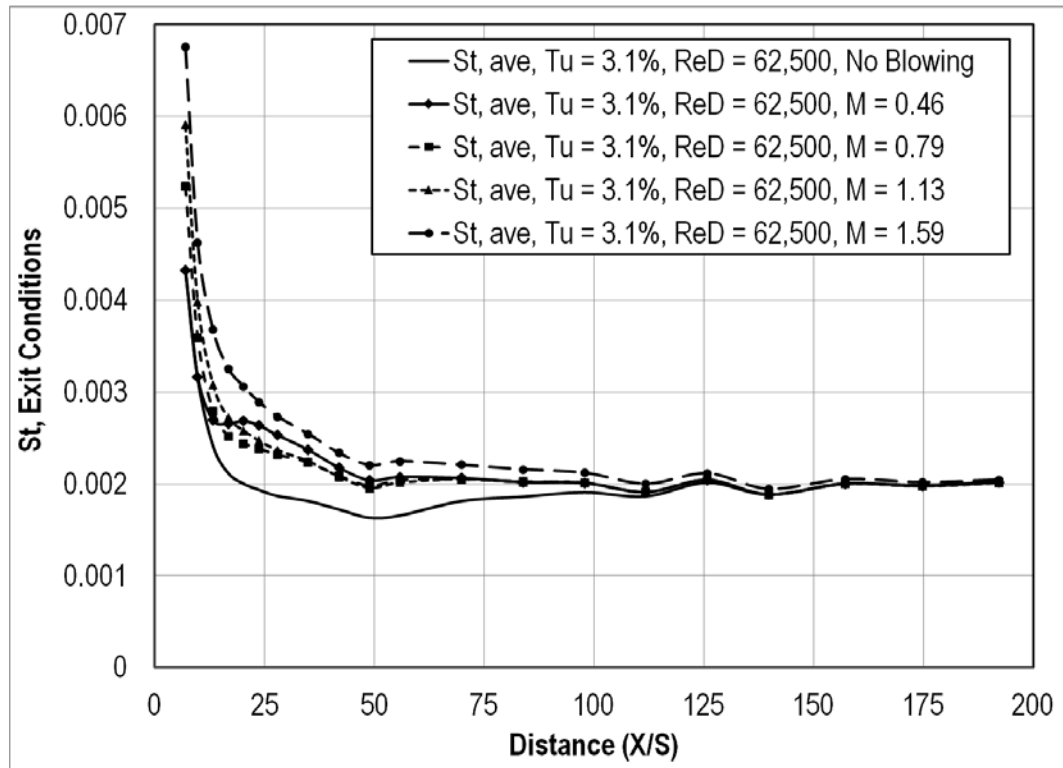


Figure 86. Effects of blowing ratio on Stanton number at small grid-far and $ReD=62.5k$.

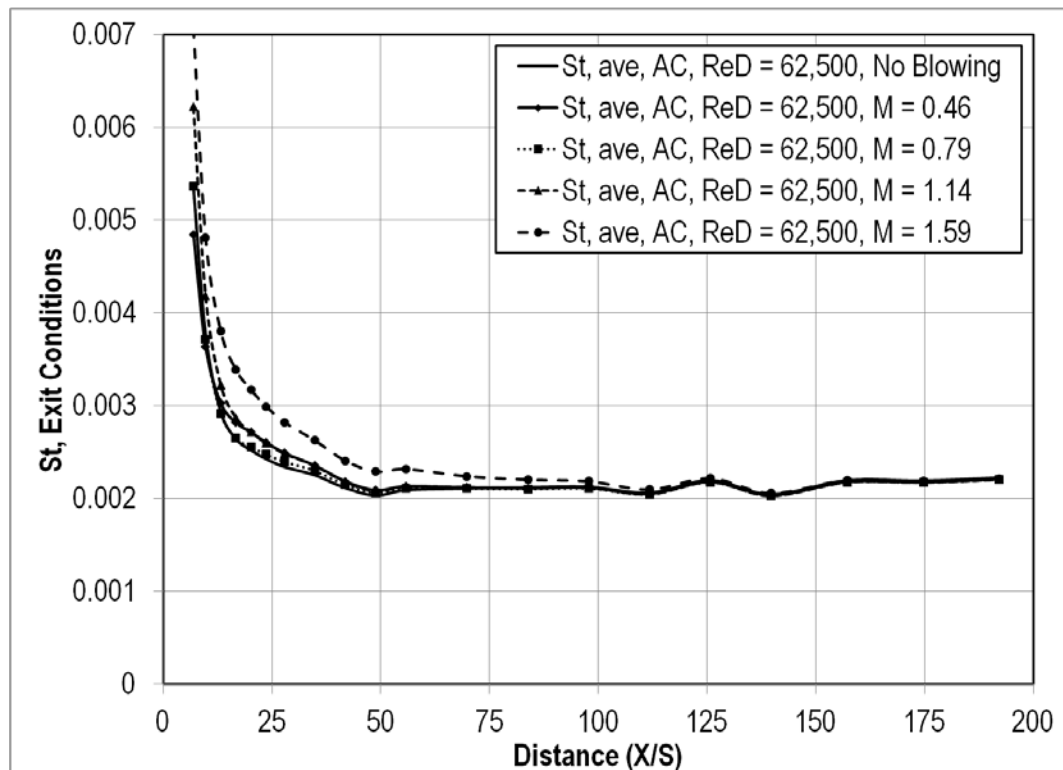


Figure 87. Effects of blowing ratio on Stanton number at aero combustor and $ReD=62.5k$.

Effects of Reynolds Number

Higher Reynolds numbers appear to have a negative effect on the Stanton number. In most cases, the Stanton number for the high Reynolds number is noticeably less close to the coolant ejection slot as seen in Figures 88 and 89. Downstream, however, the Stanton number appears to be very similar if not the same as the low Reynolds number values. The downstream value of the Stanton number was around 0.0018 for the low turbulence condition. The small grid near turbulence condition had a downstream Stanton number around 0.002 as seen in Figure 89. In Figure 90, the high Reynolds number has a higher starting value for Stanton number. Increasing the Reynolds number has the added effect of reaching the minimum Stanton number earlier and leveling off sooner.

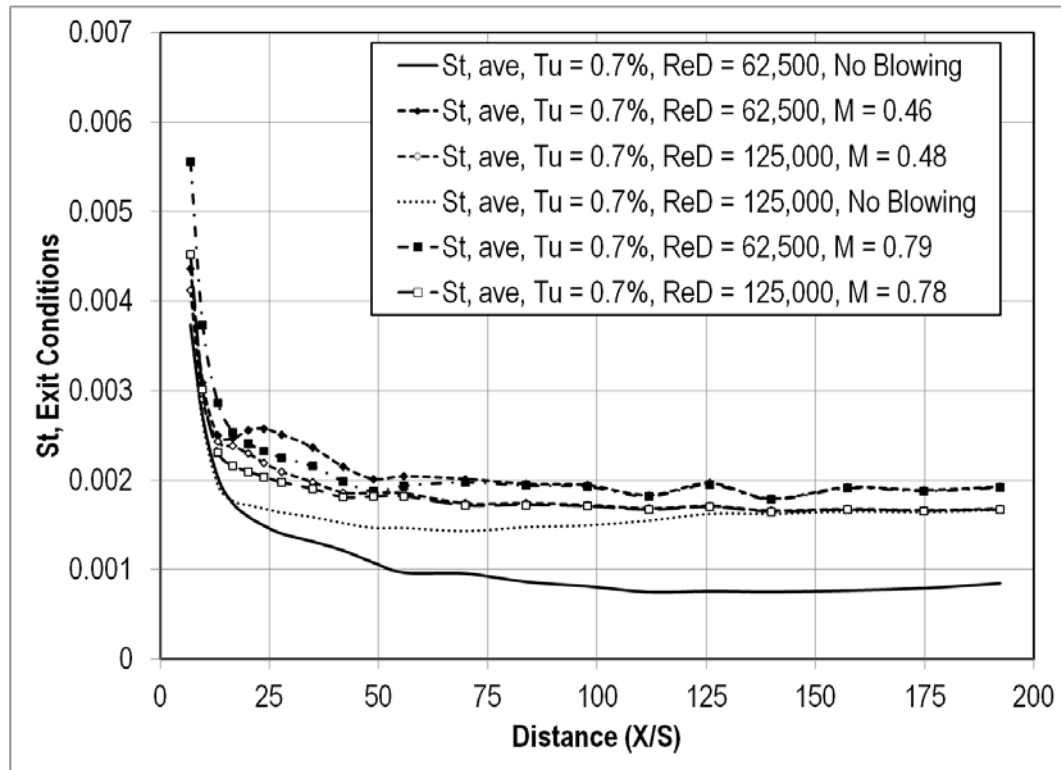


Figure 88. Effects of ReD on Stanton number at low Tu.

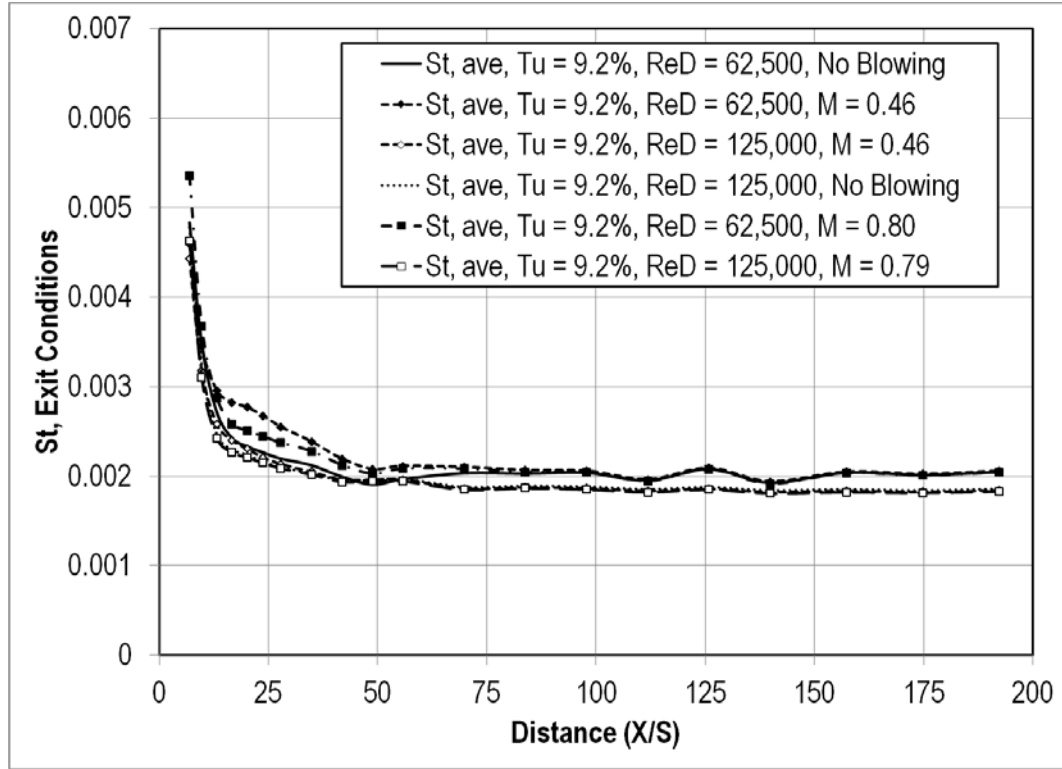


Figure 89. Effects of ReD on Stanton number at small grid-near Tu .

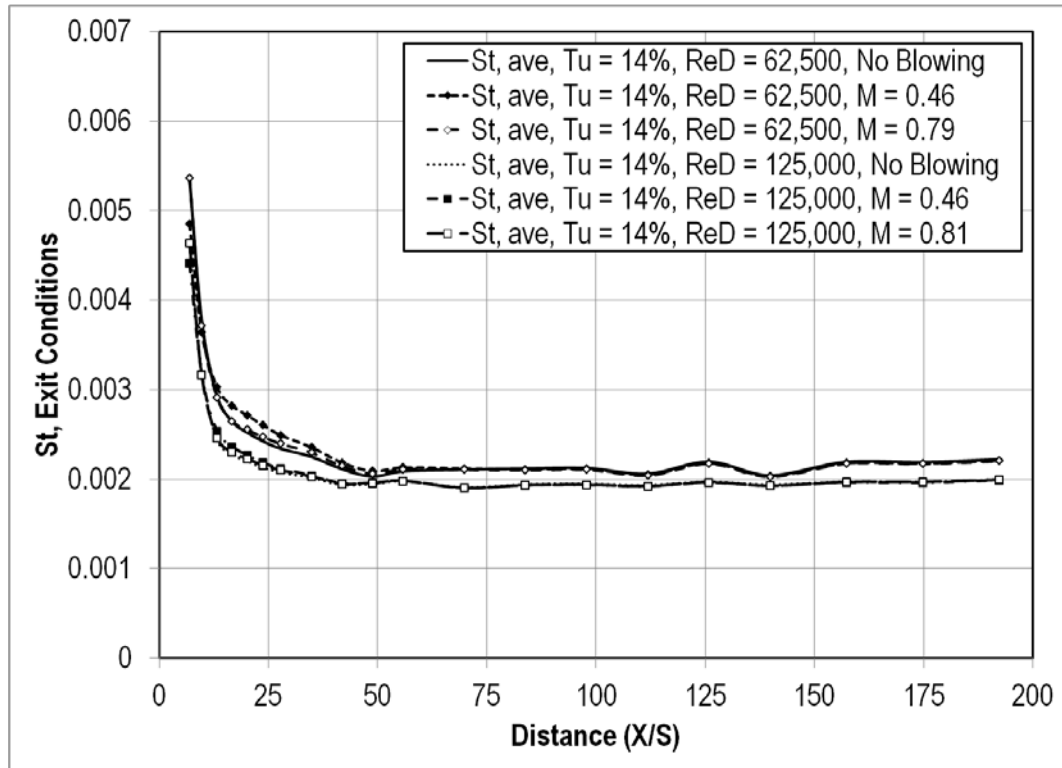


Figure 90. Effects of ReD on Stanton number at aero combustor Tu .

Effects of Turbulence

Increasing the turbulence intensity increases the Stanton number for the small cylindrical leading edge test section. The difference can be seen across the entire measured length of the test section. That is, higher turbulence intensities have increased Stanton numbers immediately after the coolant ejection slot and all the way downstream. The difference in Stanton number between the low turbulence intensity and high turbulence intensity was around ten percent. Figure 91 shows how turbulence intensities change the values for Stanton number at the low Reynolds number and low blowing ratio condition. Here, there are some dips in the Stanton number around a slot height distance of eighteen that is not seen in the other blowing ratio conditions. In Figure 92, the blowing ratio was increased and so were the Stanton numbers. Here, the average downstream Stanton number was around 0.002. Figure 93 shows a similar result for the second highest blowing ratio condition. In this plot, the values for the Stanton number are much closer together throughout the range of turbulence intensities. This effect was also noticed at the high Reynolds numbers and high blowing ratios as well. Figure 94 shows the effects of turbulence on Stanton number at the high Reynolds number and low blowing ratio condition. Here, the downstream Stanton number has very little variations. Once again, a small dip can be seen at a slot height distance of around thirteen for the low turbulence conditions. Figure 95 shows a similar plot but for the high blowing ratio at the high Reynolds number. The values for Stanton number are consistent after a slot height distance of around seventy five. At this increased blowing ratio, no dip in Stanton number is noticed behind the ejection slot at the low turbulence intensities.

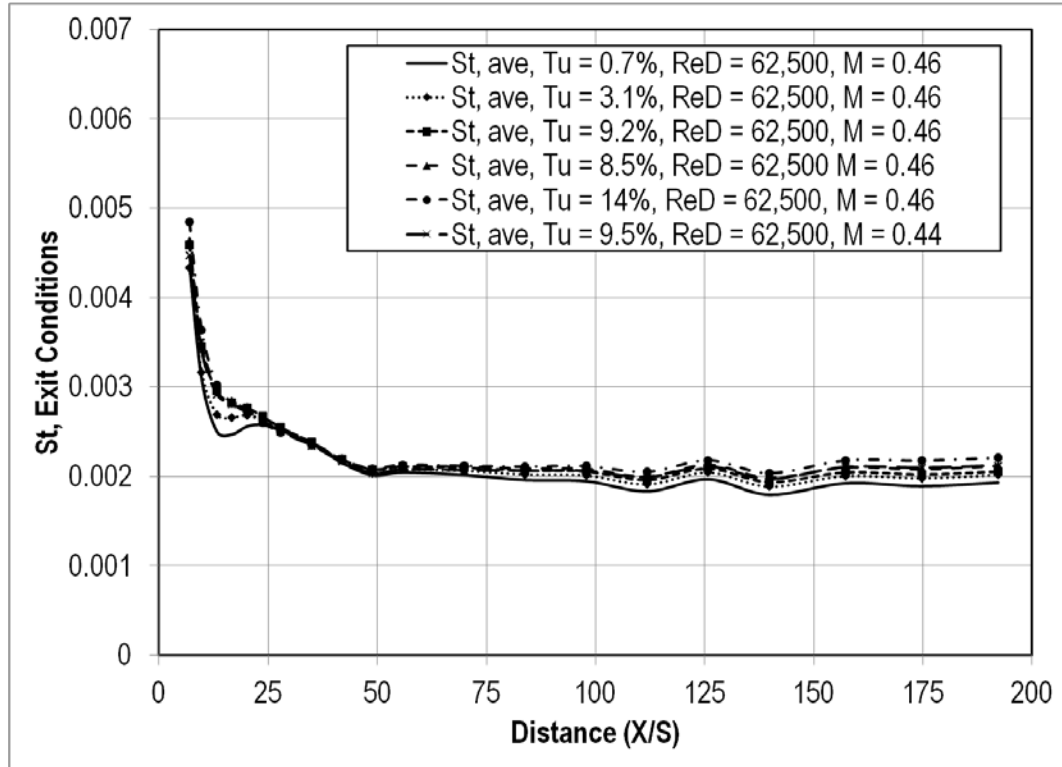


Figure 91. Effects of turbulence intensity on Stanton number at $ReD=62.5k$ and $M=0.46$.

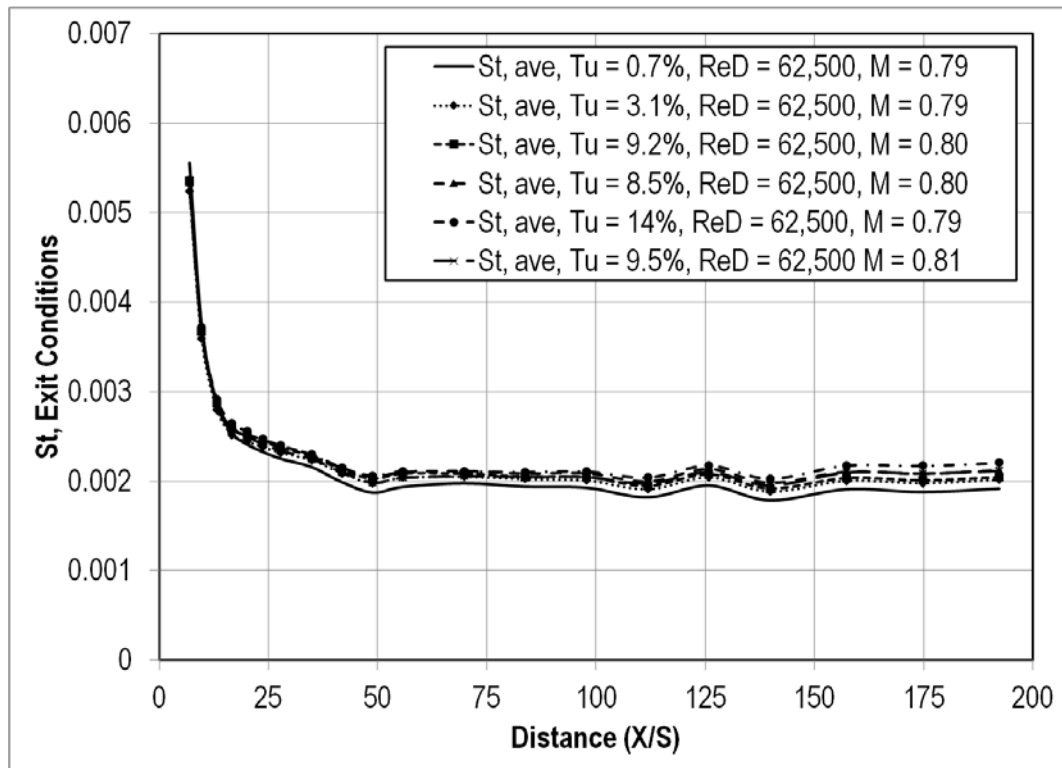


Figure 92. Effects of turbulence intensity on Stanton number at $ReD=62.5k$ and $M=0.80$.

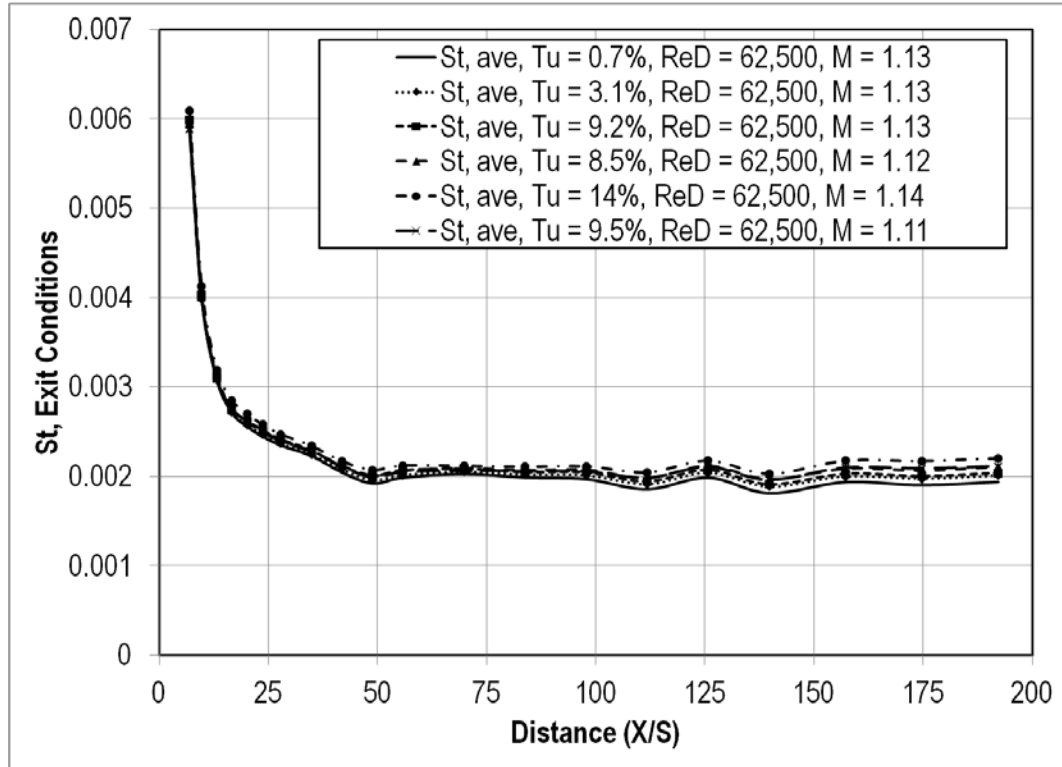


Figure 93. Effects of turbulence intensity on Stanton number at $ReD=62.5k$ and $M=1.12$.

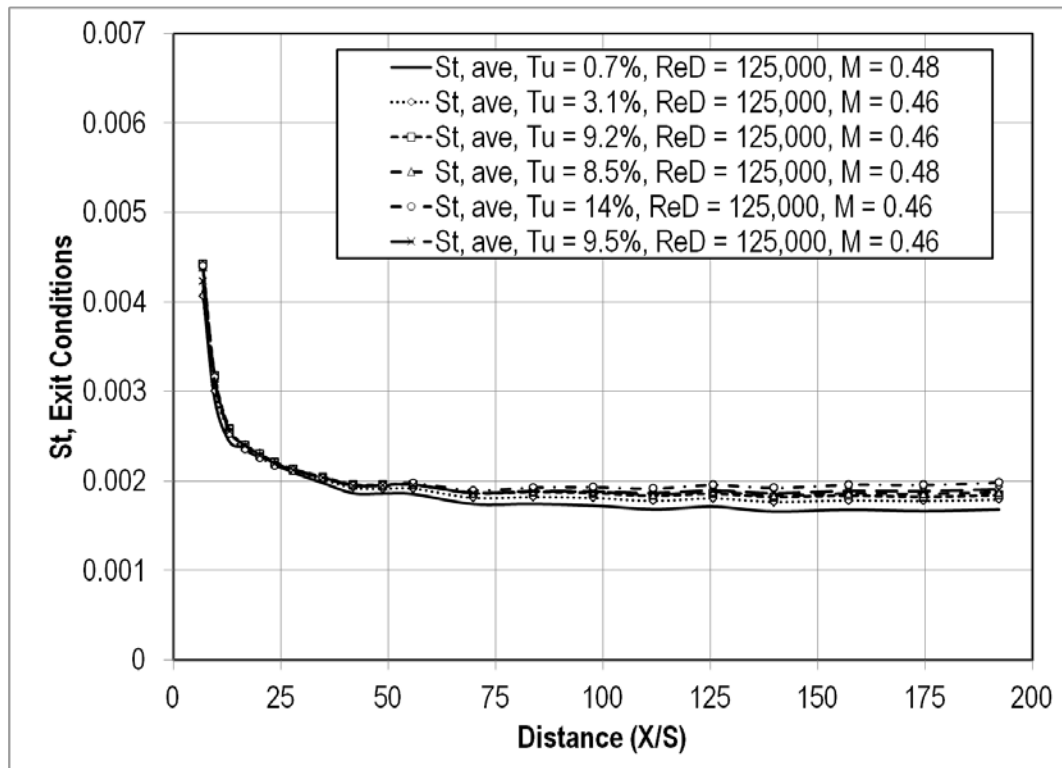


Figure 94. Effects of turbulence intensity on Stanton number at $ReD=125k$ and $M=0.46$.

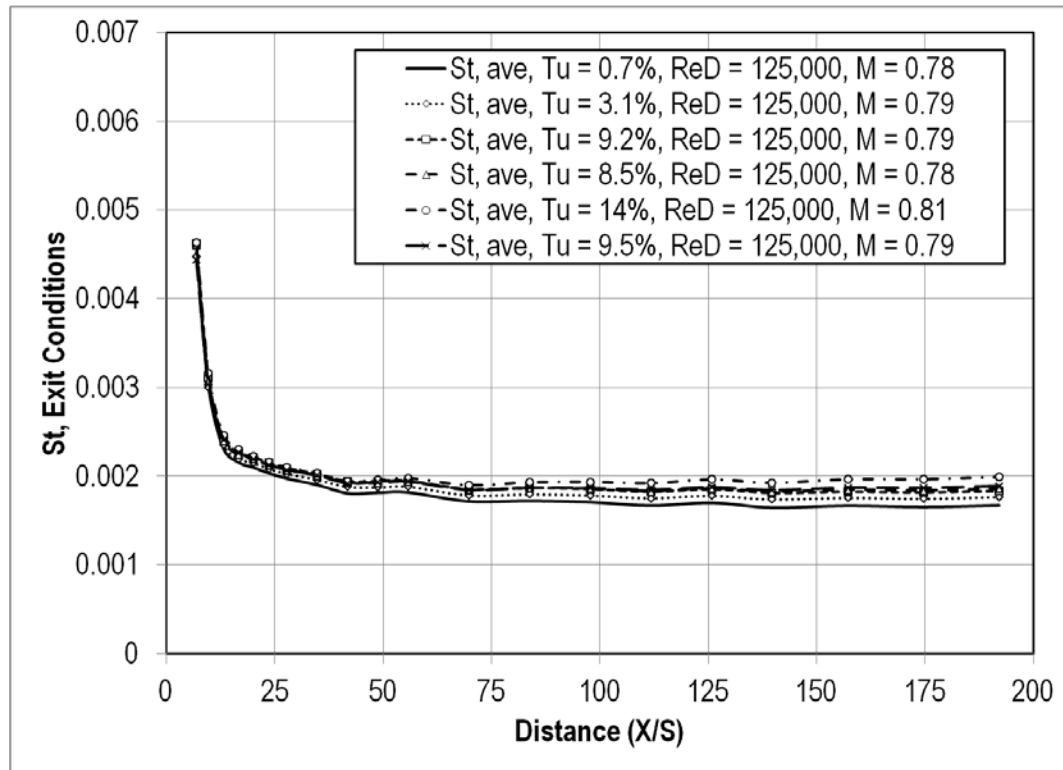


Figure 95. Effects of turbulence intensity on Stanton number at $ReD=125k$ and $M=0.80$.

CHAPTER V

CONCLUSIONS

A pin fin array was designed and integrated into a unique cylindrical leading edge with slot film cooling. Two cylindrical leading edge test sections were designed and constructed, one with a 10.16cm (4.0in) diameter leading edge, and another with a 40.64cm (16.0in) leading edge. The test surfaces were fitted into UND's large scale turbine vane cascade wind tunnel and tested. Equipment was fabricated to deliver film cooling air to the test sections. This research project investigated three parameters that could possibly influence the adiabatic effectiveness of film cooling a cylindrical leading edge test section and the heat transfer of the downstream surfaces. The three parameters were: blowing ratio, free stream Reynolds number, and turbulence intensity. Different turbulence intensities were achieved by integrating a turbulence generating grid into the flow, or by replacing the outlet nozzle with a mock aero combustor. The Reynolds number was controlled by increasing or decreasing the large blower speed, while the blowing ratio was controlled by the small blower. Temperature, pressure, and heater voltage data was acquired using an HP data acquisition unit and a QuickBasic program.

Adiabatic Effectiveness

The data shows that for both the large and the small cylindrical test surfaces, that an increase in turbulence intensity will decrease the adiabatic effectiveness. Higher levels of turbulence will reduce the effectiveness more. The effectiveness values for the

mock aero combustor for example, are shifted farther down to the left than the values for the small grid-far. This reduce in adiabatic effectiveness is thought to be a result of the film cooling mixing out with the turbulence in the freestream flow around the test section. From the data, it can be said that the Reynolds number does have an effect on adiabatic effectiveness. It seems that an increase in the Reynolds number decreases the adiabatic effectiveness at first, but by the end of the test section, the effectiveness values were usually greater than that of the lower Reynolds number. This could be because the film cooling at the high Reynolds number lifts off the test section but then reattaches later on downstream. At the higher Reynolds number condition, the velocity of the film coolant leaving the slot is greater than the velocity would be at the low Reynolds number. It is possible that the flow is partially penetrating into the freestream flow. The coolant blowing ratio has a very large effect on the adiabatic effectiveness. In all cases, large blowing ratios at the same Reynolds number and same turbulence intensity equated to larger adiabatic effectiveness levels across the test section. This increase in adiabatic effectiveness is attributed to the larger amount of coolant air being supplied to the test surface.

Stanton Number

In this research, data was acquired to allow for the calculation of the Stanton number based on exit conditions of the test. This is typical of what is done in industry. It was found that for both cylinders, an increase in blowing ratio causes an increase in the Stanton number. The greatest effect can be seen directly behind the coolant ejection slot. The effects of the increased blowing ratio are not as pronounced far downstream towards the end of the test section. For both cylindrical leading edge test sections, increased

Reynolds number had a lower Stanton number. The Stanton number also reached a minimum closer to the coolant ejection slot before recovering a little. Turbulence had a very noticeable effect on the Stanton number for both test sections. Increasing the turbulence intensity had the effect of increasing the heat transfer. This held true for all blowing ratios and Reynolds numbers tested, and was seen throughout the entire length of the test section. One possible reason for the increased Stanton numbers directly behind the slot is because of the unheated starting length. The cool air ejected from the slot where it flowed over a part of the mounting bracket before flowing over the Inconel foil heater. This created an unheated starting length, where the velocity boundary layer started to develop before the thermal boundary layer developed. This growth of the thermal boundary layer can push the film cooling off of the surface and into the free stream flow. The higher velocity of the free stream flow at the high Reynolds number changed the growth rate of the boundary layer. As mentioned earlier, turbulent boundary layers can be two to four times thicker than a laminar boundary layer. They also have a larger growth rate. This larger boundary layer could be a possible reason why the Stanton number is lower for the high Reynolds numbers. Another possibility for the increased Stanton number directly behind the coolant ejection slot is the turbulence generated inside of the cylindrical leading edge due to the pin fin array. This turbulence promoted better mixing within the coolant film. The small fluctuations in the downstream Stanton number could be a sign of transition in the flow around the test section from laminar to turbulent and back to laminar.

APPENDICES

the ejection slot (in mm). Using data from the taped, no blowing condition, a correction factor for U_{ex} ratio was made. The correction factor was used along with the measured values for U_{∞} and U_{ex} , to calculate the true U_{ex} value. The corrected blowing ratio was calculated by the following equation:

$$M = \frac{\dot{m}_{corr}}{U_{ex,corr}} \quad (B.1)$$

Table 3. Change in temperature between heated and ambient conditions.

N1 is est	del-T,far	del-T,mid	del-T,near	Averaged
0.2	0.628	0.567	0.412	0.535667
0.7	7.083	7.036	6.545	6.888
1.4	10.048	10.23	10.077	10.11833
1.9	12.678	13.435	13.261	13.12467
2.4	14.746	14.94	14.592	14.75933
2.9	15.634	15.55	15.272	15.48533
3.4	16.187	15.765	16.081	16.011
4	16.435	16.487	16.685	16.53567
5	17.092	17.609	16.958	17.21967
6	18.4	18.9	18.585	18.62833
7	18.798	19.965	20.476	19.74633
8	18.991	19.424	18.871	19.09533
10	18.525	19.067	18.583	18.725
12	19.314	19.119	18.75779	19.0636
14	19.268	19.184	19.069	19.17367
16	19.903	20.486	20.38	20.25633
18	18.884	18.994	18.931	18.93633
20	20.513	21.215	20.187	20.63833
25	19.293	19.576	19.122	19.33033
30	19.886	19.674	19.348	19.636
35	18.979	19.438	19.364	19.26033

Using the temperatures for the two conditions, a ΔT was calculated for each thermocouple. The first column is the position of the thermocouple in the x-direction, while the far, mid, and near denotes the position in the z-direction, with mid being the midpoint. A correction factor was used for the T_{in} and T_{co} between the heated and ambient conditions and is given by:

$$(T_h - T_a) - (\eta) * (T_{co,h} - T_{co,a}) + (1 - \eta) * (T_{in,a} - T_{in,h}) \quad (B.2)$$

This equation was used for each thermocouple, and the results were averaged for each row of thermocouples.

Table 4. Average Stanton number for each row of thermocouples.

N1 is est	Average					Averaged					0 X(m)	St. ave, Low Turb, ReD = 62.5k, M = 0.7
	h (W/m ² /Fh)	h (W/m ² /Fh)	h (W/m ² /Fh)	h (W/m ² /Fh)	X(m)	St,far	St,mid	St,near	St,ave, Lc			
0.985726	117.2517	118.0439	126.9992	120.7649	0.025037	0.005314	0.00535	0.005756	0.005473	0	0.025037	0.0054731
1.385726	82.25222	80.76428	82.01138	81.67596	0.035197	0.003728	0.00366	0.003717	0.003702	0	0.035197	0.0037016
1.885726	64.90001	61.16317	61.98453	62.68257	0.047897	0.002941	0.002772	0.002809	0.002841	0	0.047897	0.0028408
2.385726	55.59828	54.8575	56.20008	55.55195	0.060597	0.00252	0.002486	0.002547	0.002518	0	0.060597	0.0025176
2.885726	52.35811	52.6488	53.63338	52.8801	0.073297	0.002373	0.002386	0.002431	0.002397	0	0.073297	0.0023965
3.385726	50.51967	51.91079	50.86184	51.09743	0.085997	0.00229	0.002353	0.002305	0.002316	0	0.085997	0.0023157
3.985726	49.73491	49.57328	48.96753	49.42524	0.101237	0.002254	0.002247	0.002219	0.00224	0	0.101237	0.00224
4.985726	47.76649	46.32061	48.15555	47.41422	0.126637	0.002165	0.002099	0.002182	0.002149	0	0.126637	0.0021488
5.985726	44.26539	43.05463	43.80993	43.70998	0.152037	0.002006	0.001951	0.001985	0.001981	0	0.152037	0.0019809
6.985726	43.29634	40.67742	39.62443	41.1994	0.177437	0.001962	0.001844	0.001796	0.001867	0	0.177437	0.0018672
7.985726	42.84123	41.85245	43.12302	42.60556	0.202837	0.001942	0.001897	0.001954	0.001931	0	0.202837	0.0019309
9.985726	43.95655	42.66424	43.81449	43.47842	0.253637	0.001992	0.001934	0.001986	0.00197	0	0.253637	0.0019704
11.985726	42.09942	42.54426	43.3924	42.67869	0.304437	0.001908	0.001928	0.001967	0.001934	0	0.304437	0.0019342
13.985726	42.20373	42.3949	42.65998	42.41954	0.355237	0.001913	0.001921	0.001933	0.001922	0	0.355237	0.0019225
15.985726	40.80913	39.60423	39.81821	40.07719	0.406037	0.001849	0.001795	0.001805	0.001816	0	0.406037	0.0018163
17.985726	43.09254	42.83405	42.98176	42.96945	0.456837	0.001953	0.001941	0.001948	0.001947	0	0.456837	0.0019474
19.985726	39.55045	38.191	40.21364	39.31836	0.507637	0.001792	0.001731	0.001822	0.001782	0	0.507637	0.0017819
22.485726	42.14726	41.51576	42.53735	42.06679	0.571137	0.00191	0.001881	0.001928	0.001906	0	0.571137	0.0019065
24.985726	40.84525	41.30144	42.023	41.3899	0.634637	0.001851	0.001872	0.001904	0.001876	0	0.634637	0.0018758
27.485726	42.8693	41.82144	41.98706	42.22594	0.698137	0.001943	0.001895	0.001903	0.001914	0	0.698137	0.0019137

The next step was to determine h for each thermocouple, which was given by:

$$\left(\frac{\text{Heater Power}}{(\text{Area of ejection slot} - 0.0000000567 + 0.21 + ((T_h(K))^4 - (T_a(K))^4))} \right) / \Delta T \quad (B.3)$$

The h for each row of thermocouples was then averaged. Using the averaged h value, the Stanton number was then calculated for each row of thermocouples.

$$St, ave = \frac{h, ave}{(U_\infty * U_{ex} * 1005)} \quad (B.4)$$

Appendix B

Adiabatic Effectiveness and Stanton Number Data

Table 5. Effectiveness data for the large test section at low Tu.

	Low Turbulence					
ReD	250477	249929	248828	249166	502002	502636
Ttin(K)	293.26	293.29	295.40	294.98	293.84	296.27
Ptin(Pa)	99214	99214	98337	98337	99848	99427
Patm(Pa)	99006	99006	98126	98126	99006	98566
Blowing Ratio	0.43	0.77	1.08	1.51	0.43	0.77
Vexit(m/s)	18.69	18.64	18.96	18.96	37.59	38.44
Free Stream Density	1.180	1.180	1.161	1.162	1.182	1.166
Exit Mach #	0.0545	0.0544	0.0551	0.0551	0.1095	0.1114
Mass Flow Rate(kg/s)	0.003897	0.006944	0.009674	0.013589	0.007685	0.013970
Tcool, avg(K)	284.60	281.99	283.33	284.24	282.25	284.67
X/S	Adiabatic Effectiveness					
1.39860	0.90601	0.92561	0.93817	0.95151	0.93000	0.95396
6.89319	0.84659	0.85087	0.83902	0.83921	0.84884	0.84839
9.69039	0.81822	0.79347	0.77855	0.77722	0.77648	0.79201
13.18690	0.79575	0.75760	0.74253	0.73866	0.72016	0.77184
16.68340	0.75644	0.72363	0.71006	0.70266	0.64712	0.74004
20.17990	0.72059	0.69826	0.68594	0.67481	0.58708	0.71222
23.67641	0.68197	0.67431	0.66250	0.64718	0.53444	0.68161
27.87221	0.63738	0.64972	0.63855	0.61693	0.48159	0.65079
34.86522	0.57188	0.61366	0.60391	0.57291	0.42109	0.60726
41.85822	0.51474	0.58365	0.57460	0.53758	0.37932	0.57155
48.85123	0.46349	0.55267	0.54494	0.50496	0.34738	0.54050
55.84424	0.41868	0.52401	0.51878	0.47705	0.32248	0.51583
69.83025	0.34290	0.46744	0.47049	0.43276	0.28542	0.46909
83.81627	0.29028	0.42272	0.43351	0.40070	0.25848	0.43276
97.80228	0.25053	0.38327	0.40137	0.37356	0.23492	0.39988
111.78829	0.22196	0.35142	0.37574	0.35230	0.21617	0.37187
125.77431	0.20162	0.32615	0.35453	0.33605	0.19998	0.34689
139.76032	0.18318	0.30224	0.33468	0.31973	0.18813	0.32667
157.24284	0.16484	0.27739	0.31409	0.30405	0.17195	0.30295
174.72536	0.15156	0.25727	0.29621	0.29090	0.16030	0.28270
192.20787	0.13935	0.23888	0.27999	0.27843	0.14921	0.26505

Table 6. Effectiveness data for the large test section at small grid far Tu.

Sm Grid Far						
ReD	250509	250396	249661	250458	501767	498516
Ttin(K)	296.64	293.88	296.10	295.76	297.26	296.98
Ptin(Pa)	97733	97728	98103	98104	98760	99995
Patm(Pa)	97516	97516	97889	97889	97889	99141
Blowing Ratio	0.43	0.74	1.09	1.52	0.43	0.76
Vexit(m/s)	19.43	19.12	19.23	19.30	38.94	38.20
Free Stream Density	1.147	1.157	1.153	1.152	1.153	1.167
Exit Mach #	0.0563	0.0556	0.0557	0.0559	0.1126	0.1105
Mass Flow Rate(kg/s)	0.003887	0.006692	0.009876	0.013807	0.007893	0.013783
Tcool, avg(K)	287.03	282.38	281.24	280.60	285.74	284.08
X/S	Adiabatic Effectiveness					
1.39860	0.91782	0.92512	0.94523	0.95428	0.93793	0.95609
6.89319	0.84790	0.84386	0.83595	0.83443	0.81784	0.83559
9.69039	0.80509	0.78769	0.77636	0.77512	0.70956	0.77485
13.18690	0.74868	0.73561	0.72951	0.72779	0.61947	0.73043
16.68340	0.68183	0.68933	0.68847	0.68529	0.53910	0.68241
20.17990	0.62381	0.65211	0.65718	0.65119	0.47888	0.64161
23.67641	0.57349	0.61738	0.62932	0.62060	0.43075	0.60181
27.87221	0.51962	0.58301	0.59915	0.58620	0.37903	0.55508
34.86522	0.44172	0.52787	0.55310	0.53384	0.31748	0.48642
41.85822	0.37948	0.47865	0.51136	0.48860	0.27456	0.43097
48.85123	0.32852	0.43243	0.47103	0.44801	0.24090	0.38477
55.84424	0.28458	0.38930	0.43124	0.41129	0.21567	0.34766
69.83025	0.21775	0.31260	0.36021	0.35148	0.17917	0.28901
83.81627	0.17459	0.25706	0.30814	0.30862	0.15399	0.24602
97.80228	0.14589	0.21772	0.26676	0.27332	0.13385	0.21413
111.78829	0.12631	0.18945	0.23691	0.24703	0.12012	0.18934
125.77431	0.11206	0.16748	0.21419	0.22653	0.10922	0.16904
139.76032	0.09935	0.15066	0.19435	0.20789	0.09956	0.15321
157.24284	0.08873	0.13447	0.17535	0.18942	0.09038	0.13726
174.72536	0.08158	0.12185	0.16187	0.17588	0.08471	0.12363
192.20787	0.07372	0.11134	0.14882	0.16142	0.07829	0.11194

Table 7. Effectiveness data for the large test section at small grid near Tu.

Sm Grid Near						
ReD	250933	250373	250286	250434	502733	504683
Ttin(K)	296.00	295.96	295.99	296.02	299.15	299.24
Ptin(Pa)	99962	99961	99962	99962	99211	99217
Patm(Pa)	99751	99751	99751	99751	98329	98329
Blowing Ratio	0.45	0.76	1.08	1.53	0.43	0.76
Vexit(m/s)	18.96	18.92	18.91	18.93	39.28	39.45
Free Stream Density	1.175	1.175	1.175	1.175	1.151	1.151
Exit Mach #	0.0550	0.0548	0.0548	0.0549	0.1133	0.1137
Mass Flow Rate(kg/s)	0.004065	0.006936	0.009836	0.013762	0.007892	0.013957
Tcool, avg(K)	287.04	284.48	282.74	281.78	287.80	287.19
X/S	Adiabatic Effectiveness					
1.39860	0.89216	0.91112	0.92835	0.94404	0.92232	0.94462
6.89319	0.81171	0.83142	0.82630	0.83274	0.71789	0.81995
9.69039	0.71590	0.75652	0.75874	0.76896	0.58920	0.74311
13.18690	0.62054	0.69214	0.70661	0.71978	0.50410	0.68161
16.68340	0.53630	0.63426	0.66103	0.67692	0.43355	0.62092
20.17990	0.47394	0.58753	0.62389	0.64166	0.38003	0.56822
23.67641	0.42290	0.54491	0.58825	0.60745	0.33632	0.51884
27.87221	0.37260	0.50108	0.55086	0.57088	0.29229	0.46558
34.86522	0.30332	0.43265	0.49060	0.51203	0.23759	0.39291
41.85822	0.25086	0.37448	0.43620	0.46048	0.19762	0.33642
48.85123	0.21263	0.32553	0.38749	0.41521	0.17044	0.29559
55.84424	0.18103	0.28412	0.34432	0.37519	0.15011	0.26303
69.83025	0.13630	0.22138	0.27609	0.31084	0.11810	0.21217
83.81627	0.10868	0.18016	0.22854	0.26367	0.09842	0.17991
97.80228	0.09164	0.15326	0.19657	0.23142	0.08397	0.15467
111.78829	0.07848	0.13235	0.17156	0.20526	0.07249	0.13532
125.77431	0.06808	0.11655	0.15263	0.18478	0.06227	0.11866
139.76032	0.06239	0.10606	0.13860	0.16908	0.05828	0.11000
157.24284	0.05415	0.09379	0.12330	0.15170	0.05168	0.09744
174.72536	0.04819	0.08437	0.11203	0.13885	0.04415	0.08603
192.20787	0.04367	0.07705	0.10202	0.12756	0.04010	0.07587

Table 8. Effectiveness data for the large test section at large grid Tu.

Large Grid									
ReD	249946	249674	250875	251053	250137	501756	498019	503883	
Ttin(K)	297.29	296.13	296.13	295.29	295.23	297.63	296.10	297.13	
Ptin(Pa)	98848	100163	100165	100096	100095	100277	100724	100748	
Patm(Pa)	98633	99954	99954	99886	99886	99412	99886	99886	
Blowing Ratio	0	0.46	0.80	1.16	1.61	0	0.46	0.78	
Vexit(m/s)	19.25	18.85	18.94	18.87	18.79	38.55	37.73	38.42	
Free Stream Density	1.157	1.177	1.177	1.179	1.179	1.169	1.179	1.175	
Exit Mach #	0.0557	0.0546	0.0549	0.0548	0.0545	0.1113	0.1093	0.1110	
Mass Flow Rate(kg/s)	0	0.003943	0.006844	0.009989	0.013755	0	0.007896	0.013569	
Tcool, avg(K)	297.74	296.29	296.36	295.40	295.42	298.07	296.34	297.54	
X/S	Stanton Number								
6.89319	0.00498	0.00466	0.00568	0.00633	0.00711	0.00477	0.00443	0.00466	
9.69039	0.00384	0.00374	0.00404	0.00436	0.00486	0.00326	0.00321	0.00325	
13.18690	0.00326	0.00333	0.00343	0.00365	0.00406	0.00274	0.00281	0.00278	
16.68340	0.00288	0.00302	0.00302	0.00317	0.00352	0.00242	0.00255	0.00249	
20.17990	0.00256	0.00274	0.00269	0.00280	0.00312	0.00221	0.00236	0.00230	
23.67641	0.00232	0.00253	0.00245	0.00254	0.00285	0.00211	0.00228	0.00222	
27.87221	0.00217	0.00241	0.00231	0.00239	0.00271	0.00215	0.00232	0.00228	
34.86522	0.00207	0.00234	0.00223	0.00228	0.00260	0.00219	0.00231	0.00229	
41.85822	0.00198	0.00225	0.00216	0.00220	0.00248	0.00219	0.00228	0.00227	
48.85123	0.00195	0.00223	0.00215	0.00218	0.00245	0.00224	0.00231	0.00230	
55.84424	0.00200	0.00228	0.00222	0.00225	0.00247	0.00226	0.00231	0.00230	
69.83025	0.00218	0.00241	0.00238	0.00240	0.00254	0.00225	0.00228	0.00228	
83.81627	0.00228	0.00243	0.00242	0.00242	0.00252	0.00217	0.00225	0.00225	
97.80228	0.00233	0.00245	0.00243	0.00244	0.00249	0.00219	0.00222	0.00221	
111.78829	0.00239	0.00247	0.00246	0.00246	0.00250	0.00217	0.00219	0.00219	
125.77431	0.00239	0.00245	0.00243	0.00244	0.00246	0.00208	0.00218	0.00217	
139.76032	0.00240	0.00245	0.00243	0.00243	0.00245	0.00213	0.00215	0.00215	
157.24284	0.00236	0.00240	0.00238	0.00238	0.00239	0.00210	0.00212	0.00212	
174.72536	0.00235	0.00239	0.00237	0.00237	0.00238	0.00208	0.00211	0.00210	
192.20787	0.00232	0.00237	0.00235	0.00235	0.00235	0.00214	0.00214	0.00222	

Table 9. Effectiveness data for the large test section at aero-combustor Tu.

Aero Comb								
ReD	249115	248869	250073	250212	249481	496376	501212	501435
Ttin(K)	295.17	296.85	296.94	297.05	297.20	297.75	297.86	297.93
Ptin(Pa)	99451	99657	99657	99659	99659	100096	100299	100312
Patm(Pa)	99243	99446	99446	99446	99446	99243	99446	99446
Blowing Ratio	0	0.59	0.80	1.15	1.61	0	0.47	0.80
Vexit(m/s)	18.83	19.03	19.06	19.09	19.05	38.23	38.55	38.58
Free Stream Density	1.173	1.161	1.168	1.167	1.166	1.166	1.167	1.167
Exit Mach #	0.0547	0.0554	0.0552	0.0552	0.0551	0.1104	0.1113	0.1114
Mass Flow Rate(kg/s)	0	0.003913	0.006847	0.009878	0.013771	0	0.008203	0.013882
Tcool, avg(K)	295.42	294.15	296.96	297.06	297.37	297.99	297.88	298.31
X/S	Stanton Number							
6.89319	0.00532	0.00509	0.00556	0.00617	0.00699	0.00467	0.00436	0.00454
9.69039	0.00392	0.00384	0.00398	0.00426	0.00477	0.00323	0.00315	0.00317
13.18690	0.00335	0.00335	0.00339	0.00357	0.00397	0.00274	0.00274	0.00272
16.68340	0.00298	0.00302	0.00302	0.00313	0.00347	0.00246	0.00249	0.00246
20.17990	0.00268	0.00274	0.00272	0.00279	0.00310	0.00227	0.00232	0.00228
23.67641	0.00247	0.00254	0.00251	0.00256	0.00285	0.00218	0.00224	0.00220
27.87221	0.00236	0.00245	0.00241	0.00244	0.00273	0.00222	0.00227	0.00224
34.86522	0.00230	0.00239	0.00235	0.00237	0.00263	0.00224	0.00227	0.00225
41.85822	0.00224	0.00232	0.00229	0.00230	0.00252	0.00225	0.00226	0.00224
48.85123	0.00224	0.00230	0.00228	0.00229	0.00247	0.00231	0.00230	0.00229
55.84424	0.00229	0.00234	0.00233	0.00233	0.00249	0.00234	0.00233	0.00231
69.83025	0.00244	0.00246	0.00245	0.00245	0.00255	0.00237	0.00235	0.00233
83.81627	0.00251	0.00251	0.00250	0.00249	0.00255	0.00236	0.00233	0.00232
97.80228	0.00254	0.00253	0.00252	0.00251	0.00255	0.00234	0.00232	0.00231
111.78829	0.00258	0.00256	0.00255	0.00255	0.00257	0.00233	0.00231	0.00230
125.77431	0.00258	0.00256	0.00255	0.00254	0.00256	0.00233	0.00230	0.00229
139.76032	0.00259	0.00257	0.00256	0.00255	0.00256	0.00231	0.00229	0.00228
157.24284	0.00255	0.00253	0.00252	0.00252	0.00252	0.00228	0.00227	0.00225
174.72536	0.00255	0.00254	0.00252	0.00252	0.00253	0.00227	0.00226	0.00225
192.20787	0.00255	0.00253	0.00252	0.00251	0.00251	0.00226	0.00223	0.00223

Table 10. Effectiveness data for the large test section at aero-combustor with spool Tu.

Aero Comb-Spool								
ReD	250038	250498	249684	250327	251281	499748	502400	497231
Ttin(K)	297.91	297.87	297.89	297.72	297.68	299.78	297.97	298.55
Ptin(Pa)	98408	98613	98612	98612	99020	99081	99661	99666
Patm(Pa)	98193	98396	98396	98396	98803	98193	98803	98803
Blowing Ratio	0	0.45	0.81	1.17	1.63	0	0.47	0.80
Vexit(m/s)	19.42	19.41	19.35	19.38	19.37	39.38	38.93	38.65
Free Stream Density	1.150	1.152	1.152	1.152	1.157	1.146	1.159	1.157
Exit Mach #	0.0561	0.0561	0.0559	0.0560	0.0560	0.1133	0.1124	0.1115
Mass Flow Rate(kg/s)	0	0.003923	0.006982	0.010063	0.014062	0	0.008243	0.013836
Tcool, avg(K)	298.20	297.86	297.58	297.71	297.65	300.04	298.20	299.04
X/S	Stanton Number							
6.89319	0.00487	0.00465	0.00584	0.00631	0.00714	0.00468	0.00436	0.00464
9.69039	0.00373	0.00368	0.00411	0.00434	0.00487	0.00320	0.00315	0.00322
13.18690	0.00317	0.00326	0.00347	0.00361	0.00404	0.00269	0.00276	0.00276
16.68340	0.00281	0.00296	0.00305	0.00315	0.00352	0.00238	0.00251	0.00247
20.17990	0.00252	0.00269	0.00272	0.00279	0.00312	0.00217	0.00232	0.00228
23.67641	0.00229	0.00249	0.00248	0.00253	0.00286	0.00207	0.00223	0.00219
27.87221	0.00215	0.00237	0.00233	0.00237	0.00272	0.00209	0.00226	0.00223
34.86522	0.00204	0.00229	0.00224	0.00226	0.00260	0.00213	0.00226	0.00225
41.85822	0.00195	0.00220	0.00215	0.00216	0.00248	0.00215	0.00223	0.00224
48.85123	0.00191	0.00216	0.00212	0.00213	0.00243	0.00221	0.00227	0.00228
55.84424	0.00193	0.00219	0.00217	0.00217	0.00246	0.00224	0.00229	0.00230
69.83025	0.00209	0.00233	0.00233	0.00233	0.00252	0.00227	0.00229	0.00230
83.81627	0.00222	0.00238	0.00239	0.00238	0.00251	0.00228	0.00227	0.00228
97.80228	0.00229	0.00242	0.00243	0.00242	0.00250	0.00223	0.00224	0.00226
111.78829	0.00237	0.00247	0.00248	0.00246	0.00252	0.00222	0.00223	0.00224
125.77431	0.00240	0.00247	0.00248	0.00246	0.00249	0.00220	0.00221	0.00223
139.76032	0.00243	0.00248	0.00249	0.00246	0.00249	0.00218	0.00220	0.00221
157.24284	0.00241	0.00245	0.00245	0.00243	0.00244	0.00215	0.00217	0.00218
174.72536	0.00241	0.00245	0.00245	0.00243	0.00243	0.00214	0.00215	0.00217
192.20787	0.00248	0.00249	0.00244	0.00242	0.00243	0.00220	0.00214	0.00216

Table 11. Effectiveness data for the small test section at low Tu.

Low Turbulence						
ReD	63046	62890	62874	62576	127538	124301
Ttin(K)	297.45	296.91	296.54	296.84	297.84	298.45
Ptin(Pa)	100794	100792	100791	100789	101514	101470
Patm(Pa)	100564	100564	100564	100564	100564	100564
Blowing Ratio	0.46	0.80	1.12	1.58	0.45	0.83
Vexit(m/s)	18.71	18.60	18.56	18.50	38.03	37.20
Free Stream Density	1.179	1.181	1.183	1.181	1.181	1.178
Exit Mach #	0.0541	0.0538	0.0538	0.0536	0.1098	0.1073
Mass Flow Rate(kg/s)	0.004666	0.008024	0.011257	0.015767	0.009021	0.016446
Tcool, avg(K)	287.63	286.96	287.04	287.41	287.54	287.68
X/S	Adiabatic Effectiveness					
1.39860	0.91177	0.92566	0.93067	0.94323	0.92897	0.94895
6.89319	0.84722	0.84700	0.84287	0.85768	0.80568	0.83060
9.69039	0.81069	0.79543	0.78872	0.79957	0.73185	0.79380
13.18690	0.73248	0.73648	0.73301	0.74147	0.58706	0.73252
16.68340	0.63492	0.69031	0.69523	0.70046	0.47611	0.68288
20.17990	0.54546	0.64937	0.66172	0.66430	0.40767	0.64018
23.67641	0.47304	0.61359	0.63568	0.63716	0.36286	0.60700
27.87221	0.41300	0.57900	0.60997	0.61005	0.32651	0.57496
34.86522	0.34618	0.53175	0.57497	0.57392	0.28406	0.53228
41.85822	0.30335	0.49397	0.54558	0.54288	0.25475	0.49677
48.85123	0.27295	0.46329	0.52157	0.51642	0.23103	0.46674
55.84424	0.24751	0.43510	0.49879	0.49016	0.21208	0.44163
69.83025	0.21145	0.38913	0.45798	0.44848	0.18539	0.40169
83.81627	0.19081	0.35649	0.42820	0.41934	0.16615	0.36928
97.80228	0.17315	0.32978	0.40330	0.39507	0.14986	0.34311
111.78829	0.15964	0.30648	0.38051	0.37412	0.13814	0.32089
125.77431	0.14746	0.28520	0.36015	0.35677	0.12774	0.29973
139.76032	0.13818	0.26932	0.34429	0.34300	0.11858	0.28310
157.24284	0.12805	0.25014	0.32465	0.32551	0.10909	0.26414
174.72536	0.11888	0.23375	0.30756	0.31097	0.10092	0.24709
192.20787	0.11149	0.22024	0.29268	0.29872	0.09305	0.23215

Table 12. Effectiveness data for the small test section at small grid far Tu.

Sm Grid Far						
ReD	62423	62564	62548	62598	125505	125662
Ttin(K)	300.01	300.31	300.44	300.51	299.56	299.66
Ptin(Pa)	99207	99209	99209	99210	99924	99934
Patm(Pa)	98972	98972	98972	98972	98972	98972
Blowing Ratio	0.46	0.79	1.12	1.57	0.47	0.79
Vexit(m/s)	19.11	19.19	19.20	19.22	38.42	38.49
Free_Stream_density	1.151	1.149	1.149	1.148	1.156	1.155
Exit_Mach_number	0.0550	0.0552	0.0552	0.0553	0.1106	0.1108
Mass_flow_rate(kg/s)	0.004590	0.007928	0.011308	0.015872	0.009505	0.016170
T_Cool_avg(K)	289.97	287.05	285.98	285.42	288.33	287.34
X/S	Adiabatic Effectiveness					
1.39860	0.91566	0.92710	0.93496	0.95550	0.93618	0.95248
6.89319	0.84184	0.83872	0.83390	0.85304	0.78461	0.82978
9.69039	0.78135	0.78460	0.77969	0.79532	0.69502	0.79051
13.18690	0.67581	0.72268	0.72513	0.73820	0.58185	0.73220
16.68340	0.56964	0.67025	0.68406	0.69518	0.50246	0.68118
20.17990	0.48541	0.62307	0.64814	0.65755	0.44820	0.63609
23.67641	0.42105	0.58282	0.61976	0.62973	0.41010	0.59969
27.87221	0.36387	0.53891	0.58810	0.59848	0.37518	0.56138
34.86522	0.30290	0.48131	0.54541	0.55899	0.33400	0.51086
41.85822	0.26389	0.43504	0.50919	0.52574	0.30480	0.46944
48.85123	0.23349	0.39618	0.47693	0.49574	0.28063	0.43426
55.84424	0.20836	0.36143	0.44605	0.46673	0.26068	0.40321
69.83025	0.17424	0.30817	0.39313	0.42073	0.23370	0.35901
83.81627	0.15283	0.27122	0.35383	0.38628	0.21302	0.32537
97.80228	0.13224	0.24014	0.31952	0.35612	0.19767	0.29888
111.78829	0.11931	0.21737	0.29195	0.33162	0.18527	0.27751
125.77431	0.10952	0.19903	0.26895	0.31126	0.17625	0.26181
139.76032	0.09904	0.18234	0.24893	0.29261	0.16881	0.24693
157.24284	0.09073	0.16643	0.22735	0.27215	0.16004	0.23239
174.72536	0.08485	0.15388	0.21115	0.25538	0.15450	0.21990
192.20787	0.07705	0.14170	0.19479	0.23931	0.14863	0.20882

Table 13. Effectiveness data for the small test section at small grid near Tu.

Sm Grid Near						
ReD	62522	62452	62521	62229	124791	123765
Ttin(K)	298.17	298.19	298.14	299.15	299.75	298.95
Ptin(Pa)	99609	99610	99610	99610	100321	100299
Patm(Pa)	99378	99378	99378	99378	99378	99378
Blowing Ratio	0.46	0.80	1.13	1.59	0.45	0.81
Vexit(m/s)	18.86	18.84	18.85	18.88	38.08	37.59
Free Stream Density	1.162	1.162	1.162	1.158	1.160	1.162
Exit Mach #	0.0545	0.0544	0.0545	0.0544	0.1096	0.1083
Mass Flow Rate(kg/s)	0.004539	0.007986	0.011255	0.015732	0.009010	0.016027
Tcool, avg(K)	287.86	285.04	283.61	286.36	287.62	287.84
X/S	Adiabatic Effectiveness					
1.39860	0.91075	0.92654	0.93428	0.95248	0.91043	0.94626
6.89319	0.79939	0.83252	0.83697	0.85883	0.64731	0.80901
9.69039	0.70236	0.76992	0.77885	0.79897	0.54887	0.76237
13.18690	0.58321	0.70075	0.72000	0.73995	0.43966	0.69109
16.68340	0.48764	0.64251	0.67507	0.69410	0.37317	0.63100
20.17990	0.41632	0.59047	0.63463	0.65499	0.32614	0.57710
23.67641	0.36279	0.54515	0.60158	0.62531	0.29141	0.53254
27.87221	0.31647	0.49847	0.56526	0.59176	0.25971	0.48969
34.86522	0.26280	0.43623	0.51509	0.54953	0.21925	0.42823
41.85822	0.22785	0.38805	0.47270	0.51394	0.18955	0.37890
48.85123	0.19970	0.34766	0.43463	0.48065	0.16770	0.34056
55.84424	0.17680	0.31295	0.39975	0.44815	0.14864	0.30929
69.83025	0.14355	0.25983	0.34223	0.39756	0.12179	0.25938
83.81627	0.12239	0.22454	0.30082	0.36031	0.10419	0.22391
97.80228	0.10630	0.19714	0.26777	0.32661	0.08999	0.19901
111.78829	0.09453	0.17688	0.24174	0.30094	0.08080	0.17956
125.77431	0.08480	0.15951	0.22008	0.27910	0.07078	0.16065
139.76032	0.07687	0.14566	0.20210	0.25849	0.06575	0.15038
157.24284	0.06942	0.13269	0.18407	0.23844	0.05993	0.13604
174.72536	0.06370	0.12195	0.16944	0.22254	0.05433	0.12400
192.20787	0.05846	0.11241	0.15696	0.20665	0.05017	0.11647

Table 14. Effectiveness data for the small test section at large grid Tu.

Large Grid						
ReD	62579	62456	62730	62648	125521	125142
Ttin(K)	298.03	298.13	298.15	298.17	300.16	300.23
Ptin(Pa)	100251	100588	100590	100591	101302	101266
Patm(Pa)	100022	100360	100360	100360	100360	100360
Blowing Ratio	0.45	0.80	1.13	1.60	0.46	0.80
Vexit(m/s)	18.74	18.65	18.73	18.71	38.03	37.94
Free Stream Density	1.170	1.174	1.174	1.174	1.169	1.169
Exit Mach #	0.0541	0.0539	0.0541	0.0540	0.1094	0.1091
Mass Flow Rate(kg/s)	0.004494	0.007890	0.011285	0.015885	0.009188	0.016154
Tcool, avg(K)	287.55	285.06	284.32	284.63	288.39	288.76
X/S	Adiabatic Effectiveness					
1.39860	0.91168	0.92430	0.93251	0.95410	0.90535	0.94677
6.89319	0.78448	0.82204	0.82904	0.85113	0.64055	0.79621
9.69039	0.67931	0.75762	0.76948	0.78972	0.54189	0.74702
13.18690	0.55694	0.68515	0.70988	0.72959	0.43257	0.67653
16.68340	0.46273	0.62488	0.66473	0.68442	0.36380	0.61488
20.17990	0.39261	0.57005	0.62322	0.64431	0.31388	0.56036
23.67641	0.33930	0.52286	0.58850	0.61334	0.27859	0.51475
27.87221	0.29348	0.47413	0.55004	0.57967	0.24417	0.46787
34.86522	0.24036	0.40956	0.49715	0.53535	0.20344	0.40740
41.85822	0.20436	0.35967	0.45225	0.49751	0.17358	0.35720
48.85123	0.17755	0.31943	0.41287	0.46406	0.14921	0.31704
55.84424	0.15463	0.28364	0.37525	0.42955	0.12875	0.28213
69.83025	0.12234	0.23037	0.31490	0.37483	0.10079	0.23232
83.81627	0.10174	0.19501	0.27163	0.33397	0.08347	0.19788
97.80228	0.08593	0.16804	0.23720	0.29914	0.06873	0.17036
111.78829	0.07592	0.14791	0.21049	0.27104	0.05730	0.14806
125.77431	0.06634	0.13127	0.18859	0.24697	0.05143	0.13232
139.76032	0.05960	0.11860	0.17058	0.22734	0.04432	0.11914
157.24284	0.05319	0.10587	0.15299	0.20584	0.03860	0.10463
174.72536	0.04798	0.09545	0.13829	0.18832	0.03416	0.09497
192.20787	0.04404	0.08669	0.12630	0.17307	0.02765	0.08366

Table 15. Effectiveness data for the small test section at aero-combustor Tu.

Aero Comb						
ReD	62210	62677	62325	62407	126914	126176
Ttin(K)	299.84	300.08	300.56	300.74	301.38	301.26
Ptin(Pa)	98290	98296	98295	98296	99042	99039
Patm(Pa)	98058	98058	98058	98058	98058	98058
Blowing Ratio	0.46	0.75	1.11	1.56	0.46	0.77
Vexit(m/s)	19.21	19.38	19.32	19.37	39.65	39.39
Free Stream Density	1.141	1.140	1.138	1.137	1.138	1.139
Exit Mach #	0.0553	0.0558	0.0556	0.0557	0.1138	0.1131
Mass Flow Rate(kg/s)	0.004522	0.007751	0.011345	0.015943	0.009654	0.016157
Tcool, avg(K)	290.35	288.78	286.78	286.22	289.74	288.84
X/S	Adiabatic Effectiveness					
1.39860	0.89904	0.91981	0.93785	0.95198	0.90478	0.94978
6.89319	0.71250	0.80468	0.83351	0.85529	0.63788	0.79541
9.69039	0.60179	0.72972	0.77114	0.79406	0.54376	0.73499
13.18690	0.48756	0.64466	0.70502	0.73026	0.43590	0.64976
16.68340	0.40443	0.57527	0.65042	0.67990	0.36664	0.57852
20.17990	0.34348	0.51518	0.60332	0.63714	0.31631	0.51852
23.67641	0.29825	0.46304	0.56236	0.60257	0.27696	0.46829
27.87221	0.25471	0.41195	0.51632	0.56428	0.24093	0.41806
34.86522	0.20540	0.34405	0.45390	0.51248	0.19709	0.35255
41.85822	0.17229	0.29349	0.40274	0.46812	0.16483	0.30127
48.85123	0.14669	0.25316	0.35739	0.42730	0.14031	0.26071
55.84424	0.12333	0.21875	0.31593	0.38754	0.11867	0.22542
69.83025	0.09471	0.16911	0.25383	0.32490	0.09009	0.17612
83.81627	0.07763	0.13537	0.21054	0.27750	0.07037	0.14119
97.80228	0.06307	0.11209	0.17609	0.23796	0.05789	0.11769
111.78829	0.05360	0.09421	0.15093	0.20774	0.04780	0.09913
125.77431	0.04767	0.08055	0.13200	0.18331	0.03961	0.08453
139.76032	0.04021	0.07071	0.11580	0.16233	0.03419	0.07393
157.24284	0.03476	0.06010	0.10012	0.14137	0.02853	0.06281
174.72536	0.03231	0.05158	0.08873	0.12542	0.02374	0.05368
192.20787	0.02819	0.04658	0.07840	0.11156	0.02086	0.04762

Table 16. Effectiveness data for the small test section at aero-combustor with spool Tu.

Aero Comb-Spool						
ReD	62443	62307	62331	62677	126125	125689
T _{tin} (K)	298.81	298.88	298.86	298.83	300.57	300.57
P _{tin} (Pa)	98159	98160	98159	98160	99514	99503
P _{atm} (Pa)	97922	97922	97922	97922	98532	98532
Blowing Ratio	0.44	0.78	1.10	1.58	0.46	0.80
V _{exit} (m/s)	19.19	19.15	19.16	19.26	39.01	38.88
Free Stream Density	1.143	1.143	1.143	1.143	1.147	1.147
Exit Mach #	0.0554	0.0553	0.0553	0.0556	0.1121	0.1117
Mass Flow Rate(kg/s)	0.004507	0.007889	0.011235	0.015765	0.009336	0.016093
T _{cool, avg} (K)	288.76	286.06	285.03	284.33	288.38	288.46
X/S	Adiabatic Effectiveness					
1.39860	0.91119	0.92246	0.93157	0.94781	0.91775	0.94821
6.89319	0.79818	0.82673	0.83360	0.85492	0.69623	0.81667
9.69039	0.70299	0.76462	0.77549	0.79551	0.59754	0.76413
13.18690	0.58421	0.69278	0.71413	0.73313	0.48876	0.69190
16.68340	0.48968	0.63240	0.66773	0.68712	0.41496	0.62796
20.17990	0.41665	0.57970	0.62757	0.64733	0.36109	0.57481
23.67641	0.36100	0.53343	0.59266	0.61547	0.32104	0.53044
27.87221	0.31251	0.48591	0.55523	0.58245	0.28536	0.48477
34.86522	0.25590	0.42161	0.50331	0.53784	0.24282	0.42594
41.85822	0.21805	0.37105	0.45892	0.49944	0.20931	0.37570
48.85123	0.18927	0.32997	0.41948	0.46503	0.18648	0.33865
55.84424	0.16383	0.29313	0.38164	0.43128	0.16161	0.30007
69.83025	0.12727	0.23645	0.31987	0.37549	0.12789	0.24658
83.81627	0.10470	0.19800	0.27357	0.33205	0.10528	0.20891
97.80228	0.08845	0.16880	0.23731	0.29631	0.08902	0.17953
111.78829	0.07607	0.14703	0.20838	0.26660	0.07746	0.15725
125.77431	0.06505	0.12812	0.18403	0.23967	0.06594	0.13719
139.76032	0.05842	0.11528	0.16525	0.21878	0.05929	0.12443
157.24284	0.04954	0.09952	0.14502	0.19514	0.05240	0.11016
174.72536	0.04349	0.08819	0.12849	0.17535	0.04665	0.09718
192.20787	0.03891	0.07918	0.11566	0.15889	0.04152	0.08717

Table 17. Stanton number data for the large test section at low Tu.

Low Turbulence									
ReD	249432	249446	250338	250420	249553	498283	500328	500073	
Ttin(K)	293.46	296.67	296.81	296.89	297.42	293.02	300.52	300.93	
Ptin(Pa)	98571	97902	97904	97904	97904	99182	98989	98985	
Patm(Pa)	98363	97685	97685	97685	97685	98363	98092	98092	
Blowing Ratio	0	0.44	0.75	1.08	1.53	0	0.43	0.76	
Vexit(m/s)	18.79	19.33	19.41	19.42	19.41	37.85	39.51	39.40	
Free Stream Density	1.168	1.148	1.148	1.147	1.145	1.171	1.143	1.144	
Exit Mach #	0.0547	0.0560	0.0562	0.0562	0.0561	0.1090	0.1137	0.1134	
Mass Flow Rate(kg/s)	0	0.003977	0.006821	0.009867	0.013858	0	0.007915	0.013909	
Tcool, avg(K)	293.41	296.55	296.68	296.86	297.30	293.40	300.29	300.27	
X/S	Stanton Number								
6.89319	0.00359	0.00408	0.00542	0.00597	0.00701	0.00393	0.00442	0.00460	
9.69039	0.00301	0.00345	0.00398	0.00420	0.00488	0.00338	0.00313	0.00323	
13.18690	0.00255	0.00287	0.00322	0.00335	0.00392	0.00274	0.00257	0.00259	
16.68340	0.00224	0.00249	0.00275	0.00285	0.00335	0.00235	0.00232	0.00226	
20.17990	0.00199	0.00220	0.00241	0.00249	0.00297	0.00210	0.00220	0.00207	
23.67641	0.00181	0.00203	0.00219	0.00227	0.00276	0.00202	0.00220	0.00203	
27.87221	0.00168	0.00193	0.00206	0.00215	0.00267	0.00209	0.00226	0.00210	
34.86522	0.00155	0.00185	0.00193	0.00203	0.00255	0.00215	0.00219	0.00209	
41.85822	0.00139	0.00174	0.00177	0.00190	0.00243	0.00221	0.00218	0.00210	
48.85123	0.00132	0.00176	0.00177	0.00194	0.00246	0.00223	0.00215	0.00209	
55.84424	0.00122	0.00176	0.00177	0.00197	0.00245	0.00221	0.00212	0.00207	
69.83025	0.00109	0.00197	0.00197	0.00214	0.00248	0.00217	0.00207	0.00204	
83.81627	0.00101	0.00217	0.00212	0.00218	0.00244	0.00213	0.00201	0.00200	
97.80228	0.00094	0.00219	0.00217	0.00217	0.00238	0.00209	0.00199	0.00197	
111.78829	0.00089	0.00223	0.00222	0.00219	0.00239	0.00206	0.00196	0.00195	
125.77431	0.00084	0.00215	0.00211	0.00208	0.00225	0.00203	0.00192	0.00192	
139.76032	0.00084	0.00219	0.00217	0.00213	0.00229	0.00200	0.00190	0.00188	
157.24284	0.00084	0.00213	0.00211	0.00206	0.00221	0.00197	0.00187	0.00186	
174.72536	0.00091	0.00214	0.00211	0.00206	0.00220	0.00194	0.00184	0.00182	
192.20787	0.00100	0.00209	0.00209	0.00202	0.00216	0.00191	0.00181	0.00180	

Table 18. Stanton number data for the large test section at small grid far Tu.

Sm Grid Far								
ReD	250842	250290	250048	249882	249478	501220	500796	499371
Ttin(K)	294.39	294.34	294.50	294.63	295.16	297.66	296.59	297.76
Ptin(Pa)	98809	98099	98099	98100	98101	99459	98753	98757
Patm(Pa)	98600	97889	97889	97889	97889	98600	97889	97889
Blowing Ratio	0	0.43	0.76	1.08	1.51	0	0.43	0.76
Vexit(m/s)	18.99	19.03	19.07	19.09	19.10	38.72	38.71	38.91
Free Stream Density	1.168	1.161	1.159	1.158	1.156	1.161	1.156	1.150
Exit Mach #	0.0552	0.0554	0.0554	0.0555	0.0555	0.1119	0.1121	0.1124
Mass Flow Rate(kg/s)	0	0.003913	0.006846	0.009755	0.013635	0	0.007810	0.013753
Tcool, avg(K)	294.40	294.15	294.48	294.74	295.17	296.86	296.31	297.83
X/S	Stanton Number							
6.89319	0.00424	0.00397	0.00520	0.00597	0.00685	0.00466	0.00420	0.00456
9.69039	0.00354	0.00313	0.00375	0.00412	0.00467	0.00316	0.00297	0.00308
13.18690	0.00298	0.00275	0.00315	0.00341	0.00386	0.00269	0.00262	0.00259
16.68340	0.00265	0.00254	0.00279	0.00298	0.00338	0.00236	0.00242	0.00233
20.17990	0.00236	0.00234	0.00249	0.00264	0.00302	0.00214	0.00227	0.00214
23.67641	0.00214	0.00216	0.00225	0.00238	0.00275	0.00201	0.00219	0.00204
27.87221	0.00198	0.00206	0.00209	0.00221	0.00261	0.00204	0.00223	0.00209
34.86522	0.00183	0.00198	0.00195	0.00206	0.00249	0.00211	0.00222	0.00216
41.85822	0.00170	0.00190	0.00184	0.00194	0.00237	0.00213	0.00219	0.00216
48.85123	0.00161	0.00187	0.00178	0.00189	0.00233	0.00218	0.00221	0.00220
55.84424	0.00158	0.00192	0.00181	0.00193	0.00237	0.00220	0.00221	0.00220
69.83025	0.00170	0.00212	0.00205	0.00215	0.00246	0.00219	0.00217	0.00217
83.81627	0.00183	0.00221	0.00218	0.00225	0.00244	0.00215	0.00212	0.00213
97.80228	0.00195	0.00227	0.00225	0.00229	0.00242	0.00213	0.00211	0.00212
111.78829	0.00207	0.00230	0.00229	0.00232	0.00241	0.00210	0.00209	0.00209
125.77431	0.00214	0.00228	0.00227	0.00229	0.00236	0.00207	0.00205	0.00205
139.76032	0.00221	0.00230	0.00228	0.00229	0.00235	0.00206	0.00204	0.00205
157.24284	0.00223	0.00226	0.00224	0.00225	0.00229	0.00203	0.00201	0.00202
174.72536	0.00224	0.00225	0.00223	0.00223	0.00227	0.00201	0.00199	0.00200
192.20787	0.00222	0.00221	0.00219	0.00220	0.00223	0.00195	0.00193	0.00194

Table 19. Stanton number data for the large test section at small grid near Tu.

Sm Grid Near								
ReD	250673	250043	249974	250276	250333	499040	500572	501253
Ttin(K)	295.62	297.07	297.17	297.15	297.10	299.08	298.36	298.58
Ptin(Pa)	99284	98577	98577	98578	98578	99933	99227	99245
Patm(Pa)	99074	98363	98363	98363	98363	99074	98363	98363
Blowing Ratio	0	0.43	0.76	1.09	1.52	0	0.44	0.75
Vexit(m/s)	18.99	19.27	19.28	19.31	19.31	38.65	38.84	38.98
Free Stream Density	1.170	1.155	1.154	1.154	1.154	1.162	1.156	1.154
Exit Mach #	0.0551	0.0558	0.0558	0.0559	0.0559	0.1115	0.1122	0.1125
Mass Flow Rate(kg/s)	0	0.003919	0.006881	0.009917	0.013854	0	0.008005	0.013756
Tcool, avg(K)	295.47	297.06	297.18	297.23	297.42	298.38	297.98	298.60
X/S	Stanton Number							
6.89319	0.00528	0.00458	0.00565	0.00629	0.00709	0.00481	0.00443	0.00469
9.69039	0.00407	0.00366	0.00401	0.00432	0.00483	0.00333	0.00322	0.00325
13.18690	0.00334	0.00327	0.00340	0.00361	0.00402	0.00278	0.00284	0.00279
16.68340	0.00294	0.00298	0.00300	0.00314	0.00350	0.00246	0.00257	0.00250
20.17990	0.00261	0.00271	0.00267	0.00278	0.00310	0.00225	0.00239	0.00231
23.67641	0.00236	0.00251	0.00244	0.00252	0.00284	0.00216	0.00232	0.00224
27.87221	0.00220	0.00240	0.00230	0.00237	0.00270	0.00221	0.00236	0.00230
34.86522	0.00209	0.00233	0.00222	0.00227	0.00260	0.00225	0.00234	0.00231
41.85822	0.00201	0.00225	0.00216	0.00218	0.00249	0.00225	0.00231	0.00230
48.85123	0.00198	0.00224	0.00216	0.00217	0.00246	0.00230	0.00233	0.00232
55.84424	0.00204	0.00229	0.00223	0.00225	0.00249	0.00231	0.00233	0.00232
69.83025	0.00224	0.00242	0.00240	0.00240	0.00256	0.00229	0.00229	0.00229
83.81627	0.00234	0.00245	0.00244	0.00244	0.00254	0.00226	0.00226	0.00226
97.80228	0.00239	0.00244	0.00243	0.00243	0.00250	0.00222	0.00222	0.00222
111.78829	0.00243	0.00245	0.00244	0.00244	0.00250	0.00219	0.00219	0.00219
125.77431	0.00243	0.00243	0.00242	0.00242	0.00247	0.00217	0.00217	0.00217
139.76032	0.00242	0.00241	0.00240	0.00240	0.00243	0.00214	0.00214	0.00214
157.24284	0.00237	0.00236	0.00235	0.00235	0.00238	0.00211	0.00211	0.00210
174.72536	0.00235	0.00234	0.00233	0.00233	0.00235	0.00208	0.00208	0.00208
192.20787	0.00233	0.00235	0.00234	0.00234	0.00235	0.00205	0.00211	0.00213

Table 20. Stanton number data for the large test section at large grid Tu.

Large Grid								
ReD	249946	249674	250875	251053	250137	501756	498019	503883
Ttin(K)	297.29	296.13	296.13	295.29	295.23	297.63	296.10	297.13
Ptin(Pa)	98848	100163	100165	100096	100095	100277	100724	100748
Patm(Pa)	98633	99954	99954	99886	99886	99412	99886	99886
Blowing Ratio	0	0.46	0.80	1.16	1.61	0	0.46	0.78
Vexit(m/s)	19.25	18.85	18.94	18.87	18.79	38.55	37.73	38.42
Free Stream Density	1.157	1.177	1.177	1.179	1.179	1.169	1.179	1.175
Exit Mach #	0.0557	0.0546	0.0549	0.0548	0.0545	0.1113	0.1093	0.1110
Mass Flow Rate(kg/s)	0	0.003943	0.006844	0.009989	0.013755	0	0.007896	0.013569
Tcool, avg(K)	297.74	296.29	296.36	295.40	295.42	298.07	296.34	297.54
X/S	Stanton Number							
6.89319	0.00498	0.00458	0.00571	0.00630	0.00698	0.00477	0.00444	0.00459
9.69039	0.00384	0.00370	0.00406	0.00434	0.00481	0.00326	0.00321	0.00321
13.18690	0.00326	0.00330	0.00344	0.00364	0.00402	0.00274	0.00282	0.00276
16.68340	0.00288	0.00300	0.00303	0.00317	0.00349	0.00242	0.00255	0.00247
20.17990	0.00256	0.00272	0.00270	0.00280	0.00310	0.00221	0.00236	0.00229
23.67641	0.00232	0.00251	0.00246	0.00254	0.00284	0.00211	0.00228	0.00221
27.87221	0.00217	0.00240	0.00232	0.00238	0.00270	0.00215	0.00232	0.00227
34.86522	0.00207	0.00233	0.00224	0.00228	0.00259	0.00219	0.00231	0.00228
41.85822	0.00198	0.00225	0.00216	0.00220	0.00248	0.00219	0.00228	0.00226
48.85123	0.00195	0.00222	0.00216	0.00218	0.00244	0.00224	0.00231	0.00229
55.84424	0.00200	0.00227	0.00222	0.00224	0.00247	0.00226	0.00231	0.00230
69.83025	0.00218	0.00240	0.00238	0.00239	0.00253	0.00225	0.00228	0.00227
83.81627	0.00228	0.00243	0.00242	0.00242	0.00251	0.00217	0.00225	0.00224
97.80228	0.00233	0.00245	0.00244	0.00244	0.00249	0.00219	0.00222	0.00221
111.78829	0.00239	0.00247	0.00246	0.00246	0.00249	0.00217	0.00220	0.00219
125.77431	0.00239	0.00245	0.00244	0.00243	0.00246	0.00208	0.00218	0.00217
139.76032	0.00240	0.00245	0.00243	0.00243	0.00244	0.00213	0.00215	0.00214
157.24284	0.00236	0.00240	0.00238	0.00238	0.00239	0.00210	0.00212	0.00212
174.72536	0.00235	0.00239	0.00237	0.00237	0.00238	0.00208	0.00211	0.00210
192.20787	0.00232	0.00237	0.00235	0.00235	0.00235	0.00214	0.00214	0.00221

Table 21. Stanton number data for the large test section at aero-combustor Tu.

Aero Comb								
ReD	249115	248869	250073	250212	249481	496376	501212	501435
Ttin(K)	295.17	296.85	296.94	297.05	297.20	297.75	297.86	297.93
Ptin(Pa)	99451	99657	99657	99659	99659	100096	100299	100312
Patm(Pa)	99243	99446	99446	99446	99446	99243	99446	99446
Blowing Ratio	0	0.59	0.80	1.15	1.61	0	0.47	0.80
Vexit(m/s)	18.83	19.03	19.06	19.09	19.05	38.23	38.55	38.58
Free Stream Density	1.173	1.161	1.168	1.167	1.166	1.166	1.167	1.167
Exit Mach #	0.0547	0.0554	0.0552	0.0552	0.0551	0.1104	0.1113	0.1114
Mass Flow Rate(kg/s)	0	0.003913	0.006847	0.009878	0.013771	0	0.008203	0.013882
Tcool, avg(K)	295.42	294.15	296.96	297.06	297.37	297.99	297.88	298.31
X/S	Stanton Number							
6.89319	0.00532	0.00511	0.00556	0.00617	0.00699	0.00467	0.00441	0.00445
9.69039	0.00392	0.00386	0.00398	0.00426	0.00477	0.00323	0.00317	0.00313
13.18690	0.00335	0.00335	0.00339	0.00357	0.00397	0.00274	0.00276	0.00270
16.68340	0.00298	0.00302	0.00302	0.00313	0.00347	0.00246	0.00250	0.00244
20.17990	0.00268	0.00275	0.00272	0.00279	0.00310	0.00227	0.00233	0.00227
23.67641	0.00247	0.00254	0.00251	0.00256	0.00285	0.00218	0.00225	0.00219
27.87221	0.00236	0.00245	0.00241	0.00244	0.00273	0.00222	0.00228	0.00223
34.86522	0.00230	0.00239	0.00235	0.00237	0.00263	0.00224	0.00227	0.00224
41.85822	0.00224	0.00232	0.00229	0.00230	0.00252	0.00225	0.00226	0.00224
48.85123	0.00224	0.00230	0.00228	0.00229	0.00247	0.00231	0.00230	0.00228
55.84424	0.00229	0.00234	0.00233	0.00233	0.00249	0.00234	0.00233	0.00231
69.83025	0.00244	0.00247	0.00245	0.00245	0.00255	0.00237	0.00235	0.00233
83.81627	0.00251	0.00251	0.00250	0.00249	0.00255	0.00236	0.00234	0.00232
97.80228	0.00254	0.00253	0.00252	0.00251	0.00255	0.00234	0.00233	0.00231
111.78829	0.00258	0.00256	0.00255	0.00255	0.00257	0.00233	0.00231	0.00230
125.77431	0.00258	0.00256	0.00255	0.00254	0.00256	0.00233	0.00230	0.00229
139.76032	0.00259	0.00257	0.00256	0.00255	0.00256	0.00231	0.00229	0.00228
157.24284	0.00255	0.00254	0.00252	0.00252	0.00252	0.00228	0.00227	0.00225
174.72536	0.00255	0.00254	0.00252	0.00252	0.00253	0.00227	0.00226	0.00225
192.20787	0.00255	0.00253	0.00252	0.00251	0.00251	0.00226	0.00223	0.00222

Table 22. Stanton number data for the large test section at aero-combustor with spool Tu.

Aero Comb-Spool								
ReD	250038	250498	249684	250327	251281	499748	502400	497231
Ttin(K)	297.91	297.87	297.89	297.72	297.68	299.78	297.97	298.55
Ptin(Pa)	98408	98613	98612	98612	99020	99081	99661	99666
Patm(Pa)	98193	98396	98396	98396	98803	98193	98803	98803
Blowing Ratio	0	0.45	0.81	1.17	1.63	0	0.47	0.80
Vexit(m/s)	19.42	19.41	19.35	19.38	19.37	39.38	38.93	38.65
Free Stream Density	1.150	1.152	1.152	1.152	1.157	1.146	1.159	1.157
Exit Mach #	0.0561	0.0561	0.0559	0.0560	0.0560	0.1133	0.1124	0.1115
Mass Flow Rate(kg/s)	0	0.003923	0.006982	0.010063	0.014062	0	0.008243	0.013836
Tcool, avg(K)	298.20	297.86	297.58	297.71	297.65	300.04	298.20	299.04
X/S	Stanton Number							
6.89319	0.00487	0.00461	0.00584	0.00615	0.00698	0.00468	0.00427	0.00440
9.69039	0.00373	0.00366	0.00411	0.00427	0.00480	0.00320	0.00311	0.00311
13.18690	0.00317	0.00324	0.00347	0.00357	0.00400	0.00269	0.00274	0.00268
16.68340	0.00281	0.00295	0.00305	0.00312	0.00348	0.00238	0.00249	0.00242
20.17990	0.00252	0.00268	0.00272	0.00277	0.00310	0.00217	0.00231	0.00224
23.67641	0.00229	0.00248	0.00248	0.00251	0.00284	0.00207	0.00222	0.00215
27.87221	0.00215	0.00237	0.00233	0.00236	0.00270	0.00209	0.00225	0.00220
34.86522	0.00204	0.00228	0.00224	0.00225	0.00259	0.00213	0.00225	0.00222
41.85822	0.00195	0.00219	0.00215	0.00215	0.00247	0.00215	0.00223	0.00222
48.85123	0.00191	0.00216	0.00212	0.00212	0.00242	0.00221	0.00227	0.00226
55.84424	0.00193	0.00219	0.00217	0.00217	0.00245	0.00224	0.00228	0.00228
69.83025	0.00209	0.00233	0.00233	0.00232	0.00252	0.00227	0.00228	0.00228
83.81627	0.00222	0.00238	0.00239	0.00237	0.00251	0.00228	0.00226	0.00227
97.80228	0.00229	0.00242	0.00243	0.00241	0.00250	0.00223	0.00224	0.00225
111.78829	0.00237	0.00247	0.00248	0.00245	0.00251	0.00222	0.00222	0.00223
125.77431	0.00240	0.00247	0.00248	0.00245	0.00249	0.00220	0.00221	0.00222
139.76032	0.00243	0.00248	0.00249	0.00246	0.00249	0.00218	0.00219	0.00220
157.24284	0.00241	0.00245	0.00245	0.00243	0.00244	0.00215	0.00217	0.00217
174.72536	0.00241	0.00245	0.00245	0.00243	0.00243	0.00214	0.00215	0.00216
192.20787	0.00248	0.00249	0.00244	0.00242	0.00243	0.00220	0.00213	0.00216

Table 23. Stanton number data for the small test section at low Tu.

Low Turbulence									
ReD	62529	62802	62852	62722	62838	126900	123444	124843	
Ttin(K)	300.38	296.99	296.79	296.97	297.02	300.88	297.37	298.28	
Ptin(Pa)	98364	100385	100386	100385	100385	99117	101034	101077	
Patm(Pa)	98126	100157	100157	100157	100157	98126	100157	100157	
Blowing Ratio	0	0.46	0.93	1.13	1.59	0	0.48	0.78	
Vexit(m/s)	19.35	18.66	18.66	18.64	18.68	39.50	36.86	37.47	
Free Stream Density	1.139	1.176	1.177	1.176	1.176	1.142	1.178	1.174	
Exit Mach #	0.0557	0.0540	0.0540	0.0539	0.0540	0.1134	0.1065	0.1081	
Mass Flow Rate(kg/s)	0	0.004546	0.009236	0.011274	0.015779	0	0.009389	0.015613	
Tcool, avg(K)	300.85	297.16	296.94	297.00	297.11	301.41	297.81	299.03	
X/S	Stanton Number								
6.89319	0.00373	0.00436	0.00555	0.00594	0.00679	0.00372	0.00412	0.00452	
9.69039	0.00271	0.00309	0.00373	0.00400	0.00463	0.00265	0.00290	0.00301	
13.18690	0.00203	0.00250	0.00286	0.00307	0.00367	0.00194	0.00243	0.00231	
16.68340	0.00174	0.00247	0.00253	0.00271	0.00325	0.00176	0.00238	0.00215	
20.17990	0.00159	0.00256	0.00241	0.00255	0.00304	0.00172	0.00230	0.00210	
23.67641	0.00150	0.00257	0.00233	0.00244	0.00288	0.00168	0.00219	0.00203	
27.87221	0.00140	0.00251	0.00225	0.00234	0.00272	0.00164	0.00209	0.00197	
34.86522	0.00132	0.00236	0.00216	0.00223	0.00255	0.00159	0.00198	0.00190	
41.85822	0.00122	0.00215	0.00199	0.00204	0.00232	0.00152	0.00186	0.00181	
48.85123	0.00108	0.00201	0.00187	0.00192	0.00220	0.00147	0.00186	0.00181	
55.84424	0.00097	0.00204	0.00194	0.00198	0.00226	0.00147	0.00185	0.00182	
69.83025	0.00096	0.00201	0.00198	0.00202	0.00221	0.00143	0.00174	0.00172	
83.81627	0.00087	0.00196	0.00194	0.00198	0.00216	0.00148	0.00174	0.00172	
97.80228	0.00082	0.00194	0.00193	0.00197	0.00212	0.00149	0.00172	0.00171	
111.78829	0.00075	0.00183	0.00182	0.00185	0.00198	0.00155	0.00168	0.00167	
125.77431	0.00076	0.00196	0.00195	0.00198	0.00210	0.00162	0.00171	0.00170	
139.76032	0.00076	0.00179	0.00178	0.00181	0.00191	0.00162	0.00166	0.00165	
157.24284	0.00077	0.00192	0.00191	0.00193	0.00203	0.00165	0.00168	0.00167	
174.72536	0.00080	0.00189	0.00188	0.00190	0.00198	0.00164	0.00166	0.00165	
192.20787	0.00085	0.00193	0.00192	0.00193	0.00201	0.00167	0.00168	0.00167	

Table 24. Stanton number data for the small test section at small grid far Tu.

Sm Grid Far								
ReD	62420	62470	62650	62730	62627	125215	125658	125343
Ttin(K)	297.39	297.63	298.40	298.75	299.14	298.93	299.58	300.58
Ptin(Pa)	99371	99371	98834	98835	98835	100081	99561	99563
Patm(Pa)	99141	99141	98600	98600	98600	99141	98600	98600
Blowing Ratio	0	0.46	0.79	1.13	1.59	0	0.46	0.79
Vexit(m/s)	18.78	18.83	19.07	19.14	19.15	38.12	38.62	38.75
Free Stream Density	1.163	1.162	1.152	1.151	1.149	1.161	1.151	1.147
Exit Mach #	0.0543	0.0544	0.0551	0.0552	0.0552	0.1099	0.1112	0.1114
Mass Flow Rate(kg/s)	0	0.004540	0.007876	0.011288	0.015896	0	0.009351	0.015961
Tcool, avg(K)	297.83	297.75	298.53	298.86	299.53	299.15	300.09	301.15
X/S	Stanton Number							
6.89319	0.00433	0.00433	0.00524	0.00591	0.00676	0.00459	0.00407	0.00447
9.69039	0.00315	0.00316	0.00359	0.00398	0.00463	0.00316	0.00301	0.00300
13.18690	0.00241	0.00269	0.00280	0.00308	0.00368	0.00238	0.00256	0.00235
16.68340	0.00212	0.00266	0.00252	0.00271	0.00326	0.00221	0.00241	0.00219
20.17990	0.00200	0.00268	0.00244	0.00258	0.00306	0.00215	0.00231	0.00214
23.67641	0.00194	0.00264	0.00238	0.00247	0.00289	0.00208	0.00220	0.00208
27.87221	0.00187	0.00253	0.00232	0.00236	0.00273	0.00202	0.00212	0.00202
34.86522	0.00181	0.00237	0.00223	0.00224	0.00254	0.00195	0.00202	0.00196
41.85822	0.00172	0.00218	0.00209	0.00208	0.00234	0.00186	0.00192	0.00188
48.85123	0.00163	0.00204	0.00198	0.00195	0.00220	0.00187	0.00191	0.00187
55.84424	0.00166	0.00207	0.00204	0.00201	0.00225	0.00188	0.00191	0.00188
69.83025	0.00181	0.00206	0.00205	0.00205	0.00221	0.00179	0.00181	0.00178
83.81627	0.00186	0.00202	0.00202	0.00202	0.00216	0.00180	0.00182	0.00179
97.80228	0.00191	0.00201	0.00201	0.00201	0.00212	0.00179	0.00181	0.00178
111.78829	0.00187	0.00191	0.00191	0.00191	0.00200	0.00176	0.00178	0.00175
125.77431	0.00201	0.00204	0.00204	0.00204	0.00211	0.00179	0.00181	0.00178
139.76032	0.00189	0.00188	0.00188	0.00188	0.00194	0.00175	0.00177	0.00174
157.24284	0.00200	0.00200	0.00200	0.00200	0.00205	0.00177	0.00178	0.00176
174.72536	0.00199	0.00198	0.00198	0.00197	0.00202	0.00176	0.00177	0.00175
192.20787	0.00202	0.00202	0.00202	0.00201	0.00204	0.00178	0.00179	0.00177

Table 25. Stanton number data for the small test section at small grid near Tu.

Sm Grid Near								
ReD	62540	62615	62626	62700	62615	124645	127733	126533
Ttin(K)	298.09	298.22	298.21	298.23	298.25	299.47	298.41	300.06
Ptin(Pa)	99373	99271	99272	99273	99274	100083	100018	100010
Patm(Pa)	99141	99040	99040	99040	99040	99141	99040	99040
Blowing Ratio	0	0.46	0.80	1.13	1.59	0	0.46	0.79
Vexit(m/s)	18.90	18.96	18.96	18.98	18.96	38.07	38.81	38.83
Free Stream Density	1.160	1.158	1.158	1.158	1.158	1.158	1.161	1.154
Exit Mach #	0.0546	0.0547	0.0548	0.0548	0.0548	0.1096	0.1119	0.1117
Mass Flow Rate(kg/s)	0	0.004531	0.007969	0.011306	0.015828	0	0.009397	0.016079
Tcool, avg(K)	298.53	298.35	298.34	298.39	298.29	299.71	298.80	300.64
X/S	Stanton Number							
6.89319	0.00484	0.00459	0.00535	0.00598	0.00683	0.00477	0.00442	0.00462
9.69039	0.00348	0.00345	0.00367	0.00403	0.00467	0.00323	0.00318	0.00310
13.18690	0.00271	0.00295	0.00287	0.00312	0.00371	0.00246	0.00258	0.00242
16.68340	0.00242	0.00282	0.00258	0.00276	0.00328	0.00229	0.00240	0.00226
20.17990	0.00233	0.00277	0.00250	0.00262	0.00309	0.00223	0.00230	0.00221
23.67641	0.00226	0.00267	0.00244	0.00251	0.00292	0.00216	0.00221	0.00215
27.87221	0.00219	0.00255	0.00237	0.00241	0.00276	0.00210	0.00213	0.00209
34.86522	0.00212	0.00238	0.00228	0.00229	0.00257	0.00202	0.00205	0.00202
41.85822	0.00199	0.00219	0.00212	0.00211	0.00236	0.00194	0.00196	0.00194
48.85123	0.00190	0.00208	0.00203	0.00200	0.00223	0.00195	0.00196	0.00194
55.84424	0.00197	0.00211	0.00208	0.00207	0.00228	0.00196	0.00196	0.00194
69.83025	0.00203	0.00210	0.00208	0.00208	0.00222	0.00187	0.00186	0.00185
83.81627	0.00203	0.00207	0.00204	0.00205	0.00218	0.00189	0.00188	0.00186
97.80228	0.00204	0.00206	0.00204	0.00204	0.00214	0.00188	0.00187	0.00185
111.78829	0.00195	0.00196	0.00194	0.00194	0.00202	0.00185	0.00184	0.00182
125.77431	0.00208	0.00209	0.00207	0.00207	0.00214	0.00187	0.00186	0.00185
139.76032	0.00193	0.00194	0.00191	0.00191	0.00196	0.00183	0.00182	0.00181
157.24284	0.00204	0.00205	0.00203	0.00203	0.00207	0.00185	0.00184	0.00182
174.72536	0.00201	0.00202	0.00201	0.00200	0.00204	0.00183	0.00182	0.00181
192.20787	0.00205	0.00206	0.00204	0.00204	0.00207	0.00185	0.00184	0.00183

Table 26. Stanton number data for the small test section at large grid Tu.

Large Grid									
ReD	62691	62701	62446	62748	62473	124470	124619	125978	
Ttin(K)	298.05	298.50	298.64	298.97	300.32	298.37	300.95	302.22	
Ptin(Pa)	99982	100117	100117	100119	100120	100675	100834	100857	
Patm(Pa)	99751	99886	99886	99886	99886	99751	99886	99886	
Blowing Ratio	0	0.46	0.80	1.12	1.59	0	0.48	0.78	
Vexit(m/s)	18.83	18.85	18.79	18.92	18.99	37.53	38.11	38.82	
Free Stream Density	1.167	1.167	1.166	1.165	1.160	1.170	1.161	1.156	
Exit Mach #	0.0544	0.0544	0.0542	0.0546	0.0546	0.1083	0.1095	0.1113	
Mass Flow Rate(kg/s)	0	0.004579	0.007924	0.011235	0.015844	0	0.009675	0.015776	
Tcool, avg(K)	298.49	298.53	298.76	299.07	300.64	298.41	301.20	302.59	
X/S	Stanton Number								
6.89319	0.00484	0.00463	0.00534	0.00594	0.00679	0.00475	0.00439	0.00460	
9.69039	0.00348	0.00349	0.00368	0.00401	0.00463	0.00321	0.00315	0.00307	
13.18690	0.00272	0.00298	0.00288	0.00310	0.00367	0.00243	0.00255	0.00239	
16.68340	0.00243	0.00284	0.00260	0.00274	0.00325	0.00226	0.00238	0.00224	
20.17990	0.00234	0.00277	0.00252	0.00260	0.00305	0.00220	0.00229	0.00219	
23.67641	0.00227	0.00267	0.00246	0.00250	0.00289	0.00213	0.00220	0.00213	
27.87221	0.00220	0.00254	0.00239	0.00240	0.00273	0.00207	0.00212	0.00207	
34.86522	0.00212	0.00238	0.00229	0.00228	0.00254	0.00200	0.00203	0.00200	
41.85822	0.00200	0.00220	0.00215	0.00212	0.00234	0.00193	0.00195	0.00192	
48.85123	0.00192	0.00208	0.00205	0.00201	0.00221	0.00193	0.00194	0.00192	
55.84424	0.00197	0.00212	0.00210	0.00206	0.00224	0.00195	0.00195	0.00193	
69.83025	0.00204	0.00211	0.00211	0.00209	0.00220	0.00187	0.00186	0.00184	
83.81627	0.00205	0.00209	0.00208	0.00207	0.00217	0.00189	0.00188	0.00186	
97.80228	0.00206	0.00209	0.00208	0.00207	0.00214	0.00188	0.00187	0.00186	
111.78829	0.00199	0.00200	0.00199	0.00198	0.00203	0.00185	0.00184	0.00183	
125.77431	0.00213	0.00213	0.00213	0.00212	0.00215	0.00189	0.00188	0.00186	
139.76032	0.00198	0.00199	0.00198	0.00196	0.00199	0.00185	0.00184	0.00182	
157.24284	0.00210	0.00210	0.00210	0.00208	0.00210	0.00187	0.00186	0.00184	
174.72536	0.00208	0.00208	0.00208	0.00206	0.00207	0.00186	0.00185	0.00183	
192.20787	0.00211	0.00212	0.00212	0.00210	0.00211	0.00188	0.00187	0.00186	

Table 27. Stanton number data for the small test section at aero-combustor Tu.

Aero Comb									
ReD	62986	63083	63118	62529	62463	124767	126043	123962	
Ttin(K)	298.44	297.33	298.23	298.88	299.43	300.34	300.46	301.14	
Ptin(Pa)	100355	99577	99577	99576	99578	101045	100300	100295	
Patm(Pa)	100123	99345	99345	99345	99345	100123	99345	99345	
Blowing Ratio	0	0.46	0.79	1.14	1.59	0	0.46	0.81	
Vexit(m/s)	18.89	18.94	19.05	18.95	18.99	37.93	38.65	38.15	
Free Stream Density	1.170	1.165	1.162	1.159	1.157	1.166	1.157	1.154	
Exit Mach #	0.0545	0.0548	0.0550	0.0547	0.0547	0.1091	0.1111	0.1095	
Mass Flow Rate(kg/s)	0	0.004553	0.007933	0.011341	0.015811	0	0.009218	0.016066	
Tcool, avg(K)	298.86	297.57	298.44	298.98	299.70	300.38	300.51	301.53	
X/S	Stanton Number								
6.89319	0.00535	0.00485	0.00536	0.00609	0.00692	0.00460	0.00441	0.00463	
9.69039	0.00377	0.00364	0.00372	0.00413	0.00475	0.00320	0.00317	0.00316	
13.18690	0.00293	0.00303	0.00291	0.00319	0.00376	0.00244	0.00253	0.00246	
16.68340	0.00264	0.00282	0.00265	0.00285	0.00336	0.00227	0.00236	0.00230	
20.17990	0.00252	0.00271	0.00255	0.00270	0.00315	0.00220	0.00226	0.00222	
23.67641	0.00242	0.00260	0.00247	0.00258	0.00297	0.00213	0.00218	0.00215	
27.87221	0.00234	0.00249	0.00239	0.00247	0.00281	0.00207	0.00212	0.00210	
34.86522	0.00225	0.00235	0.00230	0.00234	0.00261	0.00201	0.00204	0.00203	
41.85822	0.00211	0.00218	0.00215	0.00217	0.00240	0.00193	0.00195	0.00194	
48.85123	0.00203	0.00209	0.00206	0.00207	0.00228	0.00194	0.00196	0.00195	
55.84424	0.00209	0.00213	0.00211	0.00212	0.00231	0.00197	0.00198	0.00198	
69.83025	0.00211	0.00212	0.00211	0.00212	0.00223	0.00191	0.00190	0.00190	
83.81627	0.00212	0.00211	0.00210	0.00211	0.00220	0.00194	0.00193	0.00193	
97.80228	0.00212	0.00211	0.00211	0.00211	0.00218	0.00194	0.00193	0.00194	
111.78829	0.00206	0.00205	0.00204	0.00204	0.00209	0.00193	0.00192	0.00192	
125.77431	0.00219	0.00218	0.00217	0.00218	0.00221	0.00197	0.00196	0.00196	
139.76032	0.00204	0.00204	0.00203	0.00203	0.00205	0.00193	0.00192	0.00192	
157.24284	0.00219	0.00218	0.00217	0.00217	0.00220	0.00197	0.00196	0.00196	
174.72536	0.00219	0.00218	0.00217	0.00217	0.00219	0.00197	0.00196	0.00197	
192.20787	0.00222	0.00221	0.00220	0.00220	0.00221	0.00199	0.00198	0.00199	

Table 28. Stanton number data for the small test section at aero-combustor with spool Tu.

Aero Comb-Spool									
ReD	61959	63249	61986	62995	62148	125643	125933	126021	
Ttin(K)	297.40	298.89	298.51	298.38	298.62	299.64	299.07	300.12	
Ptin(Pa)	99976	99108	99098	99108	98597	100697	99334	99338	
Patm(Pa)	99751	98871	98871	98871	98363	99751	98363	98363	
Blowing Ratio	0	0.44	0.81	1.11	1.62	0	0.46	0.79	
Vexit(m/s)	18.53	19.26	18.83	19.12	18.99	38.18	38.68	38.95	
Free Stream Density	1.170	1.154	1.155	1.156	1.149	1.165	1.151	1.147	
Exit Mach #	0.0536	0.0556	0.0544	0.0552	0.0548	0.1099	0.1114	0.1120	
Mass Flow Rate(kg/s)	0	0.004460	0.007985	0.011127	0.016040	0	0.009306	0.016028	
Tcool, avg(K)	297.85	299.04	299.19	299.07	298.76	299.93	299.21	300.30	
X/S	Stanton Number								
6.89319	0.00465	0.00447	0.00528	0.00589	0.00686	0.00453	0.00424	0.00444	
9.69039	0.00338	0.00340	0.00367	0.00400	0.00472	0.00314	0.00310	0.00303	
13.18690	0.00264	0.00292	0.00286	0.00309	0.00374	0.00239	0.00256	0.00241	
16.68340	0.00239	0.00281	0.00259	0.00276	0.00334	0.00225	0.00239	0.00226	
20.17990	0.00228	0.00273	0.00249	0.00261	0.00312	0.00217	0.00229	0.00219	
23.67641	0.00221	0.00262	0.00242	0.00249	0.00294	0.00209	0.00219	0.00212	
27.87221	0.00214	0.00250	0.00234	0.00239	0.00278	0.00203	0.00212	0.00207	
34.86522	0.00207	0.00235	0.00225	0.00227	0.00259	0.00197	0.00204	0.00200	
41.85822	0.00196	0.00216	0.00210	0.00211	0.00237	0.00189	0.00194	0.00192	
48.85123	0.00186	0.00204	0.00199	0.00199	0.00224	0.00189	0.00195	0.00193	
55.84424	0.00191	0.00208	0.00204	0.00205	0.00228	0.00192	0.00196	0.00194	
69.83025	0.00198	0.00207	0.00206	0.00206	0.00221	0.00185	0.00186	0.00184	
83.81627	0.00201	0.00206	0.00205	0.00206	0.00217	0.00187	0.00188	0.00186	
97.80228	0.00203	0.00206	0.00205	0.00205	0.00215	0.00187	0.00188	0.00186	
111.78829	0.00198	0.00199	0.00197	0.00198	0.00205	0.00185	0.00186	0.00184	
125.77431	0.00211	0.00211	0.00210	0.00210	0.00216	0.00188	0.00189	0.00187	
139.76032	0.00198	0.00197	0.00195	0.00196	0.00200	0.00185	0.00186	0.00184	
157.24284	0.00211	0.00210	0.00210	0.00210	0.00213	0.00188	0.00188	0.00187	
174.72536	0.00211	0.00210	0.00209	0.00209	0.00211	0.00187	0.00188	0.00186	
192.20787	0.00214	0.00212	0.00211	0.00211	0.00213	0.00189	0.00190	0.00189	

Appendix C

Uncertainty Analysis

There exists a possibility that the research performed could have erroneous data due to errors in the data acquisition equipment, errors in fabrication, or errors in the data acquisition procedure. An uncertainty analysis was performed using the root sum square method described by Moffat [41]. All uncertainty estimates for the experimental test is based on a ninety five percent confidence interval.

Adiabatic Effectiveness Uncertainty.

The uncertainty for the effectiveness has two values based on the errors of the thermocouples: one value directly behind the film cooling slot, and another value downstream, close to the end of the Inconel foil heater. The uncertainty upstream was 0.024 degrees Celsius while the uncertainty downstream was 0.013 degrees Celsius. These values are based off of unsteadiness and calibration. Factors for unsteadiness include but are not limited to: change in temperature of the room, coolant air temperature change, freestream temperature change, and the system not being at steady state when the data was collected. Factors for calibration include but are not limited to: ice bath not properly maintained, program issues, thermocouple issues, and equipment issues.

Stanton Number Uncertainty

The uncertainty analysis was performed at two different locations on the test surface: directly behind the ejection slot and downstream at the end of the Inconel foil. The analysis was performed for the difference in temperatures between the heated and unheated case (ΔT), the heat transfer coefficient (h), and the Stanton number (St). At both locations, the uncertainty of ΔT was 0.28 degrees Celsius. The parameters that had

the most effect were the adiabatic wall temperatures. The uncertainty in h was much larger at the upstream location than at the downstream location, with the uncertainty at the upstream location of $6.1 \frac{W}{m^2K}$ while the downstream location had an uncertainty of $1.5 \frac{W}{m^2K}$. There is three times more heat transfer upstream than downstream, so it makes sense that the uncertainty is greater upstream. The uncertainty in Stanton number was also higher upstream, with a value of 0.00030 versus the uncertainty of the downstream location of 0.00008.

Appendix D

QuickBasic Program for the Big Cylindrical Leading Edge Test Section

```
DECLARE SUB siflow (dorf!, dpipe!, LUP!, LDOWN!, torf!, p1!, dp!, siflw!)
DECLARE SUB tempca (volt!, temp!)
DECLARE SUB clrdvm ()
DECLARE SUB setdvm ()
DECLARE SUB rdscnefm (ichnl%, volt!)
DECLARE SUB zerop (vz1, vz2)
DECLARE SUB svalve (port1%, port2%)
.....
' program bigcylfc.bas
  REM $INCLUDE: 'turb.BAS'
'declare two dimensions t(90) and v!(90), will be used to store voltages and
'temperatures
  DIM t(100), v!(100), v2!(100), sumv!(100), pin(40), Pex(40), Pvane(100)
  DIM xin(40), ytrav(25), ztrav(27), p1s(30), p2s(30), p3s(30), p4s(30)
  DIM p5s(30), volt(20, 60), tempt(20, 60)
  DIM p1f(25, 27), p2f(25, 27), p3f(25, 27), p4f(25, 27), p5f(25, 27)
  DIM idtc(85), sumt(85), vt(85), tc(85)
  b11 = 2.486554 'high input transducer parameters (2 Sept 2005)
  b21 = .1267044 'low input transducer parameters (2 Sept 2005)
  ORIFICEDIAMETER = 1.25 '1.823 or 3"
  PRINT "ORIFICE DIAMETER IS CURRENTLY"; ORIFICEDIAMETER; " inches"
  INPUT "Input the barometric pressure (in hg): ", Patm
  IF Patm < 28.4 OR Patm > 29.9 THEN Patm = 29.1
  Patm = Patm * 13.6 * .03611 * 101325 / 14.696
  PRINT Patm; "Pa"
  CLS
istrt1: CALL zerop(vz1, vz2)
  vzero1 = vz1
  vzero2 = vz2
  PRINT "Average: "; "sensor1_zero="; vz1; " sensor2_zero="; vz2
  INPUT "Type 1 to continue, Enter to rezero."; ickz
  IF ickz <> 1 THEN GOTO istrt1
ioption:
  CLS
  ON KEY(1) GOSUB ioption 'Main Menu
  KEY(1) ON
  LOCATE 1, 2: PRINT ""
  LOCATE 2, 2: PRINT "This program section provides a menu of program options"
  LOCATE 3, 2: PRINT "To return to this menu at any time hit function key, F1"
  LOCATE 4, 2: PRINT "To monitor the wind tunnel conditions, type 1"
  LOCATE 5, 2: PRINT "To monitor the wind tunnel conditions with temperatures, type
2"
```

```

LOCATE 6, 2: PRINT "To acquire blowing ratio, type 3"
LOCATE 11, 2: PRINT "To check the orifice flow rate and fc temps, type 8"
LOCATE 12, 2: PRINT "To rezero pressure transducers, type 9"
LOCATE 14, 2: PRINT "To end the program, type 11"
LOCATE 15, 2: INPUT "Type in the number corresponding to your selection:"; iselect
IF iselect = 1 THEN GOTO imonitor
IF iselect = 2 THEN GOTO imon2
IF iselect = 3 THEN GOTO iblowrat
IF iselect = 8 THEN GOTO ichkflw
IF iselect = 9 THEN GOTO istr1
IF iselect = 11 THEN GOTO iend
IF iselect < 1 OR iselect > 8 THEN GOTO ioption
CLS
ON KEY(1) GOSUB ioption 'Main Menu
KEY(1) ON
imonitor:
CLS
' measure inlet total to atmospheric pressure difference -----
port1% = 44      ' should be connected to atm
port2% = 48      ' should be connected to inlet total pressure
settle = 25      'time to wait
CALL svalve(port1%, port2%)
start = TIMER
ichkt: current = TIMER
IF (current - start) < settle GOTO ichkt
'read transducer voltages and change it into Pressures
FOR i = 91 TO 92      'transducer use hp3497's port90 and port91
j% = i - 1
sum = 0!
FOR kj = 1 TO 20
CALL rdscnefm(j%, volt!)
sum = sum + volt!
NEXT kj
v2!(j%) = sum / 20!
NEXT i
pres1 = b11 * (v2!(90) - vz1) 'calculate pressure
pres2 = b21 * (v2!(91) - vz2) 'calculate pressure
' Now calculate pressures based on most applicable range. Transducer #1
' has a range to about 20 inwg. Transducer #2 has a range to about
' 1 inwg. The lowest applicable range will be selected.
IF pres1 < .95 THEN ptain! = pres2
IF pres1 >= .95 AND pres2 <= 20 THEN ptain! = pres1
'measure the inlet total exit static pressure -----
port1% = 43      ' should be connected to pressure representing Pstat,ex
port2% = 48      ' should be connected to the inlet total pressure
settle = 25      ' time to waite

```

```

CALL svalve(port1%, port2%)
start = TIMER
ichktm: current = TIMER
IF (current - start) < settle GOTO ichktm
'read transducer voltages and change it into Pressures
  FOR i = 91 TO 92    'transducer use hp3497's port90 and port91
    j% = i - 1
    sum = 0
    FOR kj = 1 TO 20
      CALL rdscnefm(j%, volt!)
      sum = sum + volt!
    NEXT kj
    v!(j%) = sum / 20!
  NEXT i
  pres1 = b11 * (v!(90) - vz1) 'calculate pressure
  pres2 = b21 * (v!(91) - vz2) 'calculate pressure
' Now calculate pressures based on most applicable range. Transducer #1
' has a range to about 20 inwg. Transducer #2 has a range to about
' 1 inwg. The lowest applicable range will be selected.
  IF pres1 < .95 THEN p14! = pres2
  IF pres1 >= .95 AND pres2 <= 20 THEN p14! = pres1
' measure the inlet air temperature
  j% = 51          'inlet total temperature #1
  sum = 0!
  FOR kj = 1 TO 10
    CALL rdscnefm(j%, volt!)
    sum = sum + volt!
  NEXT kj
  v!(j%) = sum / 10
  j% = 56          'ice bath reference
  sum = 0!
  FOR kj = 1 TO 10
    CALL rdscnefm(j%, volt!)
    sum = sum + volt!
  NEXT kj
  v!(j%) = sum / 10
  j% = 52          'inlet total temperature #2
  sum = 0!
  FOR kj = 1 TO 10
    CALL rdscnefm(j%, volt!)
    sum = sum + volt!
  NEXT kj
  v!(j%) = sum / 10
  v!(51) = v!(51) - v!(56)
  CALL tempca(v!(51), temp!)
  tink! = temp! + 273.15

```

```

v!(52) = v!(52) - v!(56)
CALL tempca(v!(52), temp!)
ttink2! = temp! + 273.15
' Now calculate and print out key variables to monitor big cylinder
pta! = ptain! * 248.976 + Patm
p14! = p14! * 248.976
psex = pta! - p14!
Maex! = SQR(((pta! / (pta! - p14!)) ^ (1! / 3.5) - 1) * (2 / .4))
Tsex! = ttink2! / (1! - .4 / 2! * Maex! * Maex!)
rhoex = (pta! - p14!) / Tsex! / 287!
sndex = SQR(1.4 * 287! * Tsex!)
Vex = Maex! * sndex
Arat = 50! / 25.356          ' Inlet to exit area ratio
visc = .00001846# * (Tsex! / 300!) ^ 1.5 * (410.556 / (110.556 + Tsex!))
Dcyl = .4064
ReD = rhoex * Vex * Dcyl / visc / Arat
Ttinav = (ttink! + ttink2) / 2!
' Print monitor variables to screen
LOCATE 2, 2: PRINT "Cylinder Reynolds number:      "; ReD
LOCATE 3, 2: PRINT "Inlet total pressure   :      "; pta!
LOCATE 4, 2: PRINT "Inlet total temperature #1:    "; ttink!
LOCATE 5, 2: PRINT "Inlet total temperature #2:    "; ttink2!
LOCATE 6, 2: PRINT "Exit velocity:                "; Vex
LOCATE 7, 2: PRINT "Exit Mach number:            "; Maex!
LOCATE 8, 2: PRINT "Pstatic #1:                  "; psex
LOCATE 11, 2: PRINT "This program is set up to monitor cascade conditions"
LOCATE 12, 2: PRINT "continually. Hit F1 to return to the menu."
LOCATE 13, 2: PRINT "APPROXIMATE RESULTS          "
GOTO ichktm
imon2:
CLS
' measure inlet total to atmospheric pressure difference -----
port1% = 44      ' should be connected to atm
port2% = 48      ' should be connected to inlet total pressure
settle = 25      'time to wait
CALL svalve(port1%, port2%)
start = TIMER
ichkt5: current = TIMER
IF (current - start) < settle GOTO ichkt5
'read transducer voltages and change it into Pressures
FOR i = 91 TO 92      'transducer use hp3497's port90 and port91
j% = i - 1
sum = 0!
FOR kj = 1 TO 20
CALL rdscnefm(j%, volt!)
sum = sum + volt!

```



```

        NEXT kj
        v2!(j%) = sum / 20!
    NEXT i
    pres1 = b11 * (v2!(90) - vz1) 'calculate pressure
    pres2 = b21 * (v2!(91) - vz2) 'calculate pressure
' Now calculate pressures based on most applicable range. Transducer #1
' has a range to about 20 inwg. Transducer #2 has a range to about
' 1 inwg. The lowest applicable range will be selected.
    IF pres1 < .95 THEN ptain! = pres2
    IF pres1 >= .95 AND pres2 <= 20 THEN ptain! = pres1
'measure the inlet total exit static pressure -----
    port1% = 43      ' should be connected to p14, representing Pstat,ave
    port2% = 48      ' should be connected to the inlet total pressure
    settle = 25      ' time to waite
    CALL svalve(port1%, port2%)
    start = TIMER
ichktn5: current = TIMER
    IF (current - start) < settle GOTO ichktn5
'read transducer voltages and change it into Pressures
    FOR i = 91 TO 92      'transducer use hp3497's port90 and port91
        j% = i - 1
        sum = 0
        FOR kj = 1 TO 20
            CALL rdscnefm(j%, volt!)
            sum = sum + volt!
        NEXT kj
        v!(j%) = sum / 20!
    NEXT i
    pres1 = b11 * (v!(90) - vz1) 'calculate pressure
    pres2 = b21 * (v!(91) - vz2) 'calculate pressure
' Now calculate pressures based on most applicable range. Transducer #1
' has a range to about 20 inwg. Transducer #2 has a range to about
' 1 inwg. The lowest applicable range will be selected.
    IF pres1 < .95 THEN p14! = pres2
    IF pres1 >= .95 AND pres2 <= 20 THEN p14! = pres1
' measure the inlet air temperature
    FOR i = 52 TO 57
        j% = i - 1
        sum = 0!
        FOR kj = 1 TO 10
            CALL rdscnefm(j%, volt!)
            sum = sum + volt!
        NEXT kj
        v!(j%) = sum / 10
    NEXT i
    v!(51) = v!(51) - v!(56)

```

```

CALL tempca(v!(51), temp!)
ttink! = temp! + 273.15
v!(52) = v!(52) - v!(56)
CALL tempca(v!(52), temp!)
ttink2! = temp! + 273.15
tt1c = ttink! - 273.15
tt2c = ttink2! - 273.15
' Now calculate and print out key variables to monitor cascade
pta! = ptain! * 248.976 + Patm
p14! = ABS(p14! * 248.976)
psex = pta! - p14!
Maex! = SQR(((pta! / (pta! - p14!)) ^ (1! / 3.5) - 1) * (2 / .4))
Tsex! = ttink2! / (1! - .4 / 2! * Maex! * Maex!)
rhoex = (pta! - p14!) / Tsex! / 287!
sndex = SQR(1.4 * 287! * Tsex!)
Vex = Maex! * sndex
visc = .00001846# * (Tsex! / 300!) ^ 1.5 * (410.556 / (110.556 + Tsex!))
Dcyl = .4064
Arat = 50 / 25.356
ReD = rhoex * Vex * Dcyl / visc / Arat
' Print monitor variables to screen
LOCATE 2, 2: PRINT "Diameter Reynolds number:      "; ReD; "      "
LOCATE 3, 2: PRINT "Inlet total temperatures:      "; ttink!; ttink2!; "      "
LOCATE 4, 2: PRINT "Inlet total temperatures: (C)      "; tt1c; tt2c; "      "
LOCATE 5, 2: PRINT "Exit velocity:      "; Vex; "      "
LOCATE 6, 2: PRINT "Exit static pressure:      "; psex; "      "
' Now set up scanner to measure cylinder thermocouples
idtc(1) = 0      ' Bracket left
idtc(2) = 1      ' Bracket mid
idtc(3) = 2      ' Bracket right
idtc(4) = 3      ' Row 0 Left
idtc(5) = 4      ' Row 0 Mid
idtc(6) = 5      ' Row 0 Right
idtc(7) = 6      ' Row 1 Left
idtc(8) = 7      ' Row 1 Mid
idtc(9) = 8      ' Row 1 Right
idtc(10) = 9     ' Row 2 Left
idtc(11) = 10    ' Row 2 Mid
idtc(12) = 11    ' Row 2 Right
idtc(13) = 12    ' Row 3 Left
idtc(14) = 13    ' Row 3 Mid
idtc(15) = 14    ' Row 3 Right
idtc(16) = 15    ' Row 4 Left
idtc(17) = 16    ' Row 4 Mid
idtc(18) = 17    ' Row 4 Right
idtc(19) = 18    ' Row 5 Left

```

idtc(20) = 19	' Row 5 Mid
idtc(21) = 20	' Row 5 Right
idtc(22) = 21	' Row 6 Left
idtc(23) = 22	' Row 6 Mid
idtc(24) = 23	' Row 6 Right
idtc(25) = 24	' Row 7 Left
idtc(26) = 25	' Row 7 Mid
idtc(27) = 26	' Row 7 Right
idtc(28) = 27	' Row 8 Left
idtc(29) = 28	' Row 8 Mid
idtc(30) = 29	' Row 8 Right
idtc(31) = 30	' Row 9 Left
idtc(32) = 31	' Row 9 Mid
idtc(33) = 32	' Row 9 Right
idtc(34) = 33	' Row 10 Left
idtc(35) = 34	' Row 10 Mid
idtc(36) = 35	' Row 10 Right
idtc(37) = 36	' Row 11 Left
idtc(38) = 37	' Row 11 Mid
idtc(39) = 38	' Row 11 Right
idtc(40) = 39	' Skip, Row 12 Left Bad
idtc(41) = 40	' Row 12 Mid
idtc(42) = 41	' Row 12 Right
idtc(43) = 42	' Row 13 Left
idtc(44) = 43	' Row 13 Mid
idtc(45) = 73	' Row 13 Right
idtc(46) = 45	' Row 14 Left
idtc(47) = 46	' Row 14 Mid
idtc(48) = 47	' Row 14 Right
idtc(49) = 48	' Row 15 Left
idtc(50) = 49	' Row 15 Mid
idtc(51) = 50	' Orifice
idtc(52) = 51	' Inlet Total Temperature 1
idtc(53) = 52	' Inlet Total Temperature 2
idtc(54) = 53	' LE Exit left
idtc(55) = 54	' LE Exit middle
idtc(56) = 55	' LE Exit right
idtc(57) = 56	' Ice Bath
idtc(58) = 57	' Warm AC
idtc(59) = 58	' Cold AC
idtc(60) = 59	' Plenum
idtc(61) = 60	' Row 15 Right
idtc(62) = 61	' Row 16 Left
idtc(63) = 62	' Row 16 Mid
idtc(64) = 63	' Row 16 Right
idtc(65) = 64	' Row 17 Left

```

idtc(66) = 65      ' Row 17 Mid
idtc(67) = 66      ' Row 17 Right
idtc(68) = 67      ' Row 18 Left
idtc(69) = 68      ' Row 18 Mid
idtc(70) = 69      ' Row 18 Right
idtc(71) = 70      ' Row 19 Left
idtc(72) = 71      ' Row 19 Mid
idtc(73) = 72      ' Row 19 Right
' Now zero sums
  FOR i = 1 TO 73
    sumt(i) = 0!
  NEXT i
' Now acquire mean voltages
  nave = 1
  FOR i = 1 TO nave
    FOR j = 1 TO 73
      jx% = idtc(j)
      CALL rdscnefm(jx%, volt!)
      sumt(j) = sumt(j) + volt!
    NEXT j
  NEXT i
  FOR i = 1 TO 73
    vt(i) = sumt(i) / nave
  NEXT i
  vtice = vt(57)
  FOR i = 1 TO 73
    vt(i) = vt(i) - vtice
    CALL tempca(vt(i), temp5!)
    tc(i) = temp5!
    IF tc(i) < -10 OR tc(i) > 100 THEN tc(i) = 99.9
  NEXT i
  tc(75) = 0!
  LOCATE 7, 2: PRINT "Slot temperatures:          "; tc(54); tc(55); tc(56); "          "
  LOCATE 8, 2: PRINT "Surface Temperatures"; " Orifice temperature"; tc(51); "
"
  LOCATE 9, 2: PRINT USING "#####.##"; tc(1); tc(2); tc(3); tc(75); tc(31); tc(32);
tc(33)
  LOCATE 10, 2: PRINT USING "#####.##"; tc(4); tc(5); tc(6); tc(75); tc(34); tc(35);
tc(36)
  LOCATE 11, 2: PRINT USING "#####.##"; tc(7); tc(8); tc(9); tc(75); tc(37); tc(38);
tc(39)
  LOCATE 12, 2: PRINT USING "#####.##"; tc(10); tc(11); tc(12); tc(75); tc(40);
tc(41); tc(42)
  LOCATE 13, 2: PRINT USING "#####.##"; tc(13); tc(14); tc(15); tc(75); tc(43);
tc(44); tc(45)

```

```

LOCATE 14, 2: PRINT USING "#####.##"; tc(16); tc(17); tc(18); tc(75); tc(46);
tc(47); tc(48)
LOCATE 15, 2: PRINT USING "#####.##"; tc(19); tc(20); tc(21); tc(75); tc(49);
tc(50); tc(61)
LOCATE 16, 2: PRINT USING "#####.##"; tc(22); tc(23); tc(24); tc(75); tc(62);
tc(63); tc(64)
LOCATE 17, 2: PRINT USING "#####.##"; tc(25); tc(26); tc(27); tc(75); tc(65);
tc(66); tc(67)
LOCATE 18, 2: PRINT USING "#####.##"; tc(28); tc(29); tc(30); tc(75); tc(68);
tc(69); tc(70)
LOCATE 19, 2: PRINT USING "#####.##"; tc(75); tc(75); tc(75); tc(75); tc(71);
tc(72); tc(73)
LOCATE 20, 2: PRINT "Plenum temperature"; tc(60); "AC in, AC out: "; tc(58);
tc(59); "      "
FOR i = 94 TO 95      'transducer use hp3497's port93 and port94
  j% = i - 1
  sum = 0
  FOR kj = 1 TO 20
    CALL rdscnefm(j%, volt!)
    sum = sum + volt!
  NEXT kj
  v(j%) = sum / 20
NEXT i
vcur = ABS(v(94)) / .001
vpwr = vcur * ABS(v(93))
LOCATE 20, 2: PRINT "Htr Vlt: "; ABS(v(93)); "Htr cur: "; vcur; "Htr pwr: "; vpwr; "
LOCATE 21, 2: PRINT "This program is set up to monitor cascade conditions"; "      "
LOCATE 22, 2: PRINT "continually. Hit F1 to return to the menu."; "      "
GOTO ichktn5
ichkflw:
'measure the upstream absolute pressure-----
CLS
PRINT "Measure the Delta pressure..."
port1% = 44      'will open valve 44 open to atmosphere
port2% = 46      'will open valve 46 upstream orifice port
settle = 25      ' time to wait
CALL svalve(port1%, port2%)
start = TIMER
bhktn2: current = TIMER
IF (current - start) < settle GOTO bhktn2
'read transducer voltages and change it into Pressures
FOR i = 91 TO 92      'transducer use hp3497's port90 and port91
  j% = i - 1
  sum = 0
  FOR kj = 1 TO 10
    CALL rdscnefm(j%, volt!)

```

```

        sum = sum + volt!
    NEXT kj
    v(j%) = sum / 10
NEXT i
pres1 = b11 * (v(90) - vz1) 'calculate pressure
pres2 = b21 * (v(91) - vz2) 'calculate pressure
' Now calculate pressures based on most applicable range. Transducer #1
' has a range to about 20 inwg. Transducer #2 has a range to about
' 1 inwg. The lowest applicable range will be selected.
IF pres1 < .95 THEN Pup = pres2
IF pres1 >= .95 AND pres2 <= 20 THEN Pup = pres1
Pup1 = Pup * 248.976 'change from inch water to pa
'measure the Delta pressure-----
PRINT "Measure the Delta pressure..."
port1% = 41 'will open valve 41 downstream port
port2% = 46 'will open valve 46 upstream port
settle = 25 'settling time (sec)
CALL svalve(port1%, port2%)
start = TIMER
bhktm: current = TIMER
IF (current - start) < settle GOTO bhktm
iflowchk:
'read transducer voltages and change it into Pressures
FOR i = 91 TO 92 'transducer use hp3497's port90 and port91
    j% = i - 1
    sum = 0
    FOR kj = 1 TO 10
        CALL rdscnefm(j%, volt!)
        sum = sum + volt!
    NEXT kj
    v(j%) = sum / 10
NEXT i
pres1 = b11 * (v(90) - vz1) 'calculate pressure
pres2 = b21 * (v(91) - vz2) 'calculate pressure
' Now calculate pressures based on most applicable range. Transducer #1
' has a range to about 20 inwg. Transducer #2 has a range to about
' 1 inwg. The lowest applicable range will be selected.
IF pres1 < .95 THEN Deltap = pres2
IF pres1 >= .95 AND pres2 <= 20 THEN Deltap = pres1
deltaP1 = Deltap * 248.976 'change from inch water to pa
PRINT "vzero1, vzero2 = "; vz1; vz2
Pup2 = Pup1 + Patm
PRINT "Deltap=", deltaP1, "pa"; "Pup = ", Pup2, "pa"
repeat1:
'measure the orifice air and the cascade inlet temperature
FOR i = 51 TO 57

```

```

j% = i - 1
sum = 0!
  FOR kj = 1 TO 10
    CALL rdscnefm(j%, volt!)
    sum = sum + volt!
  NEXT kj
v!(j%) = sum / 10
NEXT i
v!(50) = v!(50) - v!(56) ' orifice
v!(51) = v!(51) - v!(56) ' Tt1 (up)
v!(52) = v!(52) - v!(56) ' Tt2 (dn)
v!(53) = v!(53) - v!(56) ' Tc1 (far)
v!(54) = v!(54) - v!(56) ' Tc2 (mid)
v!(55) = v!(55) - v!(56) ' Tc3 (near)
CALL tempca(v!(50), temp1!)
torf! = temp1! + 273.15
CALL tempca(v!(51), temp2!)
ttun! = temp2! + 273.15
CALL tempca(v!(52), temp3!)
ttunb! = temp3! + 273.15
CALL tempca(v!(53), temp4!)
tcf! = temp4! + 273.15
CALL tempca(v!(54), temp5!)
tcm! = temp5! + 273.15
CALL tempca(v!(55), temp6!)
tcn! = temp6! + 273.15
' begin flow rate calculation-----
dorf = ORIFICEDIAMETER * .0254
dpipe = 3.03 * .0254
LUP! = (2.015) * .0254 ' (1.3 + 13! / 8) * .0254
LDOWN! = (2.015) * .0254
CALL siflow(dorf, dpipe, LUP!, LDOWN!, torf!, Pup2, deltaP1, siflw!)
Aslot = 9! * .143 * .0254 * .0254 ' m2
rhoVc = siflw! / Aslot
brate = rhoVc / (rhoex * Vex * .5329)
CLS
LOCATE 2, 2: PRINT "Cascade inlet air temperature is: "; ttun!; " K"
LOCATE 3, 2: PRINT "Cooling air temperature is: "; torf!; " K"
LOCATE 4, 2: PRINT "Film cooling temperature is (far)"; tcf!; " K"
' LOCATE 5, 2: PRINT "Film cooling temperature is:(mid)"; tcm!; " K"
LOCATE 5, 2: PRINT "Film cooling temperature is:(near)"; tcn!; " K"
LOCATE 6, 2: PRINT "Cooling air flow rate--mass flux: "; siflw!; " Kg/s "; rhoVc;
"kg/s/m2"
LOCATE 7, 2: PRINT "Estimated Blowing ratio: "; brate
LOCATE 8, 2: PRINT "Cascade inlet air temperature:(1)"; ttun1!; " K"
LOCATE 9, 2: PRINT "Cooling air temperature is: (1)"; torf1!; " K"

```

```

LOCATE 10, 2: PRINT "Film cooling temperature is (far)"; tcf1!; " K"
' LOCATE 11, 2: PRINT "Film cooling temperature is:(mid)"; tcm1!; " K"
LOCATE 11, 2: PRINT "Film cooling temperature is:(near)"; tcn1!; " K"
LOCATE 12, 2: PRINT "Cooling air flow rate is--mass flux: (1)"; siflw1!; " Kg/s ";
rhoVc1; "kg/s/m2"
LOCATE 13, 2: PRINT "Estimated Blowing ratio:      "; brate1
LOCATE 14, 2: PRINT "Cascade inlet air temperature:(2)"; ttun2!; " K"
LOCATE 15, 2: PRINT "Cooling air temperature is: (2)"; torf2!; " K"
LOCATE 16, 2: PRINT "Film cooling temperature is (far)"; tcf2!; " K"
' LOCATE 17, 2: PRINT "Film cooling temperature is:(mid)"; tcm2!; " K"
LOCATE 17, 2: PRINT "Film cooling temperature is:(near)"; tcn2!; " K"
LOCATE 18, 2: PRINT "Cooling air flow rate is--mass flux: (2)"; siflw2!; " Kg/s ";
rhoVc2; "kg/s/m2"
LOCATE 19, 2: PRINT "Estimated Blowing ratio:      "; brate2
LOCATE 20, 2: PRINT "Orifice diameter ="; ORIFICEDIAMETER; " inches"
rhoVc2 = rhoVc1
brate2 = brate1
tcf2! = tcf1!
tcm2! = tcm1!
tcn2! = tcn1!
siflw2! = siflw1!
siflw1! = siflw!
torf2! = torf1!
ttun2! = ttun1!
ttun1! = ttun!
torf1! = torf!
tcf1! = tcf!
tcm1! = tcm!
tcn1! = tcn!
rhoVc1 = rhoVc
brate1 = brate
GOTO iflowchk
iblowrat:
' This subroutine has been written to acquire inlet static pressures
CLS
FOR k = 1 TO 9
ip% = k
IF k = 9 THEN ip% = 43 ' reading exit static
IF k = 8 THEN ip% = 44 ' reading atmospheric
IF k = 7 THEN ip% = 44 ' reading atmospheric
IF k = 6 THEN ip% = 41 ' reading downstream orifice
port1% = ip% ' scanning ports attached to inlet statics
port2% = 48 ' should be connected to the inlet total pressure
IF k = 5 THEN port2% = 46
IF k = 6 THEN port2% = 46
IF k = 7 THEN port2% = 46

```



```

settle = 20      ' time to wait
CALL svalve(port1%, port2%)
start = TIMER
ichktm2: current = TIMER
  IF (current - start) < settle GOTO ichktm2
'read transducer voltages and change it into Pressures
  FOR i = 91 TO 92    'transducer use hp3497's port90 and port91
    j% = i - 1
    sum = 0!
    FOR kj = 1 TO 20
      CALL rdscnefm(j%, volt!)
      sum = sum + volt!
    NEXT kj
    v!(j%) = sum / 20!
  NEXT i
  pres1 = b11 * (v!(90) - vz1) 'calculate pressure
  pres2 = b21 * (v!(91) - vz2) 'calculate pressure
' Now calculate pressures based on most applicable range. Transducer #1
' has a range to about 20 inwg. Transducer #2 has a range to about
' 1 inwg. The lowest applicable range will be selected.
  IF pres1 < .95 THEN pin(k) = pres2
  IF pres1 >= .95 AND pres2 <= 20 THEN pin(k) = pres1
  NEXT k
'measure the inlet air temperature
  FOR i = 51 TO 57
    j% = i - 1
    sum = 0!
    FOR kj = 1 TO 10
      CALL rdscnefm(j%, volt!)
      sum = sum + volt!
    NEXT kj
    v!(j%) = sum / 10
  NEXT i
  v!(50) = v!(50) - v!(56) ' orifice
  v!(51) = v!(51) - v!(56) ' Tt1 (up)
  v!(52) = v!(52) - v!(56) ' Tt2 (dn)
  v!(53) = v!(53) - v!(56) ' Tc1 (far)
  v!(54) = v!(54) - v!(56) ' Tc2 (mid)
  v!(55) = v!(55) - v!(56) ' Tc3 (near)
  CALL tempca(v!(50), temp1!)
  torf! = temp1! + 273.15
  CALL tempca(v!(51), temp2!)
  ttun! = temp2! + 273.15
  CALL tempca(v!(52), temp3!)
  ttunb! = temp3! + 273.15
  CALL tempca(v!(53), temp4!)

```

```

tcf! = temp4! + 273.15
CALL tempca(v!(54), temp5!)
tcm! = temp5! + 273.15
CALL tempca(v!(55), temp6!)
tcn! = temp6! + 273.15
deltaP1 = pin(6) * 248.976
Pup2 = pin(7) * 248.976 + Patm
dorf = ORIFICEDIAMETER * .0254
dpipe = 3.03 * .0254
LUP! = (2.015) * .0254 * (1.3 + 13! / 8) * .0254
LDOWN! = (2.015) * .0254
CALL siflow(dorf, dpipe, LUP!, LDOWN!, torf!, Pup2, deltaP1, siflw!)
' Now calculate and print out key variables to monitor cascade
pta! = pin(8) * 248.976 + Patm
pin(9) = pin(9) * 248.976
Maex! = SQR(((pta! / (pta! - pin(9)))) ^ (1! / 3.5) - 1) * (2 / .4))
Tsex! = ttink! / (1! - .4 / 2! * Maex! * Maex!)
rhoex = (pta! - pin(9)) / Tsex! / 287!
sndex = SQR(1.4 * 287! * Tsex!)
Vex = Maex! * sndex
visc = .00001846# * (Tsex! / 300!) ^ 1.5 * (410.556 / (110.556 + Tsex!))
Dcyl = .4064
Arat = 50 / 25.356
ReD = rhoex * Vex * Dcyl / visc / Arat
pin1c = pin(1) * 248.976
pin2c = pin(2) * 248.976
pex1 = (pin1c + pin2c) / 2
Mafs! = SQR(((pta! / (pta! - pex1))) ^ (1! / 3.5) - 1) * (2 / .4))
Tsfs! = ttink! / (1! - .4 / 2! * Mafs! * Mafs!)
rhofs = (pta! - pex1) / Tsex! / 287!
sndfs = SQR(1.4 * 287! * Tsex!)
Vfs = Mafs! * sndfs
Afc = 9 * .143 * .0254 * .0254
rhoVfc = siflw! / Afc
Brat = rhoVfc / rhofs / Vfs
pslt1 = pin(3) * 248.976
pslt2 = pin(4) * 248.976
Pplm3 = pin(5) * 248.976
Tcoolave = (tcf! + tcn!) / 2 'T middle eliminated, touching plastic
' Now zero sums
FOR i = 1 TO 73
    sumt(i) = 0!
NEXT i
' Now acquire mean voltages
nave = 15
FOR i = 1 TO nave

```

```

FOR j = 1 TO 73
  jx% = idtc(j)
  CALL rdscnefm(jx%, volt!)
  sumt(j) = sumt(j) + volt!
NEXT j
NEXT i
FOR i = 1 TO 73
  vt(i) = sumt(i) / nave
NEXT i
vtice = vt(57)
FOR i = 1 TO 73
  vt(i) = vt(i) - vtice
  CALL tempca(vt(i), temp5!)
  tc(i) = temp5!
  IF tc(i) < -10 OR tc(i) > 100 THEN tc(i) = 99.9
NEXT i
' Print monitor variables to screen
LOCATE 2, 2: PRINT "Exit Reynolds number: "; ReD
LOCATE 3, 2: PRINT "Inlet total temperature: "; ttink!
LOCATE 4, 2: PRINT "Inlet total pressure: "; pta!
LOCATE 5, 2: PRINT "Blowing ratio: "; Brat
LOCATE 6, 2: PRINT "Free Stream vel. & density: "; Vfs; rhofs
LOCATE 7, 2: PRINT "Exit Mach number: "; Maex!
LOCATE 8, 2: PRINT "Coolant out temps & average "; tcf!; tcm!; tcn!; Tcoolave
LOCATE 9, 2: PRINT "Slot exit pressures & ave "; pin1c; pin2c; pex1
LOCATE 10, 2: PRINT "Slot, plm internal pressures "; pslt1; pslt2; Pplm3
LOCATE 11, 2: INPUT "Input the film cooling output name: "; outfile$
IF outfile$ = "" THEN outfile$ = "bigfctst.prn"
OPEN outfile$ FOR OUTPUT AS #1
PRINT #1, "ReD "; ReD
PRINT #1, "Ttin(K) "; ttink!
PRINT #1, "Ptin(Pa) "; pta!
PRINT #1, "Patm(Pa) "; Patm
PRINT #1, "Blowing_ratio "; Brat
PRINT #1, "Vfreestm_slot(m/s) "; Vfs
PRINT #1, "Vexit(m/s) "; Vex
PRINT #1, "Free_Stream_density "; rhofs
PRINT #1, "Exit_Mach_number "; Maex!
PRINT #1, "Mass_flow_rate(kg/s) "; siflw!
PRINT #1, "T_Cool_temps&avg(K) "; tcf!; tcm!; tcn!; Tcoolave
PRINT #1, "Surf_press_slt&avg(Pa) "; pin1c; pin2c; pex1
PRINT #1, "Slot&plm_int_press(Pa) "; pslt1; pslt2; Pplm3
PRINT #1, "Temp_legend_Torf,Tin1,Tin2;Tc123;Tc12;Tbrk123;Tsrfl-60"
PRINT #1, USING "#####.###"; tc(51); tc(52); tc(53)
PRINT #1, USING "#####.###"; tc(54); tc(55); tc(56)
PRINT #1, USING "#####.###"; tc(58); tc(59)

```

```

PRINT #1, USING "####.###"; tc(1); tc(2); tc(3)
PRINT #1, USING "####.###"; tc(4); tc(5); tc(6)
PRINT #1, USING "####.###"; tc(7); tc(8); tc(9)
PRINT #1, USING "####.###"; tc(10); tc(11); tc(12)
PRINT #1, USING "####.###"; tc(13); tc(14); tc(15)
PRINT #1, USING "####.###"; tc(16); tc(17); tc(18)
PRINT #1, USING "####.###"; tc(19); tc(20); tc(21)
PRINT #1, USING "####.###"; tc(22); tc(23); tc(24)
PRINT #1, USING "####.###"; tc(25); tc(26); tc(27)
PRINT #1, USING "####.###"; tc(28); tc(29); tc(30)
PRINT #1, USING "####.###"; tc(31); tc(32); tc(33)
PRINT #1, USING "####.###"; tc(34); tc(35); tc(36)
PRINT #1, USING "####.###"; tc(37); tc(38); tc(39)
PRINT #1, USING "####.###"; tc(40); tc(41); tc(42)
PRINT #1, USING "####.###"; tc(43); tc(44); tc(45)
PRINT #1, USING "####.###"; tc(46); tc(47); tc(48)
PRINT #1, USING "####.###"; tc(49); tc(50); tc(61)
PRINT #1, USING "####.###"; tc(62); tc(63); tc(64)
PRINT #1, USING "####.###"; tc(65); tc(66); tc(67)
PRINT #1, USING "####.###"; tc(68); tc(69); tc(70)
PRINT #1, USING "####.###"; tc(71); tc(72); tc(73)
PRINT #1, "HtrVlt_Cur&Power          "; ABS(v(93)); vcur; vpw
PRINT #1, "Orifice_pressure(Pa)      "; Pup2
PRINT #1, "DeltaP_orf(Pa)            "; deltaP1
PRINT #1, "Torific(K)                "; torf!
PRINT #1, "Pexit_static(Pa)          "; pin(9)
PRINT #1, "Pressure_legend_Pbrk12;Pslt12;Plnm;Pta,Pts;Pua,dPorf"
PRINT #1, USING "####.###"; pin(1); pin(2)
PRINT #1, USING "####.###"; pin(3); pin(4)
PRINT #1, USING "####.###"; pin(5)
PRINT #1, USING "####.###"; pin(6); pin(7)
PRINT #1, USING "####.###"; pin(8); pin(9)
CLOSE #1
INPUT "Hit return to go back to option menu: "; cr$
GOTO ioption
iend:
END
SUB clrdvm STATIC
' this subroutine is used for clear the board and instruments
SHARED PCIB.ERR, PCIB.BASERR, NOERR
ISC& = 7
dvm& = 709
scanner& = 709
CALL IORESET(ISC&)
IF PCIB.ERR <> NOERR THEN ERROR PCIB.BASERR
CALL IOCLEAR(ISC&)

```

```

    IF PCIB.ERR <> NOERR THEN ERROR PCIB.BASERR
END SUB
    SUB rdscnefm (ichnl%, volt!) STATIC
' this subroutine is used for sending control string to hp3497 to
' call in channel
    SHARED PCIB.ERR, PCIB.BASERR, NOERR
    ISC& = 7
    dvm& = 709
    scanner& = 709
    wrt$ = "AC" + STR$(ichnl%)
    CALL IOOUTPUTS(scanner&, wrt$, LEN(wrt$))
    IF PCIB.ERR <> NOERR THEN ERROR PCIB.BASERR
    wrt$ = "AI" + STR$(ichnl%)
    CALL IOOUTPUTS(scanner&, wrt$, LEN(wrt$))
    IF PCIB.ERR <> NOERR THEN ERROR PCIB.BASERR
" now read the digital voltmeter
    MAXL% = 20
    actual% = 0
    rd$ = SPACE$(20)
    CALL IOENTERS(dvm&, rd$, MAXL%, actual%)
    rd$ = LEFT$(rd$, actual%)
    volt! = VAL(rd$)
    IF PCIB.ERR <> NOERR THEN ERROR PCIB.BASERR
END SUB
' this program is used to set hp3497 for data acquisition
SUB setdvm STATIC
    SHARED PCIB.ERR, PCIB.BASERR, NOERR
    ISC& = 7
    dvm& = 709
    scanner& = 709
    CALL IORESET(ISC&)
    IF PCIB.ERR <> NOERR THEN ERROR PCIB.BASERR
    CALL IOTIMEOUT(ISC&, 5!)
    IF PCIB.ERR <> NOERR THEN ERROR PCIB.BASERR
    CALL IOCLEAR(ISC&)
    IF PCIB.ERR <> NOERR THEN ERROR PCIB.BASERR
' send hp3497 the setup code, SET "Programming a software trigger "
    CODE$ = "VT3" ' software trigger
    CALL IOOUTPUTS(dvm&, CODE$, LEN(CODE$))
    IF PCIB.ERR <> NOERR THEN ERROR PCIB.BASERR
" Send the hp3497 the setup code,SET "IT AS AUTORANGE"
    CODE$ = "VR5" ' autorange
    CALL IOOUTPUTS(dvm&, CODE$, LEN(CODE$))
    IF PCIB.ERR <> NOERR THEN ERROR PCIB.BASERR
" Send the HP3497 the setup code,Set up "5 1/2 digit display"
    CODE$ = "VD5" ' 5 1/2 digit display

```

```

CALL IOOUTPUTS(dvm&, CODE$, LEN(CODE$))
IF PCIB.ERR <> NOERR THEN ERROR PCIB.BASERR
" Send the HP3497 the setup code,SET "AUTOZERO"
CODE$ = "VA1" ' autozero
CALL IOOUTPUTS(dvm&, CODE$, LEN(CODE$))
IF PCIB.ERR <> NOERR THEN ERROR PCIB.BASERR
" Send code to voltmeter, SET "1 readings per trigger"
CODE$ = "VN1" ' Number of readings per trigger
CALL IOOUTPUTS(dvm&, CODE$, LEN(CODE$))
IF PCIB.ERR <> NOERR THEN ERROR PCIB.BASERR
END SUB
DEFINT I-N
SUB siflow (dorf!, dpipe!, LUP!, LDOWN!, torf, p1, dp!, siflw) STATIC
'PRINT #2, "dorf=", dorf!
'PRINT #2, "dpipe=", dpipe!
'PRINT #2, "Lup=", LUP!
'PRINT #2, "Ldown=", LDOWN!
'PRINT #2, "torf=", torf!
"PRINT #2, "p1=", p1
'PRINT #2, "dp=", dp!
' Convert to calculated output variables
'-----
' SUBROUTINE NAME: SIFLOW.BAS
' ISO 5167 orifice plate calculations
' Developed from the Stolz equation as given by R. W. Miller, 1989 "Flow
' Measurement Engineering Handbook," 2nd Ed. McGraw-Hill Publishing Co.
' by Forrest Ames September 1998
' Definition of Variables used:
' DORF - orifice diameter in meters
' DPIPE - pipe diameter in meters
' TORF - Temperature in degrees K
' LUP - Distance from orifice plate to upstream pressure tap
' LDOWN - Distance from orifice plate to downstream pressure tap
' P1 - orifice upstream pressure in Pa
' P2 - orifice downstream pressure in Pa
' CD - discharge coefficient (calculated)
' SIFLW - mass flow rate in kg/s
' REYNO - Pipe Reynolds number
DIM t$(3)
gamma = 1.4
r = 287!
pi = 3.14159
H$ = "N"
pass = 0
AREAP = (3.14159 * dpipe! ^ 2) / 4!: ' AREA OF PIPE
AREA0 = (3.14159 * dorf! ^ 2) / 4!: ' AREA OF ORIFICE

```

```

reyno = 35000!: ' FIRST CRACK AT IT, ANYWAY
GOSUB 9500: ' DISCHARGE COEFFIECIENT ROUTINE
GOSUB 1120: ' FLOW THROUGH ORIFICES ROUTINE
GOSUB 1600: ' OUTPUT ROUTINE
' Discharge Coefficient Routine
9500 beta = dorf! / dpipe!: 'Beta Factor
' This routine calculates a discharge coefficient
' using the Stolz equations from Miller's Flow Measurement
' Engineering Handbook , 2th Edition, P. 9-115 for Square-Edged
' Orifices with either Flange, 1D-1/2D, or Vena Contracta
' pressure taps. This routine uses the variables BETA, LUP,
' LDOWN, DPIPE, DORF, AND REYNO . It calculates CD.
' First determine the Cd for flange taps
CD1 = .5959 + .0317 * beta ^ 2.1 - .1848 * beta ^ 8
' Now determine the influence of pressure tap position
L1! = LUP! / dpipe!
IF L1! > .44 THEN L1! = .44
L2! = LDOWN! / dpipe! + .03
IF LUP! = 0 THEN L1! = .008
IF LDOWN! = 0 THEN L2! = .038
CD2 = .0909 * L1! * beta ^ 4 / (1 - beta ^ 4) - .0335 * L2! * beta ^ 3
' Now determine the influence for Reynolds number
CD3 = 91.71 * beta ^ 2.5 * reyno ^ -.75
' Now add up all the effects
CD = CD1 + CD2 + CD3
RETURN
' This next routine calculates flow rates through
' orifices. The flow equations used are from Miller's
' Flow Measurement Engineering Handbook, 2nd Edition.
1120
QFLOW = 0
siflw = 0
beta = dorf! / dpipe!
RNO = 35000!
reyno = RNO
IF dp! < .001 GOTO 1500 'before change: dp!<0!
' CALCULATE ABSOLUTE VISCOSITY (PA-SEC)
U = .0000184 * (torf / 300!) ^ 1.5 * (410.556 / (110.556 + torf))
' CALCULATE EXPANSION FACTOR (9.56) P. 9-21
Y1 = 1! - (.41 + .35 * beta ^ 4) * ((dp!) / (p1 * gamma))
' CALCULATE DENSITY (KG/M^3)
rho = p1 / r / torf
' CALCULATE ORIFICE AREA THERMAL EXPANSION FOR ALUMINUM
FA = 1! + 2! * .000013 * 1.8 * (torf - 293.15)
' CALCULATE FLOW RATES, CD, AND REYNOLDS NOS.
FOR pass = 1 TO 10

```

```

GOSUB 9500: ' GO TO DISCHARGE COEFFICIENT ROUTINE
' PRINT pass; beta; rho; Y1; FA
QFLOW = CD * Y1 * (pi * dorf! ^ 2 / 4!) / SQR(1! - beta ^ 4) * SQR(2! * dp! / rho)
QFLOW = FA * QFLOW
siflw = rho * QFLOW
reyno = 4! * siflw / (pi * dpipe! * U)
  DIFF = ABS((RNO - reyno) / reyno)
  IF DIFF <= .002 GOTO 1490
  RNO = reyno
  NEXT pass
  PRINT "ORIFICE ITERATION FAILS TO CONVERGE!"
1490 REYNP = reyno
1500 RETURN
1600 PRINT "'CD; reyno "; CD; reyno
" PRINT #1, CD; reyno;
END SUB
DEFSNG I-N
SUB svalve (port1%, port2%) STATIC
  PRINT "Valve "; port1%; " and valve "; port2%; " are open."
' configure DIO-48 cards as digital output
  OUT (&H310 + 3), &H80 'first part of DIO-48 configuration
  OUT (&H310 + 7), &H80 'second part of DIO-48 configuration
' try to map port1% and port2% number to relays of CIO-ERB48
  port2% = 65 - port2% ' map port2% number to relay
  ' map port1% number to CIO_ERB48' relay:
  IF (port1% >= 1) AND (port1% <= 8) THEN
    port1% = 33 - port1%
  ELSEIF (port1% >= 9) AND (port1% <= 16) THEN
    port1% = 49 - port1%
  ELSEIF (port1% >= 17) AND (port1% <= 24) THEN
    port1% = 65 - port1%
  ELSEIF (port1% >= 25) AND (port1% <= 32) THEN
    port1% = 33 - port1%
  ELSEIF (port1% >= 33) AND (port1% <= 40) THEN
    port1% = 49 - port1%
  ELSE
    port1% = 65 - port1%
  END IF
  adbase1 = &H310 ' base address
  adbase2 = &H310
  IF (port1% >= 21) AND (port1% <= 24) THEN 'port1 and port2 at same register
    'otherwise there must be two output
    prt1% = 2 ^ ABS(port1% - 24) + 2 ^ ABS(port2% - 24)
    adbase1 = adbase1 + 6
  irtn3:
  OUT (adbase1), prt1% 'open two valve at the same time

```



```

FOR i = 1 TO 1000
NEXT i
raw2% = INP(adbase1)
IF raw2% > 0 THEN
  raw3% = LOG(raw2%) / LOG(2) + 1
ELSE
  raw3% = 0
END IF
FOR i = 1 TO 1000
NEXT i
IF raw2% <> prt1% THEN GOTO irtn3
GOTO lastline
'otherwise, try to map the port number to two different register
'first try to map port1
ELSEIF (port1% >= 1) AND (port1% <= 8) THEN
  prt1% = 2 ^ ABS(port1% - 8) 'prt1% is the number used to output
  adbase1 = adbase1 + 4 'adbase1 is the address of DIO-48 register
ELSEIF (port1% >= 9) AND (port1% <= 16) THEN
  prt1% = 2 ^ ABS(port1% - 16)
  adbase1 = adbase1 + 5
ELSEIF (port1% >= 25) AND (port1% <= 32) THEN
  prt1% = 2 ^ ABS(port1% - 32)
  adbase1 = adbase1 + 0
ELSEIF (port1% >= 33) AND (port1% <= 40) THEN
  prt1% = 2 ^ ABS(port1% - 40)
  adbase1 = adbase1 + 1
ELSEIF (port1% >= 41) AND (port1% <= 48) THEN
  prt1% = 2 ^ ABS(port1% - 48)
  adbase1 = adbase1 + 2
END IF
'then try to map port2% number to DIO-48 registers
prt2% = 2 ^ ABS(port2% - 24)
adbase2 = adbase2 + 6
'begin two outputs for two registers:
irtn:
OUT (adbase1), prt1% ' open first valve
FOR i = 1 TO 1000
NEXT i
raw% = INP(adbase1)
IF raw% > 0 THEN
  raw1% = LOG(raw%) / LOG(2) + 1
ELSE
  raw1% = 0
END IF
FOR i = 1 TO 1000
NEXT i

```

```

IF raw% <> prt1% THEN GOTO irtn
irtn2:
OUT (adbase2), prt2% 'open second valve
FOR i = 1 TO 1000
NEXT i
raw2% = INP(adbase2)
IF raw2% > 0 THEN
  raw3% = LOG(raw2%) / LOG(2) + 1
ELSE
  raw3% = 0
END IF
FOR i = 1 TO 1000
NEXT i
IF raw2% <> prt2% THEN GOTO irtn2
lastline: END SUB

```

```

.....
' subroutine tempca
' This subroutine converts a type K (chromel/alumel) thermocouple emf into
' a temperature. The conversion is made by an thrid order polynomial fit
' to the National Bureau of Standards Thermocouple Reference Tables, NBS
' Monograph 125, 1979, and quoted on page T-12 of the OMEGA Temperature
' Measurement Handbook and Encyclopedia, 1987. The polynomial fit is
' applicable from 0 to 100 degrees C. The polynomial deviates from the
' NBS reference table by less than .013 degrees C, about equal to the
' precision of the reference tables.
' Last edit: 24 Sept. 1987
SUB tempca (volt, temp) STATIC
  a0 = -.01075
  a1 = 25.37273
  a2 = -.40435
  a3 = .042067
  v = volt * 1000
  temp = a0 + v * (a1 + v * (a2 + v * a3))
END SUB
SUB zerop (vz1, vz2)
CALL setdvm
DIM sumz(20), volt(120)
PRINT "Measure the Zero Point..."
port1% = 44
port2% = 45
istr2:
CALL svalve(port1%, port2%)
start = TIMER
ichkt2: current = TIMER
IF (current - start) < 20 GOTO ichkt2
sumz(1) = 0!

```

```

sumz(2) = 0!
FOR i = 1 TO 2
  FOR j = 1 TO 16
    ichn% = i + 89 'the output signals are connected with channel 90&91
    CALL rdscnefm(ichn%, volt((i - 1) * 16 + j))
    sumz(i) = sumz(i) + volt((i - 1) * 16 + j)
  NEXT j
NEXT i
FOR i = 1 TO 16
  PRINT volt(i); volt(i + 16)
NEXT i
  vz1 = sumz(1) / 16!
  vz2 = sumz(2) / 16!
END SUB

```

REFERENCES

- [1] Bathie, W.W., "Fundamentals of Gas Turbines", J. Wiley, New York, 1996, pp. 453.
- [2] Ames, F.E., and Bons, J., "Cooling Strategies for Vane Leading Edges in a Syngas Environment Including Effects of Deposition and Turbulence", *UTSR Workshop - Aerodynamics/Heat Transfer Breakout*, 2011, pp. 1-39.
- [3] Cengel, Y.A., "Heat and Mass Transfer - A Practical Approach", McGraw-Hill, New York, 2007, pp. 901.
- [4] Colban, W.F., Thole, K.A., Bogard, D., "A Film-Cooling Correlation for Shaped Holes on a Flat-Plate Surface", *Journal of Turbomachinery*, Vol. 133, 2011, pp. 1-11.
- [5] Bunker, R.S., "A Study of Mesh-Fed Slot Film Cooling", *Journal of Turbomachinery*, Vol. 133, 2011, pp. 1-8
- [6] Bogard, D.G., Bruce-Black, J.E., Davidson, F.T., and Johns, D.R., "Practical Slot Configurations for Turbine Film Cooling Applications", *Proceedings of ASME Turbo Expo*, No. GT2009-59674.
- [7] Smith, A.C., Hatchett, J.H., Nix, A.C., Ng, W.F., Thole, K.A., and Cunha, F.J., "Effectiveness of Normal and Angled Slot Cooling", *Proceedings of ASME Turbo Expo*, No. GT2004-53248.
- [8] Brauckmann, D., and von Wolfersdorf, J., "Influence of Compound Angle on Adiabatic Film Cooling Effectiveness and Heat Transfer Coefficient for a Row of Shaped Film Cooling Holes", *Proceedings of ASME Turbo Expo*, No. GT2005-68036.
- [9] Knost, D.G., and Thole, K.A., "Adiabatic Effectiveness Measurements of Endwall Film-Cooling for a First Stage Vane", *Proceedings of ASME Turbo Expo*, No. GT2004-53326.
- [10] Mhetras, S., Han, J., and Rudolph, R., "Effect of Flow Parameter Variations on Full Coverage Film-Cooling Effectiveness for a Gas Turbine Blade", *Proceedings of ASME Turbo Expo*, No. GT2007-27071.
- [11] Colban, W., Thole, K.A., and Haendler, M., "A Comparison of Cylindrical and Fan-Shaped Film-Cooling Holes on a Vane Endwall at Low and High Freestream Turbulence Levels", *Proceedings of ASME Turbo Expo*, No. GT-2006-90021.

- [12] Bunker, R.S., "A Review of Shaped Hole Turbine Film-Cooling Technology", *Journal of Heat Transfer*, Vol. 127, 2005, pp. 441-453.
- [13] Dittmar, J., Schulz, A., and Wittig, S., "Assessment of Various Film-Cooling Configurations Including Shaped and Compound Angle Holes Based on Large-Scale Experiments", *Journal of Turbomachinery*, Vol. 125, 2003, pp. 57-64.
- [14] Ligrani, P., Goodro, M., Fox, M., Moon, H., "Full-Coverage Film Cooling: Film Effectiveness and Heat Transfer Coefficients for Dense and Sparse Hole Arrays at Different Blowing Ratios", *Journal of Turbomachinery*, Vol. 134, 2012, pp. 1-13.
- [15] Nasir, S., Bolchoz, T., Ng, W., Zhang, L., Moon, H., Anthony, R. J., "Showerhead Film Cooling Performance of a Turbine Vane at High Freestream Turbulence in a Transonic Cascade", *Journal of Turbomachinery*, Vol. 134, 2012, pp. 1-11
- [16] Van Fossen, G.J., and Bunker, R.S., "Augmentation of Stagnation Region Heat Transfer Due to Turbulence from an Advanced Dual-Annular Combustor", *Proceedings of ASME Turbo Expo*, No. GT2002-30184.
- [17] Goebel, S.G., Abuaf, N., Lovett, J.A., and Lee, C.P., "Measurements of Combustor Velocity and Turbulence Profiles", *ASME Paper*, No. 93-GT-228, 1993.
- [18] Ames, F.E., "Aspects of Vane Film Cooling with High Turbulence: Part I - Heat Transfer", *Journal of Turbomachinery*, Vol. 120, 1998, pp. 768-776.
- [19] Saumweber, C., Schulz, A., and Wittig, S., "Free-Stream Turbulence Effects on Film-Cooling with Shaped Holes", *Journal of Turbomachinery*, Vol. 125, 2003, pp. 65-73.
- [20] Mayhew, J.E., Baughn, J.W., and Byerley, A.R., "The Effect of Freestream Turbulence on Film Cooling Heat Transfer Coefficient and Adiabatic Effectiveness Using Compound Angle Holes", *Proceedings of ASME Turbo Expo*, No. GT-2004-53230.
- [21] Teng, S., Sohn, D.K., and Han, J.C., "Unsteady Wake Effect on Film Temperature and Effectiveness Distributions for a Gas Turbine Blade", *Journal of Turbomachinery*, Vol. 122, 2000, pp. 340-347.
- [22] Ou, S., Han, J.C., Mehandale, A.B., and Lee, C.P., "Unsteady Wake Over a Linear Turbine Blade Cascade with Air and CO₂ Film Injection: Part I - Effect on Heat Transfer Coefficients", *Journal of Turbomachinery*, Vol. 116, 1994, pp. 721-729.
- [23] Sautner, M., Clouser, S., and Han, J.C., "Determination of Surface Heat Transfer and Film Cooling Effectiveness in Unsteady Wake Flow Conditions", AGARD-CP-527, Paper No. 6, 1993.

- [24] Du, H., Han, J.C., and Ekkad, S.V., "Effect of Unsteady Wake on Detailed Heat Transfer Coefficient and Film Effectiveness Distributions for a Gas Turbine Blade", *Journal of Turbomachinery*, Vol. 120, 1998, pp. 808-817.
- [25] Saumweber, C., and Schulz, A., "Free-Stream Effects on the Cooling Performance of Cylindrical and Fan-Shaped Cooling Holes", *Journal of Turbomachinery*, Vol. 134, 2012, pp. 1-12.
- [26] Wright, L.M., McClain, S.T., and Clemenson, M.D., "Effect of Freestream Turbulence Intensity on Film Cooling Jet Structure and Surface Effectiveness Using PIV and PSP", *Journal of Turbomachinery*, Vol. 133, 2011, pp. 1-12.
- [27] Bons, J.P., MacArthur, C.D., and Rivir, R.B., "The Effect of High Freestream Turbulence on Film Cooling Effectiveness", ASME Paper 94-GT-51, 1994.
- [28] Mayhew, J.E., Baughn, J.W., and Byerley, A.R., "The Effect of Freestream Turbulence on Film Cooling Heat Transfer Coefficient", *Proceedings of ASME Turbo Expo*, No. GT-2002-30173.
- [29] Mayhew, J.E., Baughn, J.W., and Byerley, A.R., "The Effect of Freestream Turbulence on Film Cooling Adiabatic Effectiveness", *Proceedings of ASME Turbo Expo*, No. GT-2002-30172.
- [30] Dees, J.E., Bogard, D.G., Ledezma, G.A., Laskowski, G.M., Tolpadi, A.K., "Momentum and Thermal Boundary Layer Development on an Internally Cooled Turbine Vane", *Journal of Turbomachinery*, Vol. 134, 2012, pp. 1-11.
- [31] Simon, F.F., "Jet Model for Slot Film Cooling with Effect of Free-Stream and Coolant Turbulence", *NASA Technical Paper*, No. 2655, 1986, pp. 1-18.
- [32] Gandavarapu, P., "The Influence of High Turbulence Intensity and Large Leading Edge Reynolds Numbers on Stagnation Region Heat Transfer", *University of North Dakota*, 2011.
- [33] Barbot, P.A., "The Effects of Combustor Generated Turbulence and Reynolds Number on Endwall Heat Transfer Distributions in a Linear Vane Cascade", *University of North Dakota*, 2003.
- [34] Ames, F.E., and Moffat, R.J., "Heat Transfer with High Intensity, Large Scale Turbulence: The Flat Plate Turbulent Boundary Layer and the Cylindrical Stagnation Point", *Stanford University*, 1990.
- [35] Ames, F.E., Barbot, P.A., and Wang, C., "Effects of Aero-derivative Combustor Turbulence on Endwall Heat Transfer Distributions Acquired in a Linear Vane Cascade", *Journal of Turbomachinery*, Vol. 125, 2003, pp. 221-231.

- [36] Ames, F.E., Wang, C., and Barbot, P.A., "Measurement and Prediction on the Influence of Catalytic and Dry Low NO_x Combustor Turbulence on Vane Surface Heat Transfer", *Journal of Turbomachinery*, Vol. 125, 2003, pp. 210-223.
- [37] Ames, F.E., Argenziano, M., Wang, C., "Measurement and Prediction of Heat Transfer Distributions on an Aft-Loaded Vane Subjected to the Influence of Catalytic and Dry Low NO_x Combustor Turbulence", *Journal of Turbomachinery*, Vol. 126, 2004, pp. 1-11.
- [38] Jaswal, I., "Aerodynamic Losses and Heat Transfer for a Covered Trailing Edge Turbine Vane with a High Solidity Low Pressure Drop Pedestal Pin Fin Array and Variable Coolant Ejection", *University of North Dakota*, 2008.
- [39] Busche, M.L., Moualeu, L.P., Chowdhury, N., Tang, C., and Ames, F.E., "Heat Transfer and Pressure Drop Measurements in High Solidity Pin Fin Cooling Arrays with Incremental Replenishment", *Proceedings of ASME Turbo Expo*, No. GT-2012-69289.
- [40] Kays, W., Crawford, M., and Weigand, B., "Convective Heat and Mass Transfer", McGraw-Hill, New York, 2005, pp. 546.
- [41] Moffat, R.J., "Describing the Uncertainties in Experimental Results", *Experimental Thermal and Fluid Science*, Vol. 1, 1988, pp. 3-17.